W7AS Contributions 1990

to

13th Int. Conference on Plasma Physics and Contr. Nuclear Fusion Research in Washington, Oct. 1 - 6, 1990;

17th EPS Conference on Controlled Fusion and Plasma Heating in Amsterdam, June 25 - 29, 1990;

9th Int. Conference on Plasma Surface Interaction in Controlled Fusion Devices in Bournemouth, May 28 - 30, 1990

IPP III/ 172

February 1991

MAX-PLANCK-INSTITUT FÜR PLASMAPHYSIK

8046 GARCHING BEI MÜNCHEN

MAX-PLANCK-INSTITUT FÜR PLASMAPHYSIK

GARCHING BEI MÜNCHEN

W7AS Contributions 1990

to

13th Int. Conference on Plasma Physics and Contr. Nuclear Fusion Research in Washington, Oct. 1 - 6, 1990;

17th EPS Conference on Controlled Fusion and Plasma Heating in Amsterdam, June 25 - 29, 1990;

9th Int. Conference on Plasma Surface Interaction in Controlled Fusion Devices in Bournemouth, May 28 - 30, 1990

IPP III/ 172

February 1991

Die nachstehende Arbeit wurde im Rahmen des Vertrages zwischen dem Max-Planck-Institut für Plasmaphysik und der Europäischen Atomgemeinschaft über die Zusammenarbeit auf dem Gebiete der Plasmaphysik durchgeführt.

W7AS-Contributions 1990
to
-13th Int. Conference on Plasma Physics and Contr. Nuclear Fusion Research in Washington, Oct. 1 - 6, 1990;

-17th EPS Conference on Controlled Fusion and Plasma Heating in Amsterdam, June 25 - 29, 1990;

-9th Int. Conference on Plasma Surface Interaction in Controlled Fusion Devices in Bournemouth, May 28 -30, 1990

INTERNATIONAL ATOMIC ENERGY AGENCY

THIRTEENTH INTERNATIONAL CONFERENCE ON
PLASMA PHYSICS AND CONTROLLED NUCLEAR FUSION RESEARCH

Washington, DC, United States of America, 1-6 October 1990

IAEA-CN-53/C-1-2

CONFINEMENT PROPERTIES OF THE "ADVANCED STELLARATOR" WENDELSTEIN W 7AS.

H. Renner, U. Gasparino, H. Maaßberg, G. Kühner,
H. Ringler, F. Sardei, A. Weller
and the W 7AS Team

V. Afanasiev*, R. Brakel, R. Burhenn, G. Cattanei, A. Dodhy, D. Dorst, A. Elsner, K. Engelhardt, V. Erckmann, U. Gasparino, S. Geißler, G. Grieger, P. Grigull, H. Hacker, H.J. Hartfuß , A. Izvozchikov*, R. Jaenicke, S. Jiang**, J. Junker, M. Kick, H. Kroiss, G. Kühner, I. Lakicevic, A. Lazaros, H. Maaßberg, C. Mahn, W. Ohlendorf, M.A. Ochando***, F. Rau, H. Renner, H. Ringler, J. Saffert, J. Sanchez***, F. Sardei, M. Tutter, A. Weller, E. Würsching, M. Zippe, S. Zöpfel, H. Zushi****

guests from:
* IOFFE-Institute, Leningrad, USSR;
** Southwestern Institute of Physics, Leshan (China);
*** CIEMAT, Madrid;
**** Kyoto University, Japan

NBI Group
F.P. Penningsfeld, W. Ott, E. Speth

Pellet Injection Group
K. Büchl, R. Lang

Max-Planck Institut für Plasmaphysik
EURATOM-IPP, D-8046 Garching, FRG

ECRH Team
W. Kasparek, G.A. Müller, P.G. Schüller, M. Thumm

Institut für Plasmaforschung der Universität Stuttgart,
D-7000 Stuttgart, FRG

ABSTRACT

An extended parameter range ($T_e \leq 3$ keV, $T_i \leq 0.7$ keV, $n_e \leq 2.5\ 10^{20}\ m^{-3}$) was explored in the new modular stellarator Wendelstein W 7AS using ECRH and NBI. At 2.5 T main field central values of ß up to 1.5 % were achieved. A reduced Shafranov shift as consequence of the reduced Pfirsch-Schlüter currents for the advanced stellarator concept is verified. Depending on the plasma parameters a net current is observed and identified as the bootstrap current. At the low shear stellarator W 7AS the magnetic configuration and the the confinement depends sensitively on the plasma currents. Thus a control of the configuration by small currents (OH, ECCD, Ohkawa current) is applied to maintain optimum confinement.

Based on profile measurements the electron heat conduction and the ion particle diffusion coefficient were evaluated for ECRH plasmas. As result of statistical analysis a phenomenological expression for the energy confinement time τ_E is derived.

After carbonization the high Z impurities (Fe, Ti) and radiation losses were significantly reduced. At first experiments with NBI ($P_{IN} \leq 1.5$ MW) discharges at density $n_e \leq 2.5\ 10^{20}$ m^{-3} could be maintained and an energy replacement time of up to 30 ms was achieved.

1. INTRODUCTION

The new stellarator at Garching, W 7AS "Advanced Stellarator" (major radius 2m, plasma radius ≤ 0.17 m) [1] is being operated since summer 1988. The experimental programme is devoted to the new possibilities offered by the concept of optimization and guides further theoretical models. The configuration of W 7AS with m=5 periods, similar to 5 toroidally linked mirrors, is produced by a system of modular coils. Each period consists of 9 individually shaped nonplanar coils [2]. The innovative engineering of the magnetic system is testing a technique for the realization of favourable magnetic configurations even for dimensions of a reactor. The improved equipment for heating includes ECRF (electron cyclotron heating: 4 gyrotrons at 70 GHz with 200 kW each), NBI (neutral beam injection heating: tangential injection with 1.5 MW), ICRF (ion cyclotron heating: "experimental antenna" with 1 MW) and allows more flexible operation of the device compared to the previous conventional stellarator W 7A [3]. Especially, the sophisticated ECRF system enables a quasioptical power launch by adjustable mirrors to vary the power deposition profiles and apply for local current drive by introducing $k_{\parallel}$ components [4].

PARAMETER RANGE

More than 10,000 plasma discharges have been recorded up to now, nearly half of them at full field of 2.5 T. Plasma build-up by ECF waves (70 GHz) works routinely for both fundamental and 2nd harmonic launching. In the first experimental periods of W 7AS stellarator, investigations have centered mainly on ECR heated discharges at Bo =1.25 T (2nd harmonic

x-mode) and B_0=2.5 T (fundamental o-mode). In these quasi-stationary ECRH discharges, the maximum densities were limited by the cut-off condition to < 3 10^{19} m^{-3} for B_0=1.25 T and to < 6 $10^{19}m^{-3}$ for B_0=2.5 T. Up to 800 kW ECF power was launched. Maximum electron temperatures of up to nearly 3 keV were measured. Typical energy exchange times of 5 up to 20 ms were evaluated. For these ECRH discharges with a duration of up to 1.5 seconds, the L/R -times were very large and up to 1 second was necessary for establishing of a stationary internal current density profile. The global confinement can depend sensitively on the internal rotational transform profile, and unstable plasma evolutions (bifurcations) were observed in phases with stored energy and line density being constant [5]. NBI heated discharges in the first experimental phase without wall conditioning were dominated by radiative losses and, in most cases, terminated by radiative collapse. After carbonization, the radiation loss mainly due to heavy impurities (iron and titanium) was significantly reduced and operation at high density became possible.

2. MAGNETIC CONFIGURATION EQUILIBRIUM AND STABILITY

Excluding the direct vicinity of ι =1/2 and ι=1/3 , very good agreement of all measured flux surfaces with code simulations was found on the plane where the cross section has a triangular shape [6]. Flux surfaces were also measured in one elliptical plane, where the deviation of the

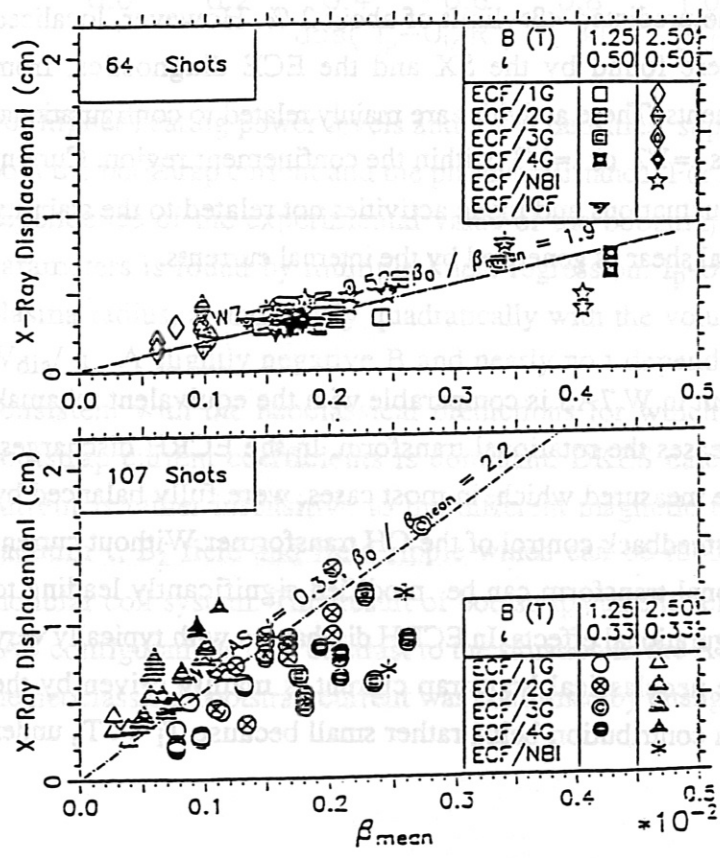

Figure 1
The horizontal shift of the magnetic axis versus the volume averaged < ß > from X-ray profile analysis for ι = 1/2 (upper plot) and for ι = 1/3 (lower plot). The straight lines result from equilibrium calculations (KW code).

measured to the predicted position of magnetic axis was within the accuracy of the method. Electron temperature profile measurements (Thomson, ECE and SX) at different toroidal positions indicate an average accuracy of the magnetic axis position of roughly 1 cm.

One of the aims of the partly optimized W 7AS field configuration was the reduction of the Pfirsch-Schlüter (PS) currents. From the W 7AS optimization, a PS current reduction by a factor of 2 was expected with respect to a standard stellarator. This leads to a reduced Shafranov shift. The outward shift of the magnetic axis with β_0 is confirmed by soft-X observations. In ECRH discharges with highly localized central power deposition, the electron temperatures are peaked. Figure 1 shows the outward shift of the measured central X-ray profile as a function of $<\beta>$ for $\iota \approx 1/2$ and $\iota \approx 1/3$. Note that the shift of the magnetic axis depending on the shape of the pressure profile is about three times larger for $\iota \approx 1/3$ than for $\iota \approx 1/2$. The comparison with predictions based on the KW equilibrium code [7] verifies the PS current reduction by a factor of 2. In addition, the B_z field component originating from the PS currents, which is related to the volume averaged $<\beta>$, is measured directly with magnetic loops and agrees with the relation $B_z \sim <\beta> B_0/\iota$ as simulated by the VMEC equilibrium code [8]. Volume-averaged β values, $<\beta>$, of up to 0.16 % and 0.28 % were found using ECRH for B_0=2.5 T and B_0=1.25 T, respectively. The maximum peak β_0 values were 0.52 % and nearly 0.8 %. Maximum values of $<\beta> = 0.62$ % and β_0=1.5 % were found with NBI. So far, the maximum values of β seem limited only by the available heating power. The experimental $<\beta>$ values were much lower than the predicted $<\beta>$ limit of about 2 %. However, localized fluctuations and mode activities were found by the SX and the ECE diagnostics, from reflectrometry and from H_α measurements. These activities are mainly related to configurational effects for discharges with resonances $\iota=1/2$ or $\iota=1/3$ within the confinement region. Current profile analysis indicates that these fluctuations and mode activities not related to the stability limit are stabilized by sufficient internal shear as generated by the internal currents.

BOOTSTRAP CURRENT

The magnitude of the bootstrap current in W 7AS is comparable with the equivalent tokamak value, and the bootstrap current increases the rotational transform. In the ECRH discharges, bootstrap currents of several kA were measured which, in most cases, were fully balanced by applying a small loop voltage, U_l, by feedback control of the OH transformer. Without current control, the edge value of the rotational transform can be modified significantly leading to confinement degradation due to configurational effects. In ECRH discharges with typically very broad n_e and peaked T_e profiles, the neoclassical bootstrap current is mainly driven by the electron temperature gradient, the ion contribution being rather small because $T_i << T_e$ under these conditions.

For each magnetic configuration in W 7AS, the bootstrap current is calculated using the DKES code. Based on measured T_e and n_e profiles, the total bootstrap current as well as the plasma resistance are calculated. In Figure 2, the neoclassical predictions for the dominant electron component, I_b^e, are compared with the experimental values defined by I_p-U_l/R for ECRH discharges. The agreement with the neoclassical predictions is very good.

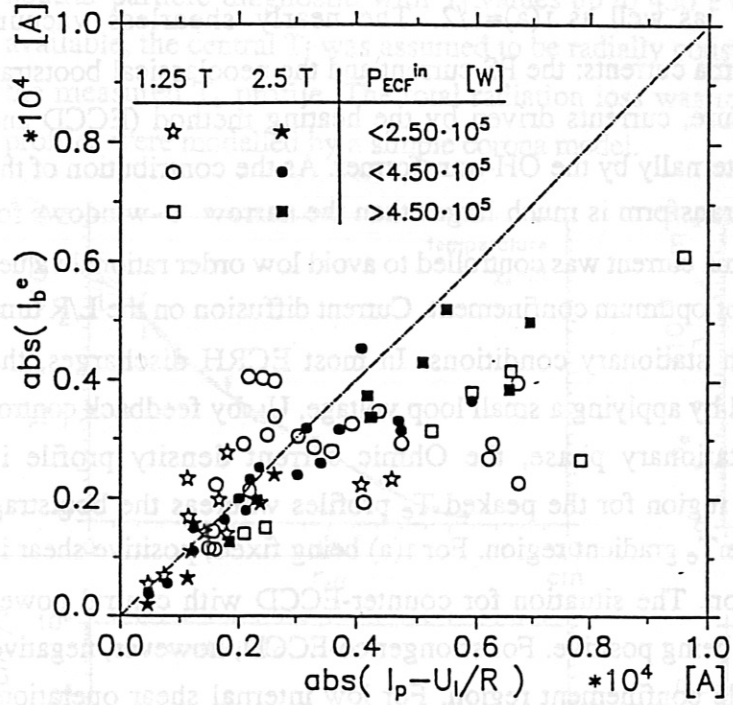

Figure 2
The electron component of the bootstrap current, I_{be}, calculated from the DKES code versus the experiment value, I_p-U_l/R, for ECRH discharges (without ECCD) with central deposition.

For higher heating power levels and lower densities, suprathermal electrons will contribute to both the bootstrap current and the plasma resistance. For ECRH discharges without ECCD, the dependence of the experimental value of the bootstrap current, I_p-U_l/R, on global plasma parameters is found by multiple linear regression. I_p-U_l/R scales linearly with the effective plasma radius, a, and nearly quadratically with the volume averaged temperature defined by W_{dia}/ n . A slightly negative B and nearly no ι dependence was found. These findings are consistent with the neoclassical predictions for which the temperature dependence of the bootstrap current coefficients is dominant. DKES calculations [9] show that the bootstrap current is rather insensitive to the different magnetic field configurations characterized by vacuum ι, B_z field and field ripple which can be modified by varying the currents in the modular coil system. This result of bootstrap current being roughly the same for different W 7AS configurations is in contrast to the situation in the ATF experiment where the existence of the neoclassical bootstrap current was confirmed by changing the additional quadrupole field.

CONFIGURATIONAL EFFECTS ON CONFINEMENT

As was the case for the W 7A stellarator, the global confinement in W 7AS depends strongly on the boundary value of the rotational transform, $\iota(a)$ [5]. A degradation of both energy and particle confinement is found for low order rational values of the rotational transform at the plasma edge, $\iota(a)$, whereas optimum confinement can be established in narrow ι-windows close to the resonances $\iota(a)\approx 1/3$ as well as $\iota(a)\approx 1/2$. The nearly shearless vacuum configurations are modified by plasma currents: the PS current and the neoclassical bootstrap current generated by plasma pressure, currents driven by the heating method (ECCD and Ohkawa currents during NBI) or externally by the OH-transformer. As the contribution of the bootstrap current to the rotational transform is much larger than the narrow ι -windows for optimum confinement, the total plasma current was controlled to avoid low order rational values of ι or to keep $\iota(a)$ within the range of optimum confinement. Current diffusion on the L/R time scale determines the time to reach stationary conditions. In most ECRH discharges, the bootstrap current was fully balanced by applying a small loop voltage, U_l, by feedback control of the OH-transformer. In the stationary phase, the Ohmic current density profile is concentrated in the central plasma region for the peaked T_e profiles whereas the bootstrap current is driven more outside in the T_e gradient region. For $\iota(a)$ being fixed, positive shear is generated in the confinement region. The situation for counter-ECCD with central power deposition is similar, the shear also being positive. For stronger co-ECCD, however, negative shear can be generated in the whole confinement region. For low internal shear operation, degraded confinement is found to be related to low order rational values of $\iota(a)$ which indicates island formation and ergodization in the magnetic configuration. Even a local flattening of the T_e profile has been resolved for these conditions. With sufficient internal shear nearly identical discharges could be established above and below both $\iota(a)=1/3$ and $\iota(a)=1/2$. Current profile estimates clearly show that the low order rational values are within the confinement region. By a scan of ECR heating power a nonlinear mechanism of "self-stabilization" of the internal shear was demonstrated [5]: both the bootstrap and compensating Ohmic currents increase with the energy content, resulting in higher positive shear and in an improved confinement which leads to increasing energy content. The W 7A experience, on the other hand, indicates a degradation of confinement with strong internal shear. As a consequence, the optimization of energy confinement depends on the optimization of the internal ι profile. First experiments using local ECCD for the ι profile shaping show promising results.

3. TRANSPORT

ELECTRON HEAT CONDUCTION

For ECRH discharges, the electron densities were less than $5\ 10^{19}\ m^{-3}$, so the collisional electron-ion coupling and the radiative losses were rather small, and the electron heat

conduction was the dominant loss channel. These discharges are the best candidates for electron energy balance analysis, which is based on density and temperature profiles measured by the Thomson scattering diagnostic. Furthermore, the n_e profiles were very broad and the T_e profiles highly peaked for central ECF power deposition. With increasing power density the density profiles become hollow. The central ion temperature was estimated by passive CX neutral particle diagnostic with T_i values up to 450 eV. As T_i-profile information was not available, the central T_i was assumed to be radially constant and the edge values were fitted to the measured T_e profile. The total radiation loss was measured by bolometry. The radiation profiles were modelled by a simple corona model.

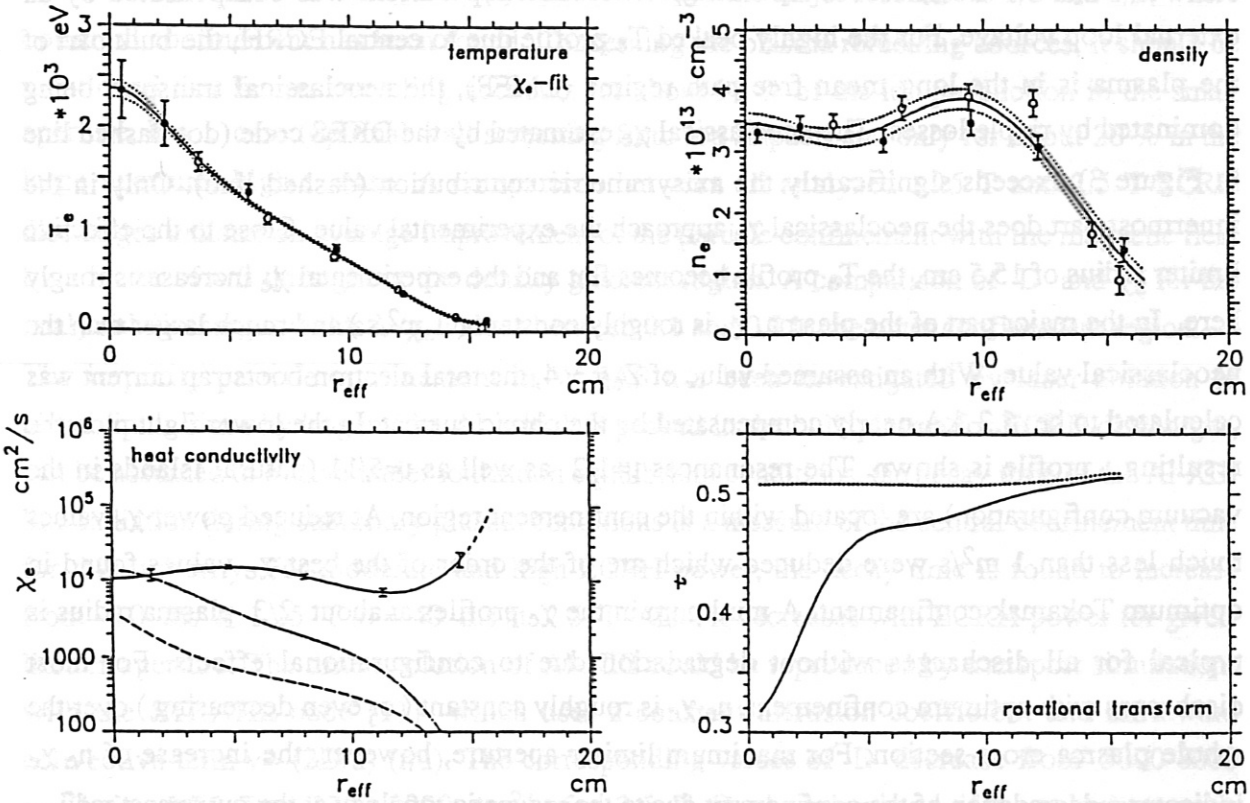

Figure 3

Transport analysis for series 7545-57. Electron temperature, T_e, density, n_e, heat conductivity, χ_e, and rotational transform profiles are shown for B_0=2.5 T and with $P_{ECF} \approx 640$ kW input power. In the experimental χ_e (lower left plot, solid line) standard errors resulting from the least-squares fit of the T_e profile (upper left plot) are given, additionally, the χ_e from the DKES code (dot-dashed line) and from the Hinton-Hazeltine model (dashed line) are shown.The rotational transform, ι, is shown in the lower right plot, the resulting $\iota(r)$ due to internal currents (solid line) and without internal currents (dotted line). collisionality : $\nu_e^* \geq 3\ 10^{-3}$

The stationary electron energy balance equation with radiative losses and electron-ion power transfer is solved with the diffusive ansatz for the radial electron energy flux, $q_e = -n_e\ \chi_e\ T_e'$,

and an analytic ECF power deposition model which is highly peaked in agreement with ray-tracing calculations. Solving the electron energy balance equation, the measured T_e profiles are fitted by a least-squares technique using a power series of log(χ_e) in normalized radius, the power series coefficients being the fit parameters. This integration method of the electron energy balance equations leads to a smoothed representation of the electron heat conductivity, χ_e. For the n_e profiles, a standard fit function is used. With these T_e and n_e profiles, all neoclassical transport properties are estimated using the DKES code [10]. In Figure 3, the electron temperature, density, heat conductivity and rotational transform profiles are shown for typical one of the high pressure (<ß> = 0.14 %) ECRH discharges at B_o=2.5 T with 640 kW ECF input power (4 gyrotrons operating). The bootstrap current was compensated by an external loop voltage. For the highly peaked T_e profile due to central ECRH, the bulk part of the plasma is in the long mean free path regime (LMFP), the neoclassical transport being dominated by ripple losses. The neoclassical χ_e estimated by the DKES code (dot-dashed line in Figure 3) exceeds significantly the axisymmetric contribution (dashed line). Only in the innermost part does the neoclassical χ_e approach the experimental value. Close to the effective limiter radius of 15.5 cm, the T_e profile becomes flat and the experimental χ_e increases strongly here. In the major part of the plasma, χ_e is roughly constant (1 m^2/s) and much larger than the neoclassical value. With an assumed value of Z_{eff} = 4, the total electron bootstrap current was calculated to be 5.2 kA nearly compensated by the ohmic current. In the lower right plot, the resulting ι profile is shown. The resonances ι=1/2 as well as ι=5/11 (natural islands in the vacuum configuration) are located within the confinement region. At reduced power χ_e values much less than 1 m^2/s were deduced which are of the order of the best χ_e values found in optimum Tokamak confinement. A minimum in the χ_e profiles at about 2/3 plasma radius is typical for all discharges without degradation due to configurational effects. For most discharges with optimum confinement, $n_e \chi_e$ is roughly constant (or even decreasing) over the whole plasma cross section. For maximum limiter aperture, however, the increase of $n_e \chi_e$ indicates a degradation of the confinement due to the magnetic topology at the outermost radii.

PARTICLE TRANSPORT

The particle confinement in W 7AS was investigated for ECRH discharges at 1.25 T and 2.5 T by coupling DEGAS code [10] simulations with H_α emissions measured at relevant toroidal positions. Radially resolved ion fluxes were obtained from calculated neutral particle distributions, after calibrating them with the H_α signals. Estimated Z_{eff} were used to derive the electron particle fluxes and diffusivities. Central electron density profiles were found to get more and more hollow as the ECR heating power with central deposition is increased. For an ECRH power scan at 2.5 T the electron fluxes in the central region have been compared with neoclassical predictions. As T_i profile information is lacking, only the neoclassical electron

fluxes were estimated by the DKES code. For the higher heating power levels, for which the central hollow profiles are more pronounced, the fluxes near the plasma center are in fairly good agreement. This means that the observed hollow density profiles can be explained reasonably well by the neoclassical temperature gradient driven particle flux (thermodiffusion), without need of additional anomalous contributions. Reduction of the heating power down to the lowest level (1 gyrotron) yields density profiles that are flat and particle fluxes much larger than the neoclassical values. In the density gradient region, as compared to the central region, the particle fluxes strongly increase whereas the neoclassical fluxes are negligible due to the neoclassical T_e dependence. The particle diffusivities, D, have been evaluated for discharges operated at half and full field, and ι(a) values close to the major resonances 1/3 and 1/2, where optimum confinement has been found. Concerning the plasma refuelling sources, it should be mentioned that limiter recycling accounts for about 90 % of the ion production in the small aperture, low ι case (optimal wall screening from ion impact) and only for about 20 % in the large aperture, high ι case. A comparison between all analyzed 1.25 T and 2.5 T ECRH discharges indicate an average improvement of the particle confinement with the magnetic field by a factor of $\approx$ 3 throughout the density gradient region. A comparison of D and χ_e for the analyzed discharges yields D/χ_e values between 0.1 and 0.3 in the outer confinement region.
The impurity particle confinement in W 7AS has been investigated by laser ablation of aluminium. Since hydrogen-like Al, which is peaked in the bulk plasma for ECRH discharges, can be assumed to evolve under ionization equilibrium conditions, the decay time of the Al-XIII line radiation during stationary plasma conditions is a measure of the central confinement time for this impurity. For moderate and high ECRH power, the decay time is found to increase from $\approx$10 ms at 1.25 T to $\approx$ 40 ms at 2.5 T. Also, it decreases with ECRH power for given limiter aperture. The time evolution of Al-XIII could be reproduced by transport simulations with the STRAHL code [11] which uses a constant diffusion coefficient and an inward convective term v=-(2D/a) (r/a). The corresponding values of D decrease from 5000-8000 cm^2/s for 1.25 T to 1200-2000 cm^2/s for 2.5 T. On the other hand, if the velocity term is omitted, these numbers reduce by only $\approx$ 20 %. Discrepancies between the measured and simulated decay times are found, however, for the lower ionization stages. More experimental data and more accurate simulations, including a spatial variation of D , are needed to improve the description of the impurity transport behaviour under different experimental conditions.

FIRST RESULTS WITH NEUTRAL INJECTION (NBI).

During July 1990 the investigations at W 7AS were concentrated on experiments using neutral beam injection. After carbonization by glow discharges with a mixture of He and 30% CD_4 (or CH_4) the content of high Z material (Fe und Ti) was significantly reduced. With reduced radiative losses the parameter range of plasmas was extended to much higher densities than

before and pulse duration up to 300 ms. The target plasma is produced by ECRH 70 GHz at main field 2.5T or 1.25 T. The full power of NBI ($P_N \leq 1.5$ MW) at W 7AS injecting H^o with an accelerating voltage of 45 kV was used for further heating, see Fig. 4.

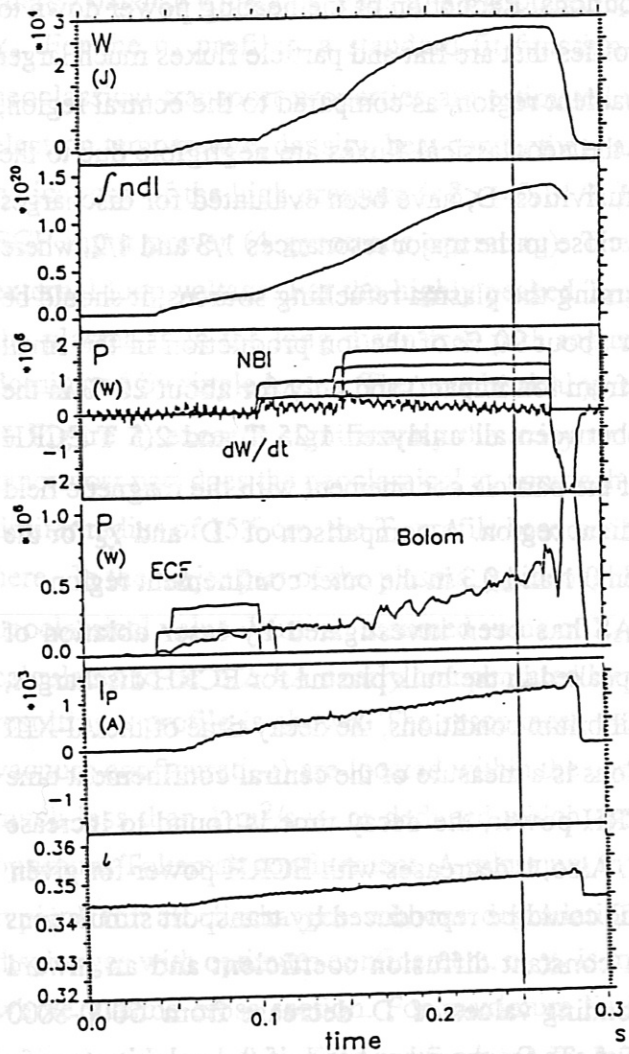

Figure 4
NBI injection after carbonization : shot 9901, 2.5 T. ι = 0.34, balanced injection using 4 beams with P_N = 1.5 MW. Development of global parameters: energy content W, line density (m^{-2}) at the elliptical plane with L=0.63 m by HCN-interferometer, input power : ECF and NBI, radiative power by bolometer, time derivative of W, plasma current, rotational transform.

With carbonized walls the recycling coefficient is larger than 1 and the evolution of the discharge is characterized by a steady increase of density. Before saturation the rate of density increase is determined by gas released by plasma/wall interaction rather than by the flux associated to NBI. The maximum energy content was 28 kJ ($\beta_0 \approx 1.5$ %) at 1.4 MW absorbed power was achieved at field 2.5 T and plasma radius 0.176 m for the rotational transform ι = 0.34. With balanced injection the observed bootstrap current of 1.2 kA agrees well with the calculated value. Unbalanced injection generates a variation of the net current by some kA depending on the density. Unfortunately, no ion temperatures could be measured at these high densities since the diagnostic beam and the CX flux from the center were completely absorbed. However, electron and ion temperatures should be equal at this very high density. The maximum obtainable density, and consequently ß, seems related to the absorbed power, as long

the electron temperature stays above 350 eV to minimize the radiative losses and prevent a radiative collapse.

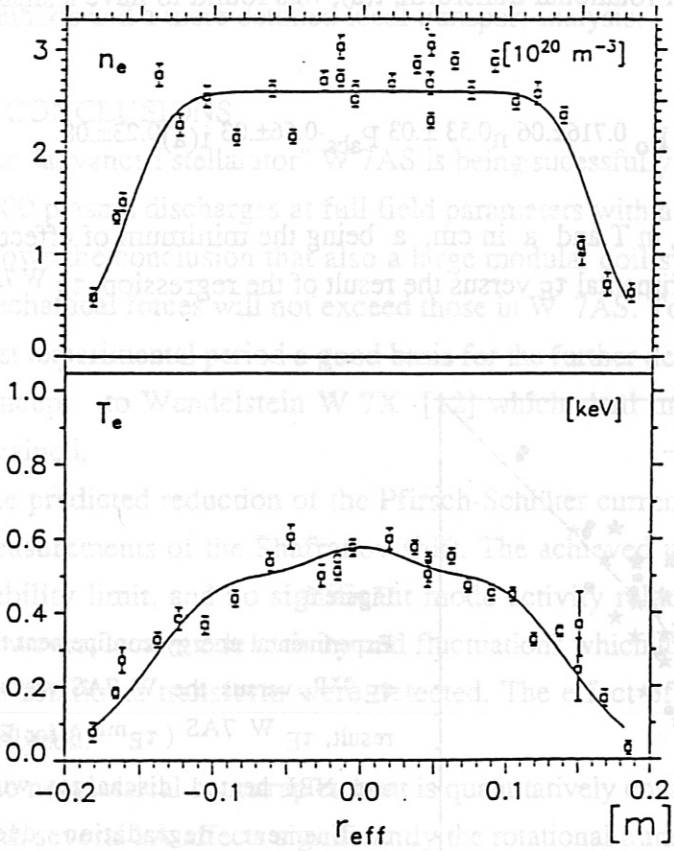

Figure 5
Density and temperature profiles for the discharge of Figure 4 at $\Delta t = 0.25$ s (series 9866-9897).

Fig. 5 presents the measured profiles. Compared to the typical situation for the ECRH discharges the ion heat losses should be significantly enlarged. More detailed information is necessary to evaluate local experimental data and deal with the influence of electric fields. Presently only a global description of the energy confinement is possible. He glow discharges and the reduction of the input power allow to stabilize the density close to $n_{eo} = 1\ 10^{20}\ m^{-3}$. At these densities with $T_{eo} \approx 0.75$ keV, $T_{io} \approx 0.6$ keV a maximum replacement time of 30 ms was achieved.

Operating at low field 1.25 T discharges at similar densities and slightly reduced temperature could be maintained. Using only 3 injectors ($P_N \leq 1.1$ MW), plasmas with an averaged $\langle \beta \rangle = 0.65\%$ and a replacement time of typical 10 ms were produced.

ENERGY CONFINEMENT SCALING

The dominant parameter dependence of the global energy confinement time, τ_E, is given by multiple linear regression analysis. This standard procedure is used to obtain the general trend in the confinement properties as well as the significant parameter dependences.

About 86 series of discharges with 2nd and 1st harmonic ECRH as well as 14 series with NBI were selected from a database system for this regression. Discharges with confinement

degradation due to configurational effects were excluded. The energy confinement time depends significantly on magnetic field strength, B_0, line averaged density, n, absorbed power, P_{abs}, and plasma radius, a. The edge value of rotational transform, $\iota(a)$, was found to have a smaller significance.

$$\tau_E^{W\,7AS} = (1.68 \pm .02)\ 10^{-8}\ a^{1.28 \pm .16}\ B_0^{\,0.716 \pm .06}\ n^{0.53 \pm .03}\ P_{abs}^{-0.56 \pm .03}\ \iota(a)^{0.23 \pm .08}$$

with τ_E in ms, n cm^{-3}, P_{abs} in W, B_0 in T and a in cm, a being the minimum of effective limiter and separatrix radius. The experimental τ_E versus the result of the regression, $\tau_E^{\,W\,7AS}$, is shown in Figure 6.

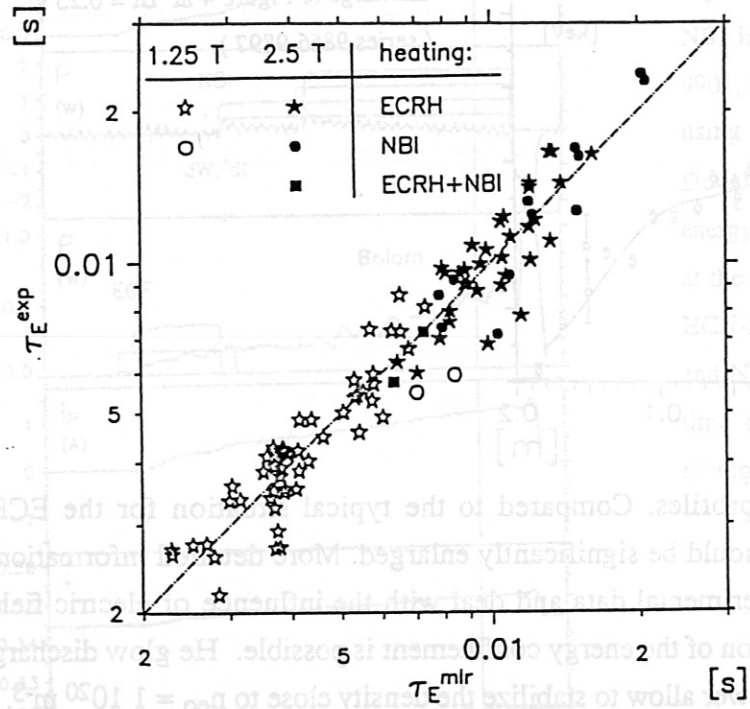

Figure 6
Experimental energy confinement times, $\tau_E^{\,exp}$, versus the W 7AS regression result, $\tau_E^{\,W\,7AS}$ (τ_E^{mlr}) for ECRH and NBI heated discharges without confinement degradation due to configurational effects.

The regression coefficients for n and P_{abs} are very similar to those of the LHS or "gyro-reduced Bohm" scalings. In spite of the differences in the parameter range for ECF ($\nu_e^*(0) \geq 10^{-3}$) and NBI discharges ($\nu_e^* \approx 0.1$), the different power deposition and different power losses by electrons, ions and radiation there is no significant deviation in such a global scaling. For pure ECRH discharges in W 7AS, where the density profiles are flat and very broad, $n_e \chi_e$ was found to be roughly constant. The shape of the T_e profiles does not change very much on variation of external plasma parameters. Within the important confinement region, the temperature gradient is only slightly affected by the heating power. A physical picture of this anomalous transport cannot be given by such a form of regression analysis. However, the fact that no local scaling of χ_e with T_e was found indicates two possible explanations. Firstly, the electron heat conduction cannot be treated by a regression ansatz as used so far for the accessible parameter range, or, secondly, the picture of transport being determined by only

local plasma parameters is inadequate. ECRH related effects (distortion of the energy distribution, localized power deposition) must be eliminated by application of different heating methods and a more detailed local transport analysis.

4. CONCLUSIONS

The "advanced stellarator" W 7AS is being sucessfully operated. To date there have been about 4000 plasma discharges at full field parameters with a duration of up to 1.5 s. This experience allows the conclusion that also a large modular coil system can be realized, especially as the mechanical forces will not exceed those in W 7AS. Together with the promising results of the first experimental period a good basis for the further development of the "Advanced stellarator" concept to Wendelstein W 7X [12] which shall include all theoretical improvements is obtained.

The predicted reduction of the Pfirsch-Schlüter currents by a factor of 2 has been verified by measurements of the Shafranov shift. The achieved pressure was much below the predicted stability limit, and no significant mode activity related to the stability limit was observed. However, local mode activity and fluctuations which are related to low order rational values of the rotational transform were detected. The effect of these activities on transport is not yet analyzed.

The neoclassical bootstrap current is quantitatively confirmed in W 7AS. The bootstrap current with several kA affects significantly the rotational transform profile and dominates the Pfirsch-Schlüter contribution. It depends sensitively on the average temperature. In order to avoid a strong modification of the ι profile, the bootstrap current has to be controlled. The control of rotational transform at the plasma edge worked well for all scenarios under consideration. Internal shear is introduced by the bootstrap current depending on the energy content achieved. A future task of W 7AS will be the analysis of confinement optimization by means of an appropriate shaping of the whole rotational transform profile using local ECCD.

For ECRH discharges, electron energy balance analysis based on measured T_e and n_e profiles yields the electron heat conductivity, $\chi_e(r)$. The best χ_e values which have been achieved are well below 10^4 cm^2/s which are in the range of the optimum χ_e values found in tokamaks. For all analyzed discharges, the neoclassical transport coefficients were calculated by using the DKES code and compared to the experimental values. Due to the strong T_e dependence, the neoclassical χ_e values decrease rapidly with radius and are typically about one order of magnitude smaller than the experimental value at half plasma radius. The neoclassical χ_e comes up to the experimental value only for central high ECF power deposition with peaked temperatures where the neoclassical ripple losses dominate. Further investigations of transport in an extended parameter range with different heating methods are necessary to discriminate effects related to particular heating scenarios.

The regression analysis of the global energy confinement time agrees rather well with predictions based on the LHS- and the "gyro-reduced Bohm" scalings.
From the DEGAS code, particle fluxes and diffusivities have been derived using measured T_e and n_e profiles and absolute H_α intensities at relevant positions around the machine. The radial range of the diffusivities includes the density gradient region up to the limiter. Here, the value of D exceeds neoclassical predictions by more than one order of magnitude. The ratio D/χ_e was between 1/10 and 1/3. For the hollow profiles at high power level, the central particle fluxes from DEGAS simulations agree fairly well with the neoclassical fluxes which are dominated by thermodiffusion. Consequently, the ECRH density pump-out in the central region is consistent with neoclassical transport in W 7AS.
Some preliminary results are obtained for NBI heated discharges. With carbonization, the very high wall recycling lead to a strong density increase, and stationary conditions could not be obtained. The radiation losses, however, were significantly reduced, and the discharges were terminated by edge cooling at very high densities. Only limited by the available heating power discharges at densities up to 2.5 10^{20} m-3 with favourable confinement were obtained. Acceptable discharge conditions with low radiation levels and lower recycling could be realized shortly after helium glow discharge cleaning. Boronization and the installation of pump limiters positioned in regions with high outward fluxes [13] may help to reduce the impurity production and to lower recycling (perhaps due to partial Ti-gettering).

REFERENCES

[1] Brossmann,U. Dommaschk,W. et alt., Plasma Physics and Controlled Nuclear Fusion Research (Proc. 9th Conf. Baltimore 1982), **Vol. 3**, IAEA, Vienna (1983), p.141
[2] Sapper, J. et alt. Transactions 8th Int. Conf. Structural Mechanics in Reactor Technology, Amsterdam (1985), **N**, p.15
[3] Renner, H. et alt., Plasma Physics and Contr. Fusion, **31**, (1989), p. 1579-1596
[4] Erckmann, V., et alt., 17th Europ. Conf. on Contr. Fusion and Plasma Physics, **14B**, p. 1271, Amsterdam 1990
[5] Ringler, H. et al., 17th EPS Conf. on Contr. Fus. and Plasma Phys., invited paper, Amsterdam, 1990
[6] Jaenicke, R., et alt., 16th Europ. Conf. on Controlled Fusion and Plasma Physics, Venedig (1989), **P8 B3**
[7] Kisslinger, J. and H.Wobig, ECA, **9F I** , p. 453, 1985
[8] Gardner, H.J., 2nd Workshop on Wendelstein VII-X, **EUR 11705 EN**, p. 51, 1988
[9] Hirshman, S.P., et alt., Phys. Fluids **29** (1986), 2951
[10] Heifetz, D.B., et alt. J. Comp. Phys. **46** (1982), 309
[11] Behringer,K., **report JET-R (87) 08** , 1987
[12] Grieger, G., et alt. , Proc. of the 13th Intern. Conf. on Plasma Phys. and Contr. Nucl. Fusion, Washington 1990, **G-1-6**
[13] Grigull, P. et al., Proceedings of the 9th Int. Conf. on Plasma Surface Interaction, Bournemouth, 1990.

INTERNATIONAL ATOMIC ENERGY AGENCY

THIRTEENTH INTERNATIONAL CONFERENCE ON
PLASMA PHYSICS AND CONTROLLED NUCLEAR FUSION RESEARCH

Washington, DC, United States of America, 1-6 October 1990

IAEA-CN-53/ C-3-1

ELECTRON CYCLOTRON CURRENT DRIVE AND WAVE ABSORPTION EXPERIMENTS IN THE W 7-AS STELLARATOR

V. Erckmann, U. Gasparino, H. Maaßberg, H. Renner, M. Tutter,
W VII-AS Team+)
Max-Planck-Institut für Plasmaphysik,
EURATOM Association, D-8046 Garching, FRG

W. Kasparek, G.A. Müller, P.G. Schüller, M. Thumm
Institut für Plasmaforschung, Universität Stuttgart, FRG

+)W 7-AS-Team

V. Afanasiev*, R. Brakel, R. Burhenn, G. Cattanei, A. Dodhy, D. Dorst, A. Elsner, K. Engelhardt, V. Erckmann, U. Gasparino, S. Geißler, P. Grigull, H. Hacker, H.J. Hartfuss, A. Izvozchikov*, R. Jaenicke, S. Jiang**, J. Junker, M. Kick, J. Kißlinger, H. Kroiss, G. Kuehner, I. Lakicevic, A. Lazaros, H. Maassberg, C. Mahn, M. Ochando***, W. Ohlendorf, F. Rau, H. Renner, H. Ringler, J. Saffert, J. Sanchez***, F. Sardei, M. Tutter, A. Weller, H. Wobig, E. Würsching, M. Zippe, S. Zöpfel, H. Zushi****.

* Guest from *IOFFE-Institute, Leningrad, USSR*
** Guest from *Southw. Institute of Physics, Leshan, China*
*** Guest from *Ciemat, Madrid, Spain*
**** Guest from *Kyoto University, Kyoto, Japan*

IAEA-CN-53/C-3-1

ELECTRON CYCLOTRON CURRENT DRIVE AND WAVE ABSORPTION EXPERIMENTS IN THE W 7-AS STELLARATOR

ABSTRACT

Experiments on non-inductive current drive by electromagnetic waves in the vicinity of the 1st and 2nd harmonic of the electron cyclotron frequency (ECCD) were performed at the W 7-AS stellarator with up to 1 MW rf-power at 70 GHz in long-pulse operation (< 1.5 s). The single pass absorption as an important input quantity for current drive investigations was directly measured for 1st harmonic O-mode and 2nd harmonic O- and X-mode operation, respectively in a wide plasma parameter range. A good agreement with a 3-D ray tracing model was found.

ECCD was investigated by

a) a toroidal launch angle variation of the microwave-beams while the total net current was kept close to zero ($I_P < 0.2$ kA) by beedback control of the OH-transformer. The change of the required loop voltage with respect to perpendicular launch (no ECCD) was measured as a function of the launch angle
b) the adjustment of the launch angle of the microwave-beams to balance the bootstrap current without making use of the OH-transformer (counter current drive). Here the EC-wave driven current is measured in units of the bootstrap current.
c) a perturbation experiment at up/down shifted frequencies, where 0.2 MW were launched at a fixed toroidal angle and the EC-resonance layer was shifted out of the confinement region (B_0 - variation). The loop voltage change required for compensation of the EC-driven current was measured as a function of the magnetic induction.

The parameter dependence on the launch angle, the electron temperature, the plasma density and the microwave-power for all types of ECCD experiments is in good agreement with a linear theoretical model, which takes into account quasilinear and trapped particle effects. The results are confirmed by Fokker-Planck calculations.

1. INTRODUCTION

Experiments on current drive by electromagnetic waves in the vicinity of the electron cyclotron frequency and the comparison with theory attract increasing interest for both, tokamak as well as stellarator research to provide a reliable data-base for Electron Cyclotron Current Drive (ECCD) scenarios in next step devices such as NET and WVII-X. The high localization of the driven currents and the capability to penetrate the plasma centre even in large machines together with the technical advantage of a simple remote launching structure may overcompensate the disadvantage of a small ECCD efficiency (compared to Lower Hybrid Current Drive) for particular applications such as MHD-mode control, current profile shaping or, especially for stellarators, bootstrap current compensation. Basic experiments were performed at the W VII-AS stellarator, where the small EC-driven currents are not masked by large inductively driven currents as in tokamaks. The control of a pressure driven net current was experimentally demonstrated and is mandatory in low vacuum shear configurations such as W VII-AS to maintain good confinement properties [1].

The theoretical treatment of ECCD would require a Fokker Planck solution in full phase space, which is out of scope. In a first approach, we compare the experimental results with a theoretical model, which in the simpliest version neglects trapped particle effects [2]. In a second step, we have analysed the sensitivity of this model with respect to simplified assumptions on trapped particle and quasi-linear effects [3,4]. The experimental investigation of the single pass absorption of a microwave beam in the electron cyclotron frequency range is of crucial importance as an input quantity for CD-calculations. Measurements of the single pass absorption are compared to ray tracing calculations.

2. WAVE ABSORPTION

Plasma build up and heating is achieved at W 7-AS with a 1 MW, 70 GHz ECRH system. The resonant magnetic field and the cutoff densities are 2.5 T and $n_{e,crit} = 6.2 \cdot 10^{19}$ m^{-3} for the 1st harmonic and 1.25 T and $n_{e,crit} = 3.1 \cdot 10^{19}$ m^{-3} for the 2nd harmonic experiments, respectively.The single pass absorption was directly measured for perpendicular launch by a 35 channel pick-up wave guide array mounted opposite to the launching mirrors at the inner vacuum vessel wall. In the investigated electron temperatures range of 0.6 keV < T_{eo} < 1.8 keV total absorption of the waves in a single transit through the plasma was found in all cases with 2nd harmonic X-mode launch, whereas for 2nd harmonic O-mode the plasma is optically thin (single pass absorption < 7 %) in agreement with theory. A deviation from total absorption is expected for 2nd harmonic X-mode at a central electron temperature of T_{eo} < 200 eV. For 2nd harmonic O-mode T_{eo} > 4 keV is required to obtain considerable absorption.

For 1st harmonic O-mode heating, however, the single pass absorption is sensitive to the electron temperature and density in the experimentally accessible parameter range of 0.6 keV <.T_{eo} < 2.7 keV and $1 \cdot 10^{19} < n_{eo} < 5 \cdot 10^{19}$ m^{-3}. The single pass absorption for a density scan at fixed central electron temperature of 1.5 keV and a temperature scan at fixed electron density of $2.5 \cdot 10^{19}$ m^{-3} was measured ranging from 60 % ± 3 % up to 95 % ± 5 %. A comparison of the measurements with a 3-D ray tracing model based on measured spatial profiles of T_e and n_e (Thomson-scattering, ECE) shows an excellent agreement within the experimental error bars.

3. ELECTRON CYCLOTRON CURRENT DRIVE - EXPERIMENTS

The ECCD-experiments were performed at the W VII-AS stellarator with up to 0.7 MW rf-power in long-pulse operation (< 1.5 s). Up to four linearly polarized rf-beams were launched at both the 1st harmonic ordinary and the 2nd harmonic extraordinary wave

polarization,respectively, from the low field side. The rf-beams were directed towards the plasma at arbitrary toroidal launch angles by a set of independently movable focussing mirrors mounted inside the vacuum chamber [5].

In a first experiment, the toroidal launch angle of the rf-beams was varied while the total net plasma current was kept close to zero ($I < 0.2$ kA) by feedback control with the OH-transformer. The measured change of the required loop voltage ΔU with respect to perpendicular launch (no ECCD) is plotted in Fig. 1(a) as a function of the launch angle at the resonance-layer for constant input power of 0.35 MW in 1st harmonic O-mode. The dots refer to experiments with one beam (0.17 MW) at perpendicular launch (no ECCD) and one beam (0.17 MW) at oblique launch angles. The crosses refer to a variation of the launch angle of both beams. The right wing of the curve with positive loop voltage increment corresponds to a situation, where the bootstrap current has the same direction as the EC-driven current. The left wing of the curve corresponds to ECCD in counter direction to the bootstrap current. Equivalent experiments at $B_0 = 1.25$ T show similar results [6]. The change of the internal current distribution results in a change of the total stored plasma energy of about 20 %. The influence on the confinement is explained by magnetic field configuration and internal shear effects [7]. The ECCD efficiency is evaluated in a 3-D ray tracing code by means of the adjoint approch [8]. In the limit of low collisionality, the evaluation of the local efficiencies was generalized to include trapped particle effects in W 7-AS magnetic configurations [4]. A comparison of the experimental data with this linear model [3] is shown in Fig. 1(b). The calculations are based on the measured n_e-profiles and the measured change of the T_e-profiles for each launch angle. The experimental findings are well described by the model. In particular, the launch angle for maximum current drive and the linear increase of ECCD with rf-power agree well. The absorption layer is shifted radially outward with increasing oblique launch. The current drive efficiency decreases for large launch angles (far in the Doppler regime) because the absorption depends sensitively on T_e and the absorption layer is then within the T_e gradient region. Furthermore, the number of trapped particles increases and the mismatch of the incident linearly polarized waves is no longer negligible [6]. It should be noted that the measured current inversion at large launch angles is also found in the calculations and is related to the particilar W 7-AS magnetic field topology. The absolute value of the EC-driven current at maximum launch angle derived from the experiment is about 3 - 5 kA, which is in satisfying agreement within the simplified assumptions of the theory and the experimental error bars.

In a second experiment, the launch angle of up to 4 microwave-beams (0.7 MW) was adjusted to balance the bootstrap current without making use of the OH-transformer (counter current drive). The net plasma current was kept below ± 0.3 kA under all plasma conditions. The EC-wave driven current is then measured under steady state conditions in units of the bootstrap current, which is varied by a variation of the plasma parameters with increasing microwave power. The dominant electron component of the bootstrap current ($T_e >> T_i$) was calculated by the DKES code for the measured spatial profiles of n_e and T_e. Scanning the rf-power from 0.17 - 0.7 MW, the electron temperature from $0.8 < T_e < 1.9$ keV and the electron density from $1.1 < n_{eo} < 2.8 \cdot 10^{19}$ m^{-3}, the bootstrap current varies from $0.8 < I_{Boot} < 4.3$ kA (2nd harmonic X-mode). The current drive model overestimates the EC driven current by typically a factor of 3, if trapped particles are neglected. If trapped particles are taken into account, this discrepancy almost vanishes within the experimental accuracy and the uncertainties to derive the bootstrap current from the measured plasma profiles.

In a third experiment, ECCD in the UP/DOWN SHIFTED REGIME was investigated by making use of a peculiarity of the magnetic field configuration of W 7-AS, i.e. wave launching at a poloidal plane with an almost vanishing magnetic field gradient. Under such conditions, a sufficiently high single pass absorption is obtained even at moderate electron temperatures of about 2 keV. Here one microwave beam (0.2 MW) is launched at a fixed angle of 11° with respect to perpendicular incidence. A magnetic field variation from 2.4 up to 2.6 T shifts the EC-resonance completely out of the confinement region in this poloidal plane as seen in Fig. 2(a). The target plasma is maintained by 0.7 MW at perpendicular launch (no ECCD) in

a poloidal plane with a strong tokamak-like magnetic field gradient, where the EC-resonance layer remains well within the confinement region for the given magnetic field variation. The calculated spatial current density distribution is given in Fig. 2(b) for the three cases of B_o = 2.4 T (up-shifted), 2.5 T (resonant), and 2.6 T (down-shifted). For the resonant case (Fig. 2(b), middle) an almost zero net current is found because the vanishing magnetic field gradient and the corresponding broad power deposition profile create counterstreaming currents on both the low and the high field sides of the resonance layer. The current inverses the sign while varying the magnetic field from an upshifted scenario (Fig. 2, top) to a downshifted scenario (Fig. 2, bottom). The measured loop voltage increment required to balance the EC-driven current is given in Fig. 3(a) for the full magnetic field scan. The change of the sign as well as the transition through zero loop voltage increment at the resonant magnetic field is in agreement with theory as shown in Fig. 3(b), where the EC-driven current is normalized to the launched microwave power. We assume, however, that only the first transit absorption, which is given in Fig. 4(a) as a funtion of the magnetic induction, contributes to current drive. The relevant EC-current drive efficiency is then obtained by normalizing the total current to the power absorbed in a single pass, which is shown in Fig.4(b). In all calculations trapped particle effects are taken into account. An improved current drive efficiency as compared to the two experiments mentioned first is clearly deduced.

4. CONCLUSIONS

Fundamental experiments on wave absorption and ECCD were performed in the W 7-AS stellarator. The single pass absorption of the microwaves was measured at perpendicular launch for 1st harmonic O-mode and 2nd harmonic O- and X-mode launch respectively. An excellent agreement with ray tracing calculations was found. The parameter dependence of ECCD on the launch angle of the incident waves, the electron temperature, the electron density and the microwave power was investigated for both 1st harmonic O-mode and 2nd harmonic X-mode operation. Perturbation experiments at up-/down-shifted resonance for first harmonic ECCD were performed by shifting the resonance layer across the confining region of the plasma. The experiments are in good agreement with a linear theoretical model and Fokker-Planck calcuations if trapped particles are taken into account.

REFERENCES

[1] H. Renner et al., Initial Operation of the WENDELSTIEN 7-AS Advanced Stellarator, Plasma Physics and Contr. Fusion, 31, (1989), 1579-1596

[2] U. Gasparino et al., Sources of Toroidal Current in the WENDELSTEIN 7-AS Stellarator, Proc. 16th Europ. Conf. on Plasma Physics and Contr. Fusion, Venice, Italy, Vol. II, 631

[3] U. Gasparino et al., Non inductive current in W 7-AS, 17th EPS Conf. on Contr. Fusion and Plasma Heating, Vol. 14B, III, p. 1275, Amsterdam, The Netherlands, 1990

[4] M. Taguchi, ECRH Current Drive in Tokamak Plasmas, Plasma Physics and Contr. Fusion 31 (1989), 241

[5] V. Erckmann et al., Electron Cyclotron Resonance Heating transmission line and launching system for the W 7-AS stellarator, Fusion Technology, Vol. 17, (1990), 76

[6] V. Erckmann et al., Current Drive experiments at the Electron Cyclotron Frequency, 17th EPS Conf. on Contr. Fusion and Plasma Heating, Vol. 14B, III, p. 1271, Amsterdam, The Netherlands, 1990

[7] H. Ringler et al., Confinement Studies on the WENDELSTEIN 7-AS Stellarator, 17th EPS Conf. on Contr. Fusion and Plasma Heating, Amsterdam, The Netherlands, 1990

[8] S.P. Hirshman, Classical collisional theory of beam-driven plasma currents, Phys. Fluids 23 (1980), 1238

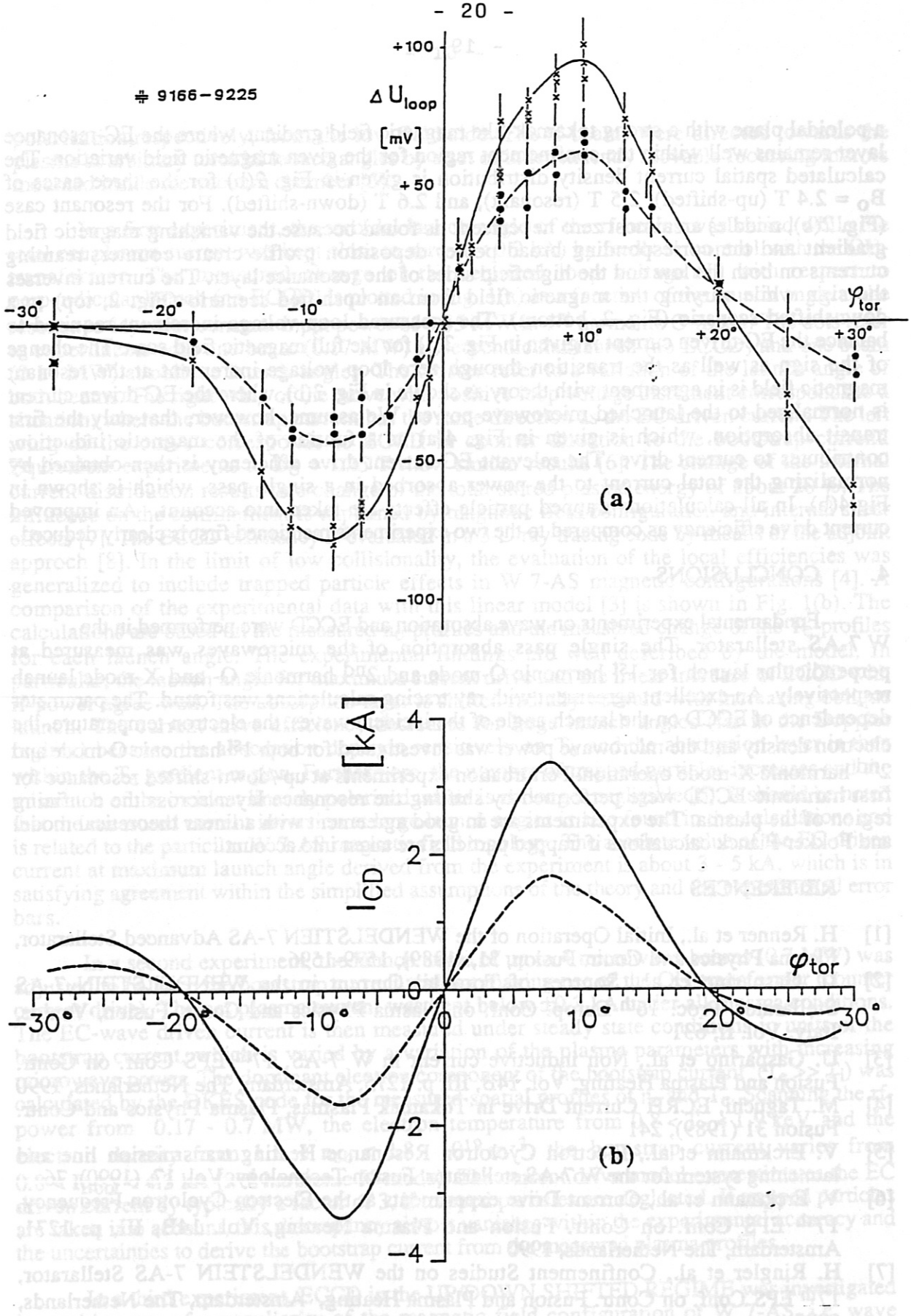

Fig. 1(a) Loop voltage increment ΔU as a function of the launch angle for 0.17 MW (dots) and 0.35 MW (crosses) ECCD power. The EC-driven current is balanced by inductive curent drive (OH-transformer feedback). The total input power for both cases is 0.35 MW.

(b) EC-Current Drive Modelling based on the measured n_e- and T_e-profiles for the same discharges at 0.17 MW (dashed curve) and 0.35 MW (solid curve).

(a) (b)

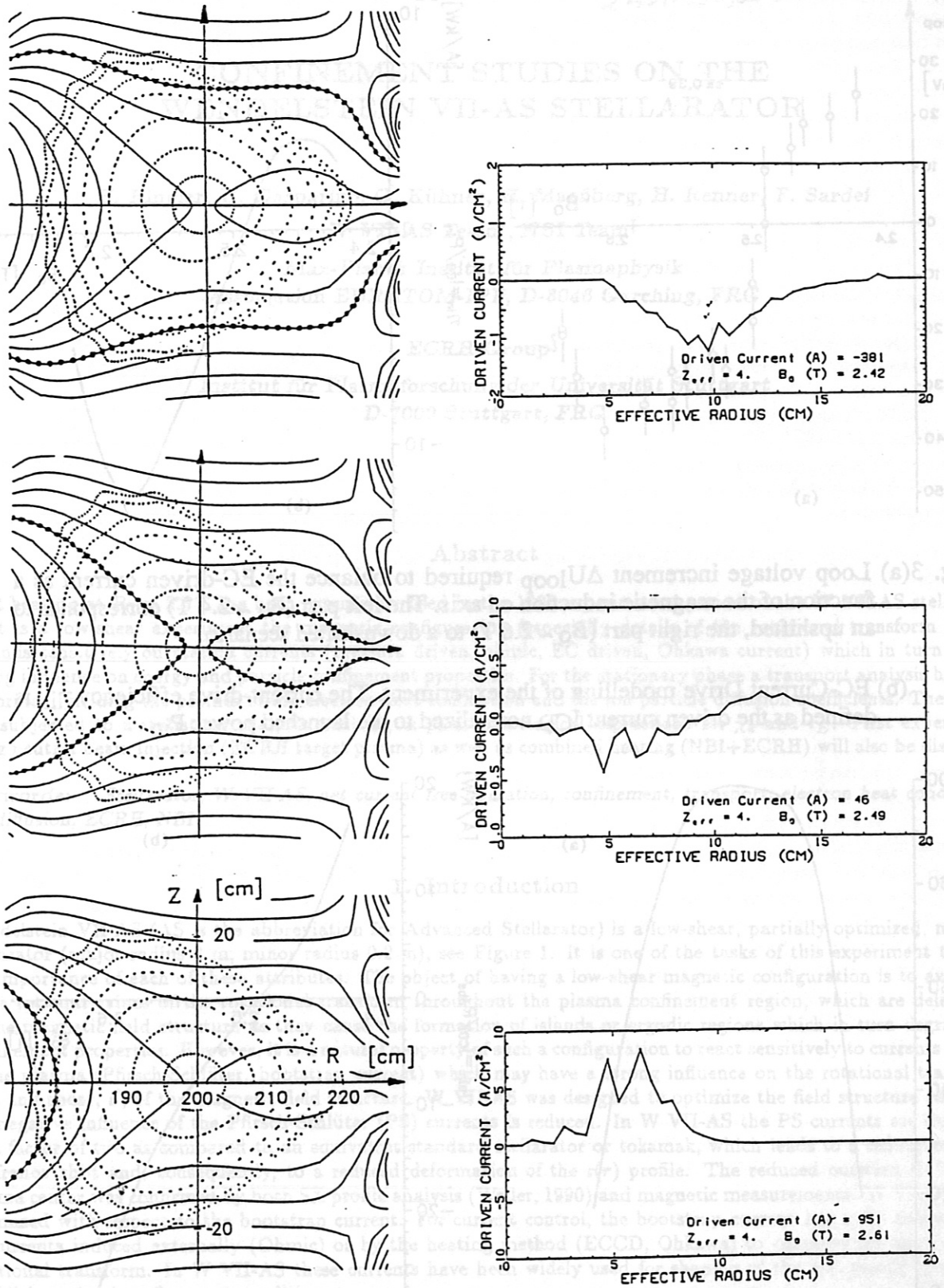

Fig. 2(a) Position of the resonance layer (dotted line) in a poloidal cross-section with small magnetic field gradient at Bo = 2.4 T (top), Bo = 2.5 T (middle) and Bo = 2.6 T (bottom). The solid lines indicate /B/ = const. contours, the dashed lines give the nested flux surfaces.

(b) EC driven current distribution from 3-D ray tracing calculations for 0.1 MW microwave power at the upshifted resonance (top), the resonant case (middle), and for the downshifted case (bottom).

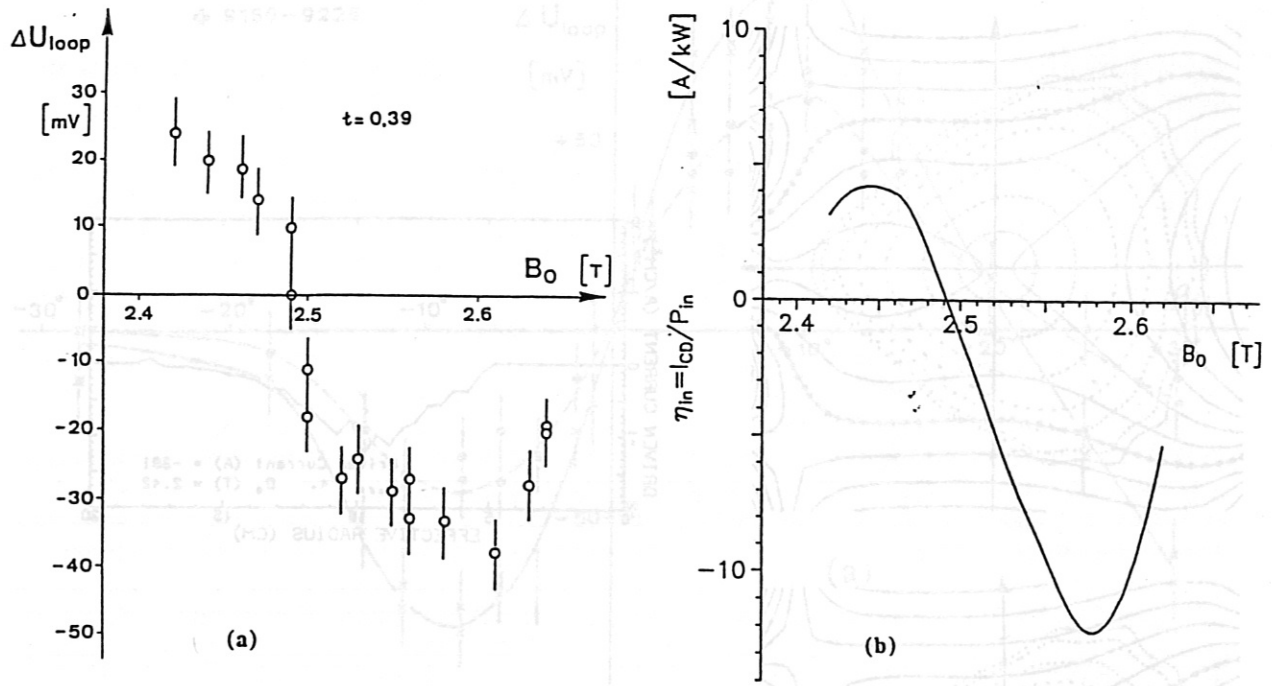

Fig. 3(a) Loop voltage increment ΔU_{loop} required to balance the EC-driven current as a function of the magnetic induction on axis. The left part ($B_0 \sim 2.4$ T) corresponds to an upshifted, the right part ($B_0 \sim 2.6$ T) to a downshifted scenario.

(b) EC-Current Drive modelling of the experiment. The current-drive efficiency η_{in} is defined as the driven current I_{CD} normalized to the launched power P_{in}

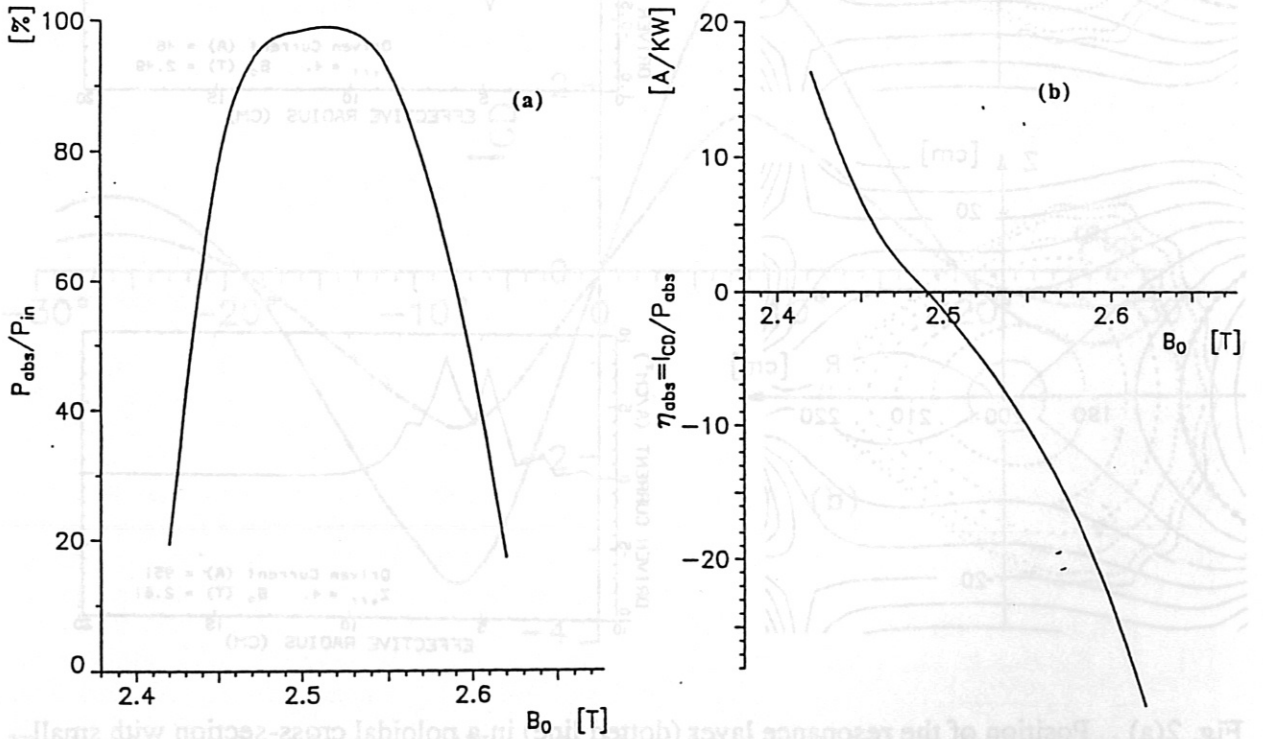

Fig. 4(a) The single pass absorption P_{abs} normalized to the launched power P_{in} from ray tracing calculation for the same discharges.

(b) EC-Current Drive efficiency η_{abs}, with the driven current I_{CD} normalized to the single pass absorption P_{abs} for the same discharges.

CONFINEMENT STUDIES ON THE WENDELSTEIN VII-AS STELLARATOR

H. Ringler, U. Gasparino, G. Kühner, H. Maaßberg, H. Renner, F. Sardei
W VII-AS Team, NBI Team†*
Max-Planck Institut für Plasmaphysik
Association EURATOM-IPP, D-8046 Garching, FRG

ECRH-Group§
Institut für Plasmaforschung der Universität Stuttgart
D-7000 Stuttgart, FRG

Abstract

ECR heating at $B_0 = 2.5T$ has been extensively used in the 1990 experimental period of the W VII-AS stellarator. As it is a low-shear experiment the magnetic configuration (especially details of the rotational transform profile) depends sensitively on plasma currents (pressure driven, ohmic, EC driven, Ohkawa current) which in turn have a strong influence on energy and particle confinement properties. For the stationary phase a transport analysis has been performed, yielding the profiles of the electron heat conduction and the ion particle diffusion coefficients. The former was subjected to a statistical analysis resulting in phenomenological expressions for χ_e and τ_E. First experiments using neutral beam injection (ECRH target plasma) as well as combined heating (NBI+ECRH) will also be discussed.

Keywords: *Stellarator, W VII-AS, net current free operation, confinement, transport, electron heat conduction, ion diffusion, ECRH, NBI*

1. Introduction

Wendelstein VII-AS (AS is the abbreviation for Advanced Stellarator) is a low-shear, partially optimized, modular stellarator (major radius 2 m, minor radius 0.2 m), see Figure 1. It is one of the tasks of this experiment to show the importance of each of these attributes. The object of having a low-shear magnetic configuration is to avoid low order rational values of the rotational transform throughout the plasma confinement region, which are deleterious to the magnetic field structure as they cause the formation of islands or ergodic regions which in turn degrade the confinement properties. However, it is a natural property of such a configuration to react sensitively to currents flowing in the plasma (Pfirsch-Schlüter, bootstrap current) which may have a strong influence on the rotational transform, $\iota(r)$, and shear, ι', of the magnetic field structure. W VII-AS was designed to optimize the field structure such that the negative influence of the Pfirsch-Schlüter (PS) currents is reduced. In W VII-AS the PS currents are decreased by a factor of two as compared to an equivalent standard stellarator or tokamak, which leads to a reduction of the Shafranov shift and, consequently, to a reduced deformation of the $\iota(r)$ profile. The reduced outward shift of the plasma center was confirmed by both SX profile analysis (Weller, 1990) and magnetic measurements. W VII-AS is not optimized with respect to the bootstrap current. For current control, the bootstrap current has to be compensated by currents induced externally (Ohmic) or by the heating method (ECCD, Ohkawa) to conserve the edge value of rotational transform. In W VII-AS these currents have been widely used for shaping of the $\iota(r)$ profile in order to establish optimal confinement conditions.

---

*N. Beredin[1)], R. Brakel, R. Burhenn, G. Cattanei, A. Dodhy, D. Dorst, A. Elsner, K. Engelhardt V. Erckmann, U. Gasparino, S. Geißler, G. Grieger, P. Grigull, U. Gutarev[1)], H. Hacker, H.J. Hartfuß, R. Jaenicke, S. Jiang[2)], J. Junker, M. Kick, H. Kroiss, G. Kühner, I. Lakicevic, A. Lazaros, M. Liniers[3)], H. Maaßberg, C. Mahn, W. Ohlendorf, M.A. Ochando[3)], H. Renner, H. Ringler, J. Saffert, F. Sardei, M. Tutter, A. Weller, E. Würsching, M. Zippe, S. Zöpfel, H. Zushi[4)]
guests from: [1)] Institute of Physics and Technology, Kharkov; [2)] Southwestern Institute of Physics, Leshan (China); [3)] CIEMAT, Madrid; [4)] Kyoto University, Japan

†F.P. Penningsfeld, W. Ott, E. Speth

§W. Kasparek, G.A. Müller, P.G. Schüller, M. Thumm, R. Wienecke

Furthermore, the reduced PS currents also give rise to a reduction of the neoclassical transport in both the plateau and the PS diffusion regime. As the electron heat and particle transport are strongly enhanced in these diffusion regimes (anomalous transport), this consequence of PS current reduction can hardly be checked in the experiment. The neoclassical transport properties in the long mean free path (LMFP) regime are determined by particles being trapped in local magnetic mirrors. In W VII-AS the neoclassical loss in the LMFP regime is dominated by particles being trapped in the regions with strong curvature (see Figure 1). The trapped particle drift orbits in the straight parts of the configuration, however, are rather close to the magnetic flux surfaces. Electron heat conduction, ion and impurity diffusion have been analyzed in a wide parameter range. Furthermore, a database has been accumulated to perform a statistical analysis of local χ_e which is very useful to find the leading parameter dependences as well as to compare present stellarator (W VII-AS, ATF, CHS, Heliotron-E) and tokamak experiments of quite different size.

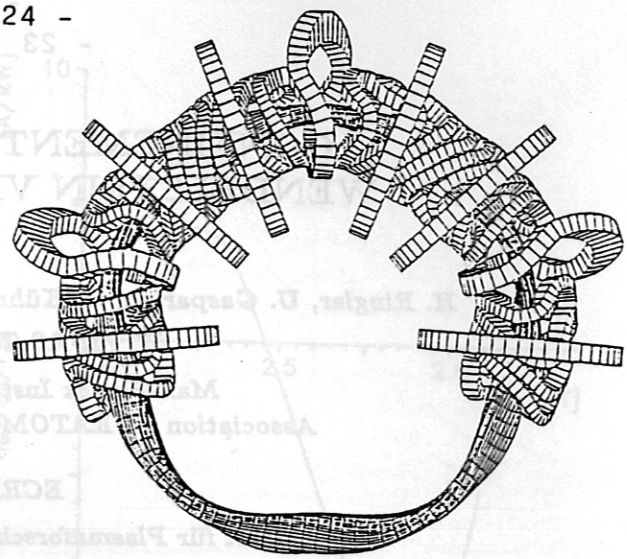

Figure 1 *Schematic view of the coil system and the plasma column of W VII-AS: the magnetic field structure is realized by 45 non-planar modular field coils and 10 planar toroidal field coils.*

An optimized configuration requires the engineering of a modular coil system which is a flexible tool for the appropriate realization of the magnetic flux surface geometry. The W VII-AS system was successfully built and is now routinely operated at full field parameters (2.5 T) after additional support structures had been introduced to limit elastic deformations of one of the coil-types.

Characteristics of the magnetic field: The magnetic field is generated by a modular system of coils which has fivefold symmetry (Fig. 1). The field is composed of two components: The "module" field consists of nine nonplanar coils per field period generating a shear free magnetic field with a rotational transform of $\iota = 0.39$. By superposition of a toroidal field generated by an addional set of two planar coils per field period, the edge value of the rotational transform, $\iota(a)$, can be varied in the range of $0.2 < \iota(a) < 0.7$. The magnetic flux surfaces are toroidally asymmetric, but exhibit the so-called stellarator symmetry. Thus, there are two planes of symmetry which are of particular interest for the experiments: the cross section of the magnetic flux surfaces in the region of maximum curvature has nearly elliptical shape, and the strong field gradient in major radius allows local heating under electron and ion cyclotron resonance conditions. The cross section in the second plane of symmetry (straight part) is triangular, the field gradient is small and inverted, thus providing the possibility of ECR heating with high field launch from the outer side. As the magnetic field topology of the W VII-AS stellarator is complex, a rigorous mapping of real space coordinates to magnetic flux coordinates (Boozer, 1981) was implemented. The TRANS code provides this coordinate transformation for all relevant vacuum and equilibrium configurations stored in Fourier representation. They were obtained by using GOURDON and KW (Kisslinger, 1985) codes. Experimental data taken at different poloidal and toroidal positions, which are nearly constant on flux surfaces, are reduced to a common radial representation, the effective radius.

ECRH: Four 70 GHz cw-gyrotrons (P = 200 kW, Δt = 3 s) have been installed for ECRH. A sophisticated transmission line (Kasparek, 1988) enables one to generate a completely polarized, almost divergence free EC wave which penetrates the plasma quasioptically. The angle of incidence of the EC wave can be varied in two directions by a set of movable mirrors, thus providing the possibility varying the location of power deposition (off-axis heating) as well as of introducing $k_{||}$ components for EC current drive. ECCD has been clearly demonstrated by this technique (see left plot of Figure 5). Off-axis heating can also be achieved by tuning of the magnetic field. ECRH has be used in most of the present experiments and two scenarios have been extensively investigated: $B_0 = 1.25$ T with x-mode launch at 2nd harmonic at densities of $n_e < 3 \cdot 10^{13}$ cm^{-3} and $B_0 = 2.50$ T with o-mode launch at fundamental with densities of $n_e < 6 \cdot 10^{13}$ cm^{-3}. Maximum temperatures of $T_e = 2.8$ keV and $T_i = 0.4$ keV and plasma energies up to 8 kJ have been obtained.

NBI: Two long-pulse beam lines have been installed on W VII-AS, injecting neutral particles (H°: E = 45 keV, Δt = 3 s) tangentially into the plasma. By co- and counter injection the Ohkawa current can be compensated. Maximum heating power is about 1.5 MW (Feist 1984). Starting from an initially ECR produced target plasma, NBI heats a plasma at densities well above the cut-off density for ECRH. Maximum temperatures of $T_e \simeq T_i = 0.7$ keV, maximum densities $n_e \leq 10^{14}$ cm^{-3} and plasma energies up to 15 kJ have been achieved.

ICRH: The power supply which was installed for ICRH provides $P_{ICF} \leq 1.5$ MW RF-power in the frequency range of 30 to 110 MHz for a time duration of $\Delta t \leq 0.5$ s. A flexible experimental antenna system is installed in W VII-AS. It consists of two classical loops with Faraday shield which allow a variation of the k-spectrum (Wesner 1988). So far, ICRH has been used only for testing purposes.

OH current control: In addition the OH-transformer of W VII-A is still available. It is used to induce small currents, $I_p < 5$ kA, or to compensate currents occurring due to the plasma pressure (bootstrap) as well as to the heating method (ECCD, Ohkawa current) by applying small loop voltages, $U_{loop} \leq 0.5$ V.

2. Configurational Effects

2.1. Rotational Transform at Plasma Edge

As was the case for the W VII-A stellarator (Wobig, 1987), the global confinement in W VII-AS depends strongly on the value of the boundary rotational transform, $\iota(a)$ (Renner, 1989). A degradation of both energy and particle confinement is found for low order rational values of the rotational transform at the plasma edge, $\iota(a)$, whereas optimum confinement can be established close to the resonances $\iota(a) \simeq 1/3$ as well as $\iota(a) \simeq 1/2$.

The W VII-AS magnetic field vacuum configuration is shearless at $\iota(a) = 0.39$. The vacuum rotational transform can be increased (decreased), introducing a very small positive (negative) shear. These vacuum configurations are modified by plasma currents: the PS current and the neoclassical bootstrap current generated by plasma pressure, currents driven by the heating method (ECCD and Ohkawa currents during NBI) or externally by the OH-transformer. For the ECRH discharges with moderate or low densities and high temperatures, the pressure effect on the ι profile is dominated by the bootstrap current, however, the PS contribution cannot be neglected in general. The bootstrap current always increases the rotational transform in W VII-AS and is localized in the T_e gradient region. The shear contribution is positive in the center and negative in the outer confinement region. Currents driven by the external loop voltage or by the heating method can be used to control $\iota(a)$ as well as the internal shear, thus current density control opens up a variety of scenarios for optimization of confinement.

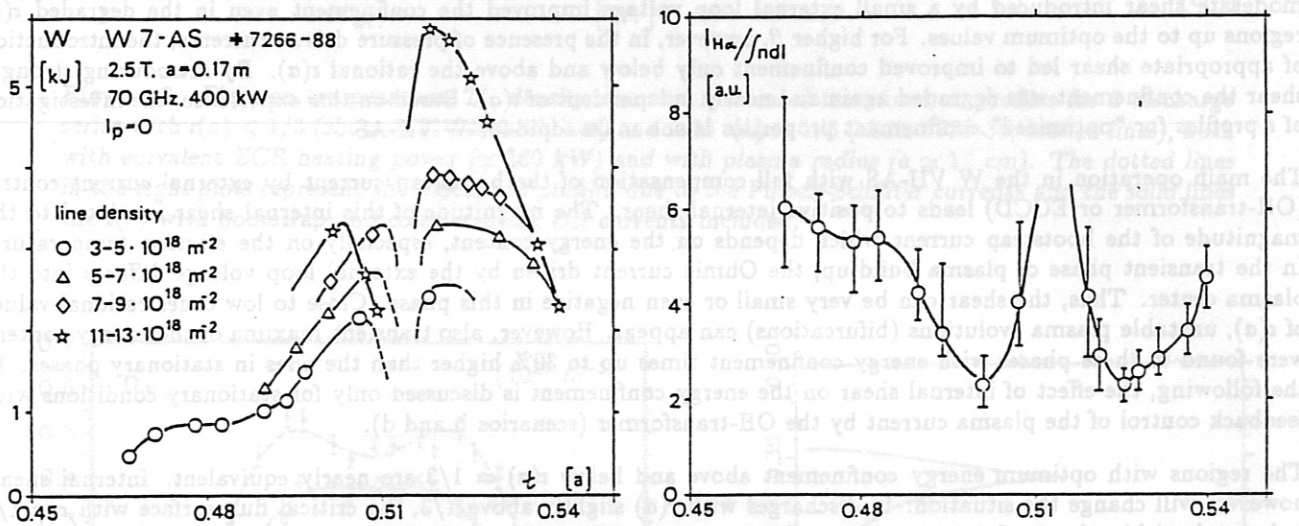

Figure 2 *Total energy, W (left plot), and normalized H_α intensity, $H_\alpha/\int ndl \propto \tau_p^{-1}$ (right plot), versus the edge value of rotational transform, $\iota(a)$. Note that there is an uncertainty in the experimental estimation of $\iota(a)$ of about 0.01.*

The global confinement properties depend sensitively on the rotational transform at the plasma edge. Figure 2 shows plasma energy, W, and the normalized H_α intensity as a measure of the inverse particle confinement time versus $\iota(a)$ in the vicinity of $\iota = 1/2$. Here, the vacuum value of $\iota(a)$ was changed shot by shot and the bootstrap current was balanced by the OH-transformer (net current-free discharges). A strong degradation of confinement is obvious at $\iota \approx 1/2$, the ι ranges for optimum confinement being very small, $\Delta\iota(a) \leq 0.01$. Above and below these two maxima, the natural islands with $\iota = 5/11$ and $\iota = 5/9$, respectively, enter the confinement region. These islands were directly observed in the vacuum magnetic field configuration (Renner, 1989). Typically, the internal contribution of the bootstrap current is much larger than the $\Delta\iota(a)$ windows for optimum confinement. Consequently, the total plasma current has to be controlled to avoid low order rational values of ι or to keep $\iota(a)$ within the range of optimum confinement. The line integrated electron density is given as a parameter in Figure 2 showing that both the energy content, W, and the energy confinement time, τ_E, increase with density for fixed heating power.

The intrinsic source for internal shear is the bootstrap current density with a maximum in the temperature gradient region and which develops as soon as the plasma pressure is built up. Typically, the other current contributions have different radial distributions. Current diffusion on the L/R time scale determines the time to reach stationary conditions. In order to analyze the confinement properties and to control the net plasma current as well as $\iota(a)$, 5 scenarios have been successfully used in W VII-AS :

a) No external loop voltage is applied: the total plasma current is driven by the bootstrap current and damped by an internal loop voltage (self-induction) on the L/R time scale. In this transient phase with a duration of up to 1 s,

the confinement properties were significantly affected by the ι profile developing with the bootstrap current, which itself depends on the confinement properties. Under stationary conditions, the shear changes sign with radius. For this scenario, a rather careful plasma operation was required, depending on the vacuum value of $\iota(a)$, and only in a few cases good confinement was obtained.

b) OH feedback: the bootstrap current was fully balanced by applying a small loop voltage, U_l, by feedback control of the OH-transformer. In the stationary phase, the Ohmic current density profile corresponds to the electrical conductivity which is concentrated in the central plasma region for the peaked T_e profiles whereas the bootstrap current is driven in the T_e gradient region. In this scenario (the one most commonly followed) $\iota(a)$ is fixed and positive shear is generated in the confinement region.

c) Electron cyclotron current drive: ECCD with a suitable $k_{||}$ spectrum (Gasparino, 1989) was used to compensate the bootstrap current completely. The current density profile driven by the ECRH is highly peaked, similarly to the power deposition profile. For central ECF power deposition, the ι profile with positive shear is comparable with the scenario of Ohmic current control. ECCD, however, offers the chance to control the rotational transform profile by adjusting the ECRH driven current density profile (partly off-axis power deposition, $k_{||}$ shaping). Only in this scenario can one generate a nearly shearless configuration with high plasma pressure.

d) The scenarios b) and c) are combined: by co- and counter ECCD with respect to the bootstrap current, both positive and negative internal shear can be generated depending on the $k_{||}$ spectrum (see Fig. 5).

e) Ohkawa currents: during NBI with co- and counter-injection, net current free discharges compensating the bootstrap current could be maintained by a corresponding mismatch of the Ohkawa currents.

2.2. Effect of Internal Shear

The effect of internal shear on the confinement had been analyzed in the predecessor W VII-A stellarator (Grieger, 1986 and Renner, 1986) which was also nearly shearless. For very low β with negligible pressure driven currents, moderate shear introduced by a small external loop voltage improved the confinement even in the degraded $\iota(a)$ regions up to the optimum values. For higher β, however, in the presence of pressure driven currents, the introduction of appropriate shear led to improved confinement only below and above the rational $\iota(a)$. By introducing stronger shear the confinement was degraded again and nearly independent of $\iota(a)$. Based on this experience, the investigation of ι profiles for "optimized" confinement properties is one main topic for W VII-AS .

The main operation in the W VII-AS with full compensation of the bootstrap current by external current control (OH-transformer or ECCD) leads to positive internal shear. The magnitude of this internal shear is related to the magnitude of the bootstrap current which depends on the energy content, especially on the electron temperature. In the transient phase of plasma build-up, the Ohmic current driven by the external loop voltage diffuses into the plasma center. Thus, the shear can be very small or even negative in this phase. Close to low order rational values of $\iota(a)$, unstable plasma evolutions (bifurcations) can appear. However, also transient maxima of the energy content were found in these phases with energy confinement times up to 30% higher than the ones in stationary phases. In the following, the effect of internal shear on the energy confinement is discussed only for stationary conditions with feedback control of the plasma current by the OH-transformer (scenarios b and d).

The regions with optimum energy confinement above and below $\iota(a) = 1/3$ are nearly equivalent. Internal shear, however, will change the situation: in discharges with $\iota(a)$ slightly above 1/3, the critical flux surface with $\iota = 1/3$ is located within the confinement region. For measured temperature and density profiles, the bootstrap current density and the electric conductivity are calculated (see Chap. 3.1.) and the internal ι profile is estimated. In these calculations, the currents are not completely balanced. These model calculations are based on Z_{eff} assumed to be constant in radius, the ion bootstrap contribution depending on the assumed T_i profile. For all ι profiles shown here the contribution of these residual currents was compensated. With sufficient internal shear depending on heating power and limiter radius, nearly identical discharges could be established above and below $\iota(a) = 1/3$, which means that the effect of island formation and ergodization at $\iota = 1/3$ could be suppressed by the internal shear. For lower heating power and small plasma radius ($a \simeq 12$ cm) in Figure 3, discharges with $\iota(a) > 1/3$ had degraded confinement properties. Even a flattening in the T_e profile was measured, indicating the $\iota = 1/3$ flux surface (Shots 8719-35 in Fig. 3). However, no degraded confinement was found for corresponding discharges with $\iota(a) < 1/3$ (Shots 8571-94 with slightly lower density), χ_e in the gradient region being more than a factor of 2 smaller than in the degraded case.

The profiles shown in Figure 4 (together with shots 8719-35 in Fig. 3) are part of an ECR-heating power scan with $\iota(a) = 0.34$ and equivalent densities. In these discharges the smallest possible limiter aperture corresponding to $a \simeq 12$ cm was used. For low heating power level (180 kW, shots 8763-78), the internal currents are very small and the internal shear in the plateau region in the T_e profiles is only weakly positive. Here, the confinement is significantly reduced, indicating island formation. Note that there is an offset of the ι-scale which is within the range of the experimental accuracy. For the higher heating power level (450 kW, shots 8638-58), however, the bootstrap current and the compensating Ohmic current are much higher, leading to stronger positive shear, $\iota' \approx 0.3$ m^{-1} at about half plasma radius. This improves the confinement, the $\iota \approx 1/3$ region is shifted outside and no flattening in the T_e profile is observed. For the two heating power levels of Figure 4, the energy content changes by a factor of 4 as compared to the power ratio of 2.5. Equivalent discharges at $\iota(a)$ slightly above 1/2 with $a = 12$ cm and with low heating power levels show that sufficient internal shear for good confinement is generated. Here, the shear in the vacuum configuration is already weakly positive which is contrary to the situation at $\iota \approx 1/3$. The scan of ECR heating power at $\iota \approx 1/3$ demonstrates a nonlinear mechanism of "self-stabilization" of the internal shear: both the

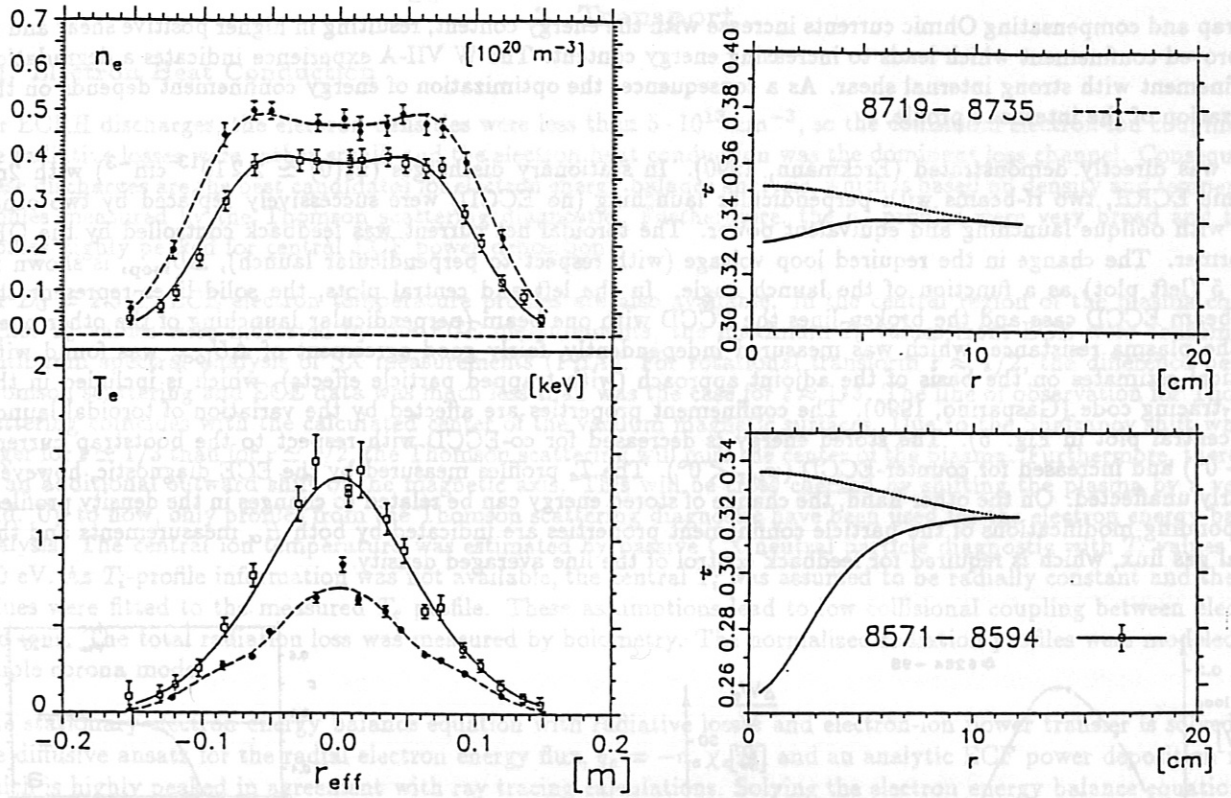

Figure 3 *Electron temperature, T_e, density, n_e, and rotational transform, ι, profiles for 2 discharge series with $\iota(a) < 1/3$ (shots 8571-94, solid lines) and with $\iota(a) > 1/3$ (shots 8719-35, broken lines), both with eqivalent ECR heating power ($\simeq$ 360 kW) and with plasma radius ($a \simeq 12$ cm). The dotted lines in the right plots represent the modified ι profiles due to the Pfirsch-Schlüter currents and the solid lines the $\iota(r)$ with bootstrap and compensating OH currents included.*

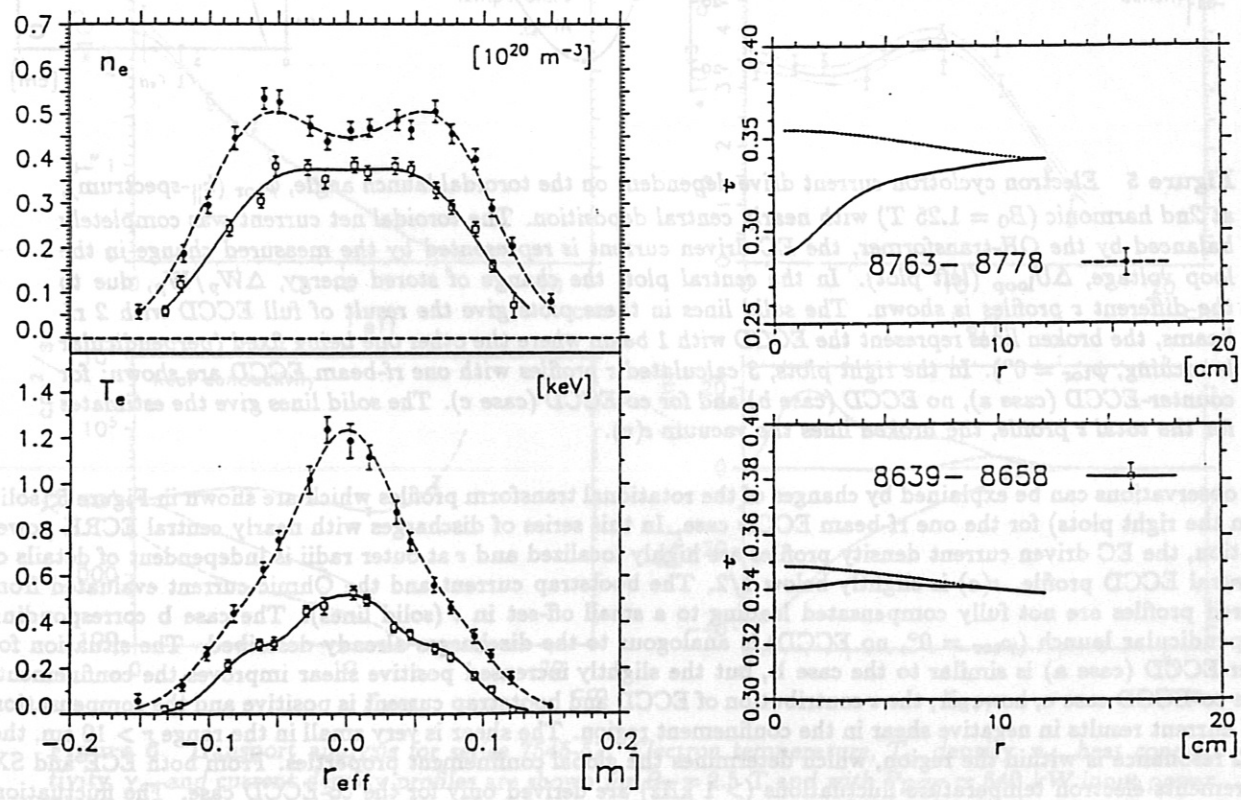

Figure 4 *Electron temperature, T_e, density, n_e, and rotational transform, ι, profiles for 2 discharge series with $P_{ECF} \simeq 180$ kW (shots 8763-78, solid lines) and with $P_{ECF} \simeq 470$ kW (shots 8739-58, broken lines), both with $\iota(a) > 1/3$ ($\simeq 0.34$) and with plasma radius ($a \simeq 12$ cm); compare Fig. 3.*

bootstrap and compensating Ohmic currents increase with the energy content, resulting in higher positive shear and in an improved confinement which leads to increasing energy content. The W VII-A experience indicates a degradation of confinement with strong internal shear. As a consequence, the optimization of energy confinement depends on the optimization of the internal ι profile.

ECCD was directly demonstrated (Erckmann, 1990). In stationary discharges ($n_e(0) \simeq 2.2\,10^{13}$ cm^{-3}) with 2nd harmonic ECRH, two rf-beams with perpendicular launching (no ECCD) were successively replaced by two other beams with oblique launching and equivalent power. The toroidal net current was feedback controlled by the OH-transformer. The change in the required loop voltage (with respect to perpendicular launch), $\Delta U_{\rm loop}$, is shown in Figure 5 (left plot) as a function of the launch angle. In the left and central plots, the solid lines represent the two rf-beam ECCD case and the broken lines the ECCD with one beam (perpendicular launching of the other one). With the plasma resistance, which was measured independently, fairly good agreement of $\Delta U_{\rm loop}$ was found with theoretical estimates on the basis of the adjoint approach (with trapped particle effects), which is included in the 3D ray-tracing code (Gasparino, 1990). The confinement properties are affected by the variation of toroidal launch angle (central plot in Fig. 5). The stored energy is decreased for co-ECCD with respect to the bootstrap current ($\varphi_{\rm tor} > 0°$) and increased for counter-ECCD ($\varphi_{\rm tor} < 0°$). The T_e profiles measured by the ECE diagnostic, however, are nearly unaffected. On the other hand, the change of stored energy can be related to changes in the density profiles. Corresponding modifications of the particle confinement properties are indicated by both H_α measurements and the external gas flux, which is required for feedback control of the line averaged density.

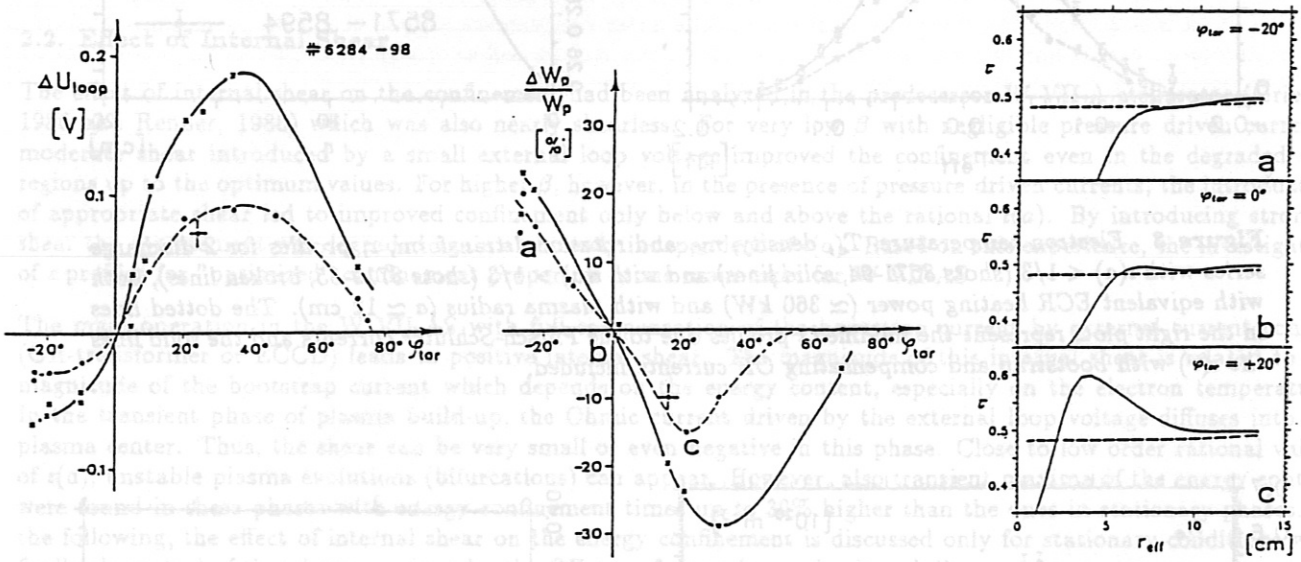

Figure 5 *Electron cyclotron current drive dependent on the toroidal launch angle, $\varphi_{\rm tor}$ ($k_\parallel$-spectrum), at 2nd harmonic ($B_0 = 1.25$ T) with nearly central deposition. The toroidal net current was completely balanced by the OH-transformer, the EC driven current is represented by the measured change in the loop voltage, $\Delta U_{\rm loop}$ (left plot). In the central plot, the change of stored energy, $\Delta W_p/W_p$, due to the different ι profiles is shown. The solid lines in these plots give the result of full ECCD with 2 rf-beams, the broken lines represent the ECCD with 1 beam where the other one being fixed (perpendicular launching, $\varphi_{\rm tor} = 0°$). In the right plots, 3 calculated ι profiles with one rf-beam ECCD are shown: for counter-ECCD (case a), no ECCD (case b) and for co-ECCD (case c). The solid lines give the estimates for the total ι profile, the broken lines the vacuum $\iota(r)$.*

These observations can be explained by changes of the rotational transform profiles which are shown in Figure 5 (solid lines in the right plots) for the one rf-beam ECCD case. In this series of discharges with nearly central ECRH power deposition, the EC driven current density profiles are highly localized and ι at outer radii is independent of details of the central ECCD profile. $\iota(a)$ is slightly below 1/2. The bootstrap current and the Ohmic current evaluated from measured profiles are not fully compensated leading to a small off-set in ι (solid lines). The case b corresponding to perpendicular launch ($\varphi_{\rm tor} = 0°$, no ECCD) is analogous to the discharges already described. The situation for counter-ECCD (case a) is similar to the case b, but the slightly increased positive shear improves the confinement. For the co-ECCD case c, however, the ι contribution of ECCD and bootstrap current is positive and the compensation by OH current results in negative shear in the confinement region. The shear is very small in the range $r > 10$ cm, the $\iota = 1/2$ resonance is within the region, which determines the global confinement properties. From both ECE and SX measurements electron temperature fluctuations (> 1 kHz) are derived only for the co-ECCD case. The fluctuation amplitudes are maximum at about 8 cm indicating the $\iota = 1/2$ resonance in agreement with the calculated ι profile (note the small off-set). In the corresponding 2 gyrotron co-ECCD case, the resonance is shifted outside (maximum of fluctuations at about 10 cm) and low frequency components (< 100 Hz) with broader radial resolution appear in the fluctuation spectrum. Furthermore, for both ECCD scenarios, equivalent fluctuation spectra are found in the H_α measurements at the limiters.

3. Transport

3.1. Electron Heat Conduction

For ECRH discharges, the electron densities were less than $5 \cdot 10^{13}$ cm^{-3}, so the collisional electron-ion coupling and the radiative losses were rather small, and the electron heat conduction was the dominant loss channel. Consequently, these discharges are the best candidates for electron energy balance analysis, which is based on density and temperature profiles measured by the Thomson scattering diagnostic. Furthermore, the n_e profiles were very broad and the T_e profiles highly peaked for central ECF power deposition.

For $B_0 = 2.5$ T, ECE electron temperature profiles are also available. In the central region of the plasma column, higher T_e values were indicated by the ECE measurements, the maximum T_e values from ECE were confirmed by continuum spectral analysis of SX measurements (PHA). For rotational transform $\iota \approx 1/2$, the difference between Thomson scattering and ECE data was much less than was the case for $\iota \approx 1/3$. The line of observation for Thomson scattering coincides with the calculated center of the vacuum magnetic surfaces. Due to the Shafranov shift which is larger for $\iota \simeq 1/3$ than for $\iota \simeq 1/2$, the Thomson scattering will miss the center of the plasma. Furthermore, there may be an additional outward shift of the magnetic axis. This will be cross checked by shifting the plasma by a vertical field. Up to now, only profiles from the Thomson scattering diagnostic have been used for the electron energy balance analysis. The central ion temperature was estimated by passive CX neutral particle diagnostic with T_i values up to 450 eV. As T_i-profile information was not available, the central T_i was assumed to be radially constant and the edge values were fitted to the measured T_e profile. These assumptions lead to low collisional coupling between electrons and ions. The total radiation loss was measured by bolometry. The normalized radiation profiles were modeled by a simple corona model.

The stationary electron energy balance equation with radiative losses and electron-ion power transfer is solved with the diffusive ansatz for the radial electron energy flux, $q_e = -n_e \chi_e T_e'$, and an analytic ECF power deposition model which is highly peaked in agreement with ray tracing calculations. Solving the electron energy balance equation, the measured T_e profiles are fitted by a least-squares technique using a power series of $log(\chi_e)$ in normalized radius, the power series coefficients being the fit parameters. This integration method of the electron energy balance equations leads to a smoothed representation of the electron heat conductivity, $\chi_e(r)$. For the n_e profiles, a standard fit function is used. With these T_e and n_e profiles, all neoclassical transport properties are estimated using the DKES-2 code (W.I. van Rij and S.P. Hirshman, 1989). The DKES code solves the monoenergetic drift kinetic equation for general magnetic field topology. Note that the W VII-AS field topology is quite different to that of standard stellarators. Energy convolution yields the full neoclassical transport matrix.

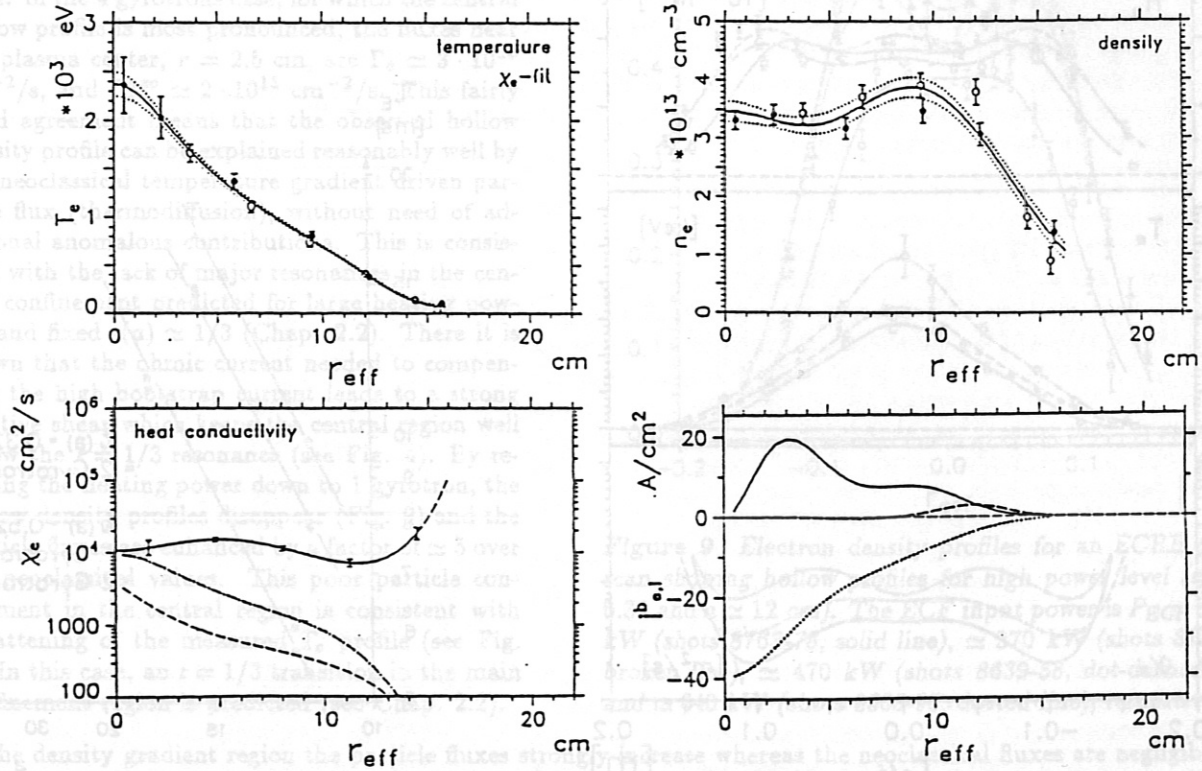

Figure 6 *Transport analysis for series 7545-57. Electron temperature, T_e, density, n_e, heat conductivity, χ_e, and current density profiles are shown for $B_0 = 2.5$ T and with $P_{ECF} \simeq 640$ kW input power. In the experimental χ_e (lower left plot, solid line) standard errors resulting from the least-squares fit of the T_e profile (upper left plot) are given, additionally, the χ_e from the DKES code (dot-dashed line) and from the Hinton-Hazeltine model (dashed line) are shown. The bootstrap current, see the profiles of j_{be} (solid line) and of j_{bi} (broken line) in the lower right plot, is compensated by an external loop voltage, see j_{OH} (dotted line).*

In Figure 6, the electron temperature, density, heat conductivity and current density profiles are shown for one of the high pressure ECRH discharges at $B_0 = 2.5$ T with 640 kW ECF input power (4 gyrotrons operating). The bootstrap current was compensated by an external loop voltage. The central β was about 0.5%. For this series of discharges with $\iota(a) \simeq 0.52$, the central T_e from ECE measurements was nearly 2.7 keV (2.4 keV from Thomson scattering). The T_e profile is highly peaked due to central ECF power deposition. For these high temperatures, the bulk part of the plasma is in the long mean free path regime (LMFP), the neoclassical transport being dominated by ripple losses. The neoclassical χ_e estimated by DKES code (dot-dashed line in Fig. 6) exceeds significantly the axisymmetric contribution (dashed line). Only in the innermost part does the neoclassical χ_e approach the experimental value. The error bars of the experimental χ_e-curve represent the standard errors of the fit given by the functional variance. Close to the effective limiter radius of 15.5 cm, the T_e profile becomes flat and the experimental χ_e increases strongly. Due to uncertainties in the outer T_e data, however, χ_e is reliable only up to 14.5 cm. In the major part of the plasma, χ_e is roughly constant (10^4 cm^2/s) and much larger than the neoclassical value. In the lower right plot, the internal current densities are shown: the electron and ion bootstrap current densities and the Ohmic current density, estimated using the measured loop voltage and the parallel electric conductivity, both current densities are estimated using the neoclassical DKES code. With an assumed value of $Z_{\text{eff}} = 4$, the total electron bootstrap current was calculated to be 4.1 kA (additionally, an ion contribution of up to 1 kA is expected) and the Ohmic current as -6.2 kA, the measured total plasma current being 0.2 kA. Typically, the agreement with the experimental data is not so good (Gasparino, 1990). This current distribution leads to a rather strong positive shear: $\Delta\iota = \iota(a) - \iota(0) \approx 0.2$, and the resonances $\iota = 1/2$ as well as $\iota = 5/11$ (natural islands in the vacuum configuration) are located within the confinement region (compare Chapter 2.1).

The series of discharges in Figure 6 is part of an ECRH power scan shown in Figure 7. In this scan, $\iota(a)$ was fixed at 0.52, the effective limiter radius was 15.5 cm and the central density was kept constant. Only for the lowest ECRH level (180 kW, solid lines in Fig. 7) was the half width of the n_e profile smaller. The T_e gradients (central plot) are only weakly dependent on heating power over the major part of the plasma column, the experimental electron heat conductivities, χ_e (lower plot) are significantly increased with heating power. The broader n_e profiles in Figure 7 at higher ECRH power levels (300 kW with 2 gyrotrons and 630 kW with 4 gyrotrons, dashed lines and dot-dashed lines, respectively) are related to a broader confinement regime with low χ_e in comparison to the discharges with low ECRH level. The χ_e profiles of this power scan with values much less than 1 m^2/s are some of the lowest values found in W VII-AS so far and of the order of the best χ_e values found in optimum Tokamak confinement.

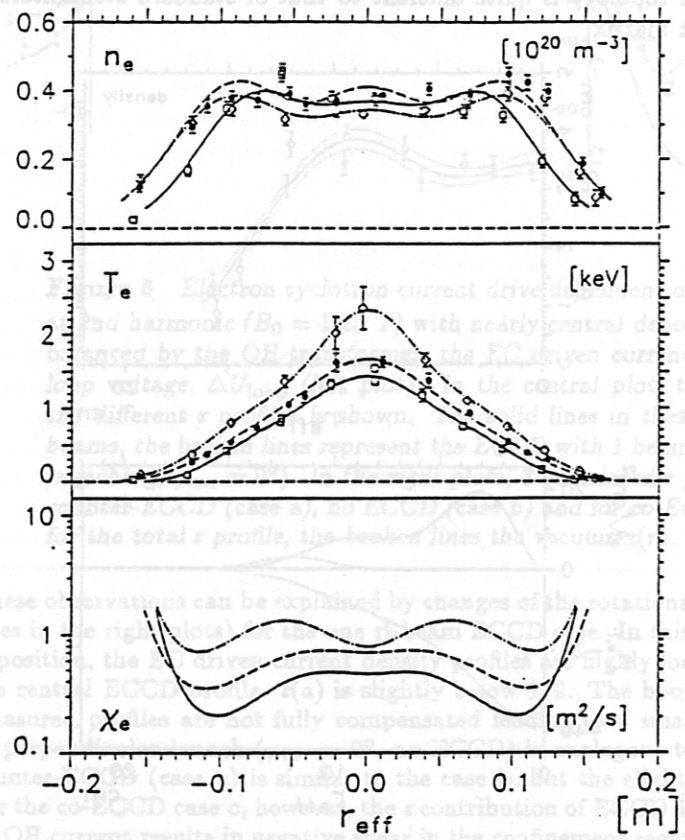

Figure 7 Profiles of electron temperature, T_e, density, n_e, heat conductivity, χ_e, for an ECRH power scan at $B_0 = 2.5$ T, with plasma radius $a \simeq 15.5$ cm and $\iota(a) > 1/2$ ($\simeq 0.52$). The input power is $P_{ECF} \simeq 200$ kW (shots 7159-72, solid lines), $\simeq 340$ kW (shots 7333-48, broken lines) and $\simeq 640$ kW (shots 7545-57, dot-dashed lines), respectively.

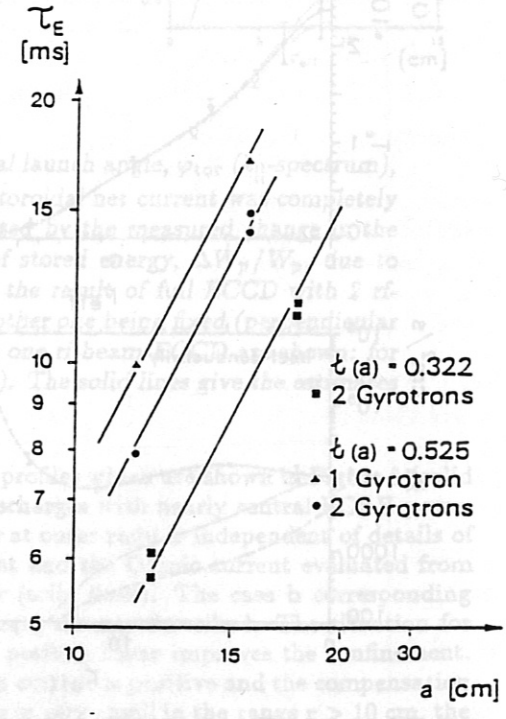

Figure 8 Energy confinemt time, τ_E, as function of limiter aperture (plasma radius a) for ECRH with 1 and 2 gyrotrons and with $\iota(a) \simeq 0.32$ and $\iota(a) \simeq 0.52$, respectively. The slope of the straight lines corresponds to an a^2-scaling.

The minimum in χ_e at about 2/3 plasma radius is typical for all discharges without degradation due to configurational effects. In the electron density gradient region, χ_e increases significantly (the n_e profiles are very broad). The electron temperature gradients of the discharges shown in Figure 7 are nearly constant versus radius. This behaviour is only found for discharges with optimum confinement (high n_e, full field). Here, $n_e \cdot \chi_e$ is roughly constant in the outer part of the plasma. For these discharges, an a^2 dependence of the global energy confinement time, τ_E, is found for fixed line averaged density, $\iota(a)$ and ECRH power, see Figure 8. This dependence can be directly explained from energy balance considerations, see Chapter 4. Figure 8 also shows that τ_E increases with $\iota(a)$ and decreases with ECRH power. For discharges without optimum confinement, however, the T_e-gradients decrease and $n_e \cdot \chi_e$ increases close to the plasma edge. Here, a different dependence of τ_E on a is found. The general trend of the energy confinement as resulting from the regression analysis in Chapter 4 shows that the dependence of τ_E on the plasma radius is weaker than a^2.

Due to ECRH cut-off, n_e at $B_0 = 1.25$ T was limited to $\leq 2.5\,10^{13}$ cm^{-3}. At high ECRH power levels, the generation of suprathermal electrons at low densities led to a broadening in the T_e profiles. Fokker-Planck model calculations indicated that ripple transport of suprathermal electrons would only result in a broadening of the effective power deposition, direct losses were negligible and a degradation of the effective heating power could be excluded. However, the minima values of the χ_e profiles were clearly higher (above 10^4 cm^2/s) for half field than for full field operation indicating an improvement of confinement with B_0 and n_e (see the regression analysis in Chapter 4).

3.2. Particle Transport

The particle confinement in W VII-AS was investigated for ECRH discharges at 1.25 and 2.5 T by coupling DEGAS code (Heifetz, 1982) simulations with H_α emissions measured at relevant toroidal positions. Radially resolved ion fluxes were obtained from calculated neutral particle distributions, after calibrating them with the H_α signals (Sardei, 1990). Estimated Z_{eff} were used to derive the electron particle fluxes and diffusivities.

The power scan at 2.5 T, $\iota(a) = 0.34$, $a = 12$ cm already discussed in Chapter 2.2., is characterized by electron density profiles which get more and more hollow as the heating power is increased, see Figure 9. In the central region the electron fluxes have been compared with neoclassical predictions. As T_i profile information is lacking, only the neoclassical electron fluxes can be estimated by DKES code. In the 4 gyrotrons case, for which the central hollow profile is most pronounced, the fluxes near the plasma center, $r = 2.5$ cm, are $\Gamma_e \simeq 3 \cdot 10^{15}$ cm^{-2}/s, and $\Gamma_e^{neo} \simeq 2 \cdot 10^{15}$ cm^{-2}/s. This fairly good agreement means that the observed hollow density profile can be explained reasonably well by the neoclassical temperature gradient driven particle flux (thermodiffusion), without need of additional anomalous contributions. This is consistent with the lack of major resonances in the central confinement predicted for large heating powers and fixed $\iota(a) \simeq 1/3$ (Chap. 2.2). There it is shown that the ohmic current needed to compensate the high bootstrap current leads to a strong positive shear which keeps the central region well below the $\iota = 1/3$ resonance (see Fig. 4). By reducing the heating power down to 1 gyrotron, the hollow density profiles disappear (Fig. 9) and the particle fluxes are enhanced by a factor of $\simeq 5$ over the neoclassical values. This poor particle confinement in the central region is consistent with a flattening of the measured T_e profile (see Fig. 4). In this case, an $\iota = 1/3$ transition in the main confinement region is predicted (see Chap. 2.2).

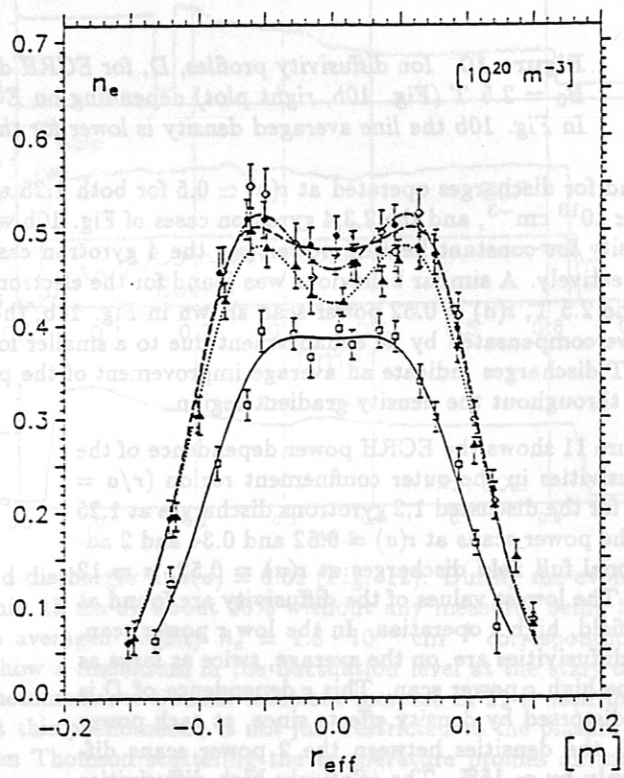

Figure 9 Electron density profiles for an ECRH power scan showing hollow profiles for high power level ($\iota(a) \simeq 0.34$ and $a \simeq 12$ cm). The ECF input power is $P_{ECF} \simeq 170$ kW (shots 8763-78, solid line), $\simeq 370$ kW (shots 8719-35, broken line), $\simeq 470$ kW (shots 8639-58, dot-dashed line) and $\simeq 640$ kW (shots 8668-95, dotted line), respectively.

In the density gradient region the particle fluxes strongly increase whereas the neoclassical fluxes are negligible with respect to the central region. For solving the particle balance equation the diffusive ansatz, $\Gamma = -D\,n'$, is used for the particle fluxes. The particle diffusivities, D, have been evaluated for discharges operated at half and full field, and $\iota(a)$ values close to the major resonances 1/3 and 1/2, where optimum confinement has been found (see Fig. 2). The radial range of the diffusivities is restricted to the density gradient region up to the limiter (D cannot be determined for flat density profiles). Here, the density profiles can be explained by diffusive transport alone.

For the power scan at $\iota(a) = 0.34$ discussed above, the diffusivities in the outer confinement region ($r \simeq 10$ cm) increase with heating power for constant density ($D \simeq 1800 - 4000$ cm^2/s from 2 to 4 gyrotrons). The same behaviour is

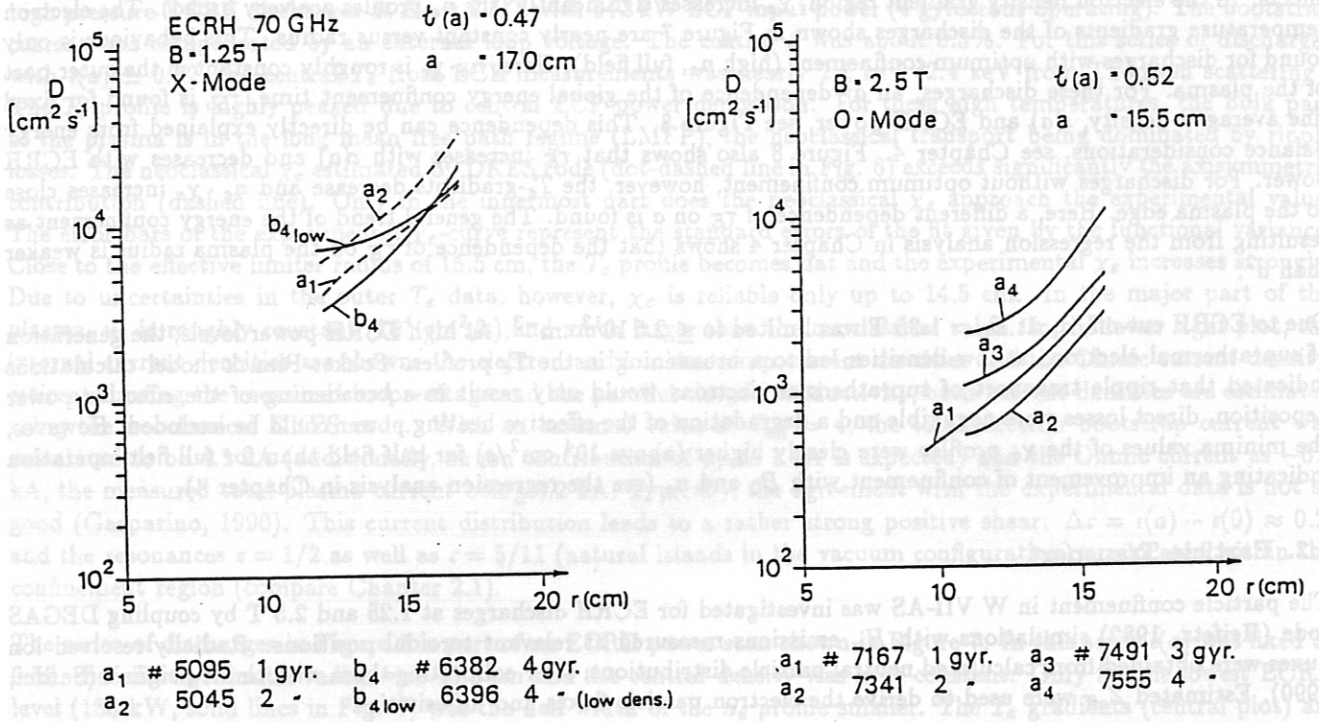

Figure 10 *Ion diffusivity profiles, D, for ECRH discharges at $B_0 = 1.25$ T (Fig. 10a, left plot) and at $B_0 = 2.5$ T (Fig. 10b, right plot) depending on ECR heating power (number of gyrotrons operating). In Fig. 10b the line averaged density is lower for the 1 gyrotron case.*

found for discharges operated at $\iota(a) \simeq 0.5$ for both 1.25 and 2.5 T, see the 1 and 2 gyrotron cases of Fig. 10a with $\bar{n}_e \simeq 10^{13}$ cm^{-3}, and the 2,3,4 gyrotron cases of Fig. 10b with $\bar{n}_e \simeq 2.8 \cdot 10^{13}$ cm^{-3}. D also increases with decreasing density for constant heating power, see the 4 gyrotron cases of Fig. 10a, with $\bar{n}_e \simeq 8.5 \cdot 10^{12}$ and $1.8 \cdot 10^{13}$ cm^{-3}, respectively. A similar behaviour was found for the electron thermal diffusivity, see Chapter 4. In the 1 gyrotron case of the 2.5 T, $\iota(a) = 0.52$ power scan shown in Fig. 10b, the expected reduction of D due to the small heating power is overcompensated by an enhancement due to a smaller local density. A comparison between the analyzed 1.25 and 2.5 T discharges indicate an average improvement of the particle confinement with the magnetic field by a factor of $\simeq 3$ throughout the density gradient region.

Figure 11 shows the ECRH power dependence of the diffusivities in the outer confinement region ($r/a = 0.8$) for the discussed 1,2 gyrotrons discharges at 1.25 T, the power scans at $\iota(a) = 0.52$ and 0.34 and 2 additional full field discharges at $\iota(a) = 0.52$, $a = 12$ cm. The lowest values of the diffusivity are found at full field, high ι operation. In the low ι power scan, the diffusivities are, on the average, twice as large as in the high ι power scan. This ι dependence of D is not distorted by density effects since, at each power level, the densities between the 2 power scans differ only by $\simeq 15\%$. The relatively high diffusivities in the 1 gyrotron case of both power scans can be explained by the local densities being 40% smaller than in the respective 2, 3, 4 gyrotron cases. All these results indicate that, at least in the outer confinement region, D scales positively with the heating power and negatively with B, ι and local plasma density. A comparison of D and χ_e for the analyzed discharges yields D/χ_e values between 0.1 and 0.3 in the outer confinement region at $r/a = 0.8$. Concerning the plasma refuelling sources, it should be mentioned that limiter recycling accounts for about 90% of the ion production in the small aperture, low ι case (optimal wall screening from ion impact) and only for about 20% in the large aperture, high ι case.

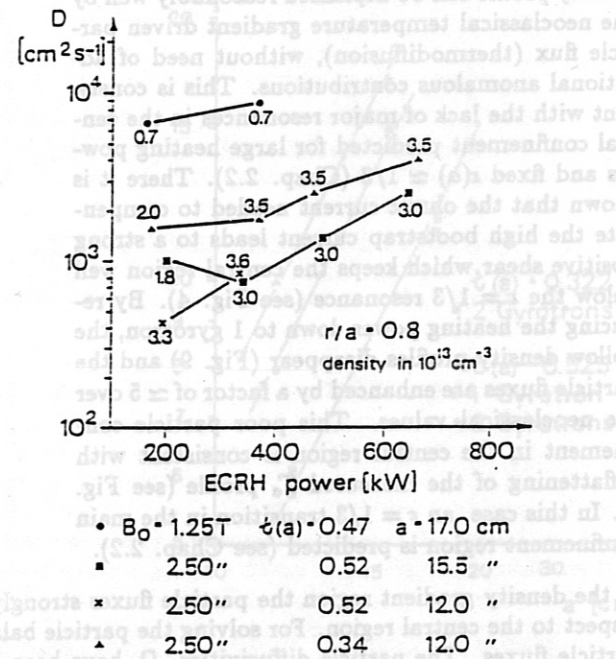

Figure 11 *Dependence of ion diffusivity, D, on ECRH power at fixed $r/a = 0.8$. The numbers in the plot give the local electron density, n_e, in units of 10^{13} cm^{-3}.*

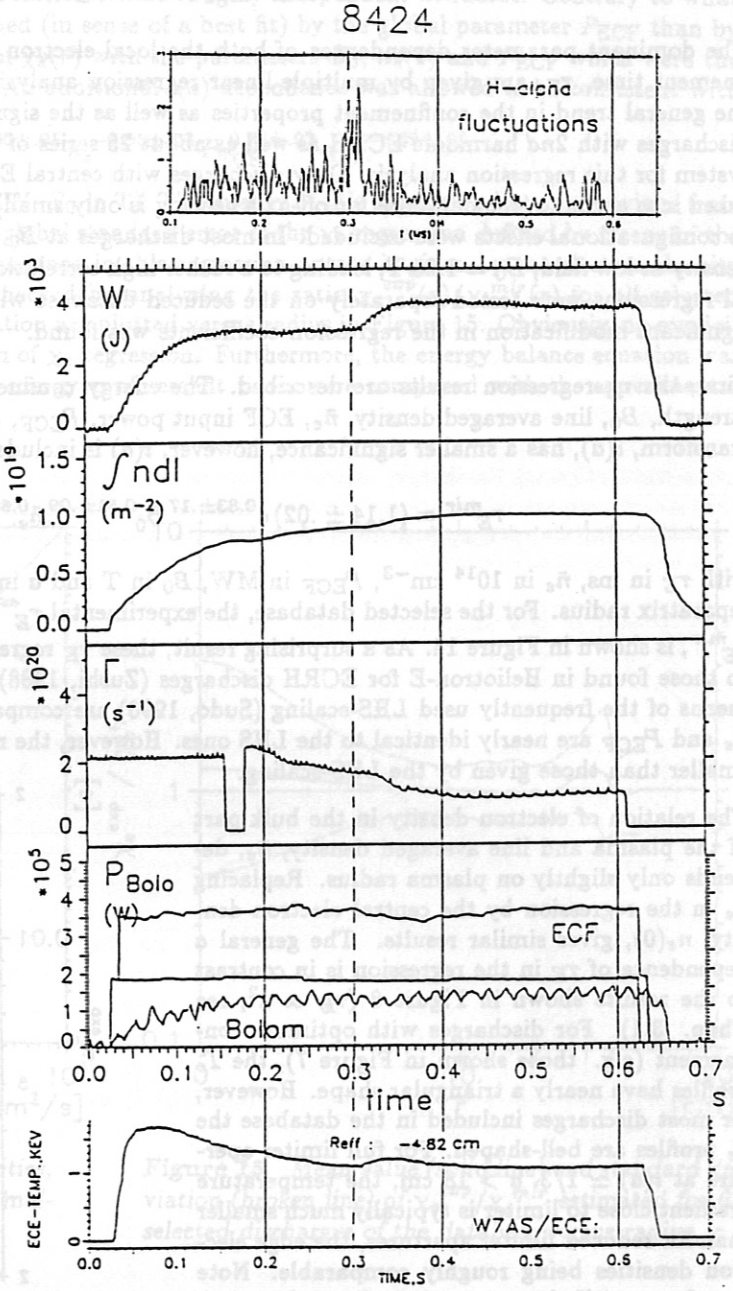

Figure 12 *Transition to improved confinement in shot 8424: the energy content, W, the line density, $\int ndl$, the gas flux, Γ, ECF input power and radiation loss, P, and, in the lowest plot, the ECE electron temperature at about $r \simeq 5$ cm are shown versus time. The H_α fluctuations (upper plot) peak at the transition (broken line) and decrease afterwards. T_e shows only a transient increase after the transition contrary to W and $\int ndl$.*

An interesting transition was observed in ECRH full field discharges at $\iota(a) = 0.32$ (Fig. 12). During the evolution of the electron density the energy content increases within 15 ms by about 30% without any measures being taken from the outside. The transition takes place at a line averaged density $\bar{n}_e = 1.8 \cdot 10^{14}$ cm^{-3} corresponding to $\int ndl = 7.5 \cdot 10^{14}$ cm^{-2} in Figure 12. The H_α signals show a maximum in the fluctuation level at the start of the transition and then relax to a lower level. From ECE measurements a small transient increase in T_e is seen during the transition at all radial positions. This indicates that this phenomenon is not just restricted to the plasma edge as one would conclude from the H_α signals alone. From Thomson scattering the temperature profiles during the steady phase after the transition turned out to be the same, but the electron density has increased, indicating better confinement, particularly as the external gas flux is even reduced. From energy and particle balance analysis, the transition to higher density is seen to correlate with an average reduction of χ_e by about 30% over the whole plasma column and with a decrease of D by about 50% in the density gradient region.

The impurity particle confinement in WVII-AS has been investigated by laser ablation of aluminium. Since hydrogen-like Al, which is peaked in the bulk plasma for ECRH discharges, can be assumed to evolve under ionization equilibrium conditions, the decay time of the Al-XIII line radiation during stationary plasma conditions is a measure of the central confinement time for this impurity. For moderate and high ECRH power, the decay time is found to increase from $\simeq$ 10 ms at 1.25 T to $\simeq$ 40 ms at 2.5 T. Also, it decreases with ECRH power for given limiter aperture. The time evolution of Al-XIII could be reproduced by transport simulations with the STRAHL code (Behringer, 1987), which uses a constant diffusion coefficient and an inward convective term $v = -(2D/a)\cdot(r/a)$. The corresponding D decrease from $5000 - 8000$ cm^2/s for 1.25 T to $1200 - 2000$ cm^2/s for 2.5 T. These numbers reduce by $\simeq$ 20%, if the velocity term is omitted. Discrepancies between the measured and simulated decay times are found, however, for the lower ionization stages. More experimental data, and more accurate simulations, including a spatial variation of D, are needed to improve the description of the impurity transport behaviour under different experimental conditions.

4. Transport Regression Analysis

The dominant parameter dependences of both the local electron heat conductivity, χ_e, and the global energy confinement time, τ_E, are given by multiple linear regression analysis. This standard procedure is only used to obtain the general trend in the confinement properties as well as the significant parameter dependences. About 40 series of discharges with *2nd* harmonic ECRH as well as about 25 series of *1st* harmonic ECRH were selected from a database system for this regression analysis. Only discharges with central ECF power deposition which is highly localized were taken into account (the database for off-axis heating is only small) and discharges with confinement degradation due to configurational effects were excluded. In most discharges at $B_0 = 2.5$ T the electron density is more than twice the density at low field, $B_0 = 1.25$ T, leading to a rather high correlation in the regressions with B_0 and n_e. Consequently, all regressions were tested separately on the reduced database with $B_0 = 1.25$ T and $B_0 = 2.5$ T, respectively. No significant modification in the regression coefficients was found.

First, the τ_E-regression results are described. The energy confinement time depends significantly on magnetic field strength, B_0, line averaged density, $\bar{n}_e$, ECF input power, P_{ECF}, and plasma radius, a. The edge value of rotational transform, $\iota(a)$, has a smaller significance, however, $\iota(a)$ is included in the regression.

$$\tau_E^{mlr} = (1.14 \pm .02)\, a^{0.83\pm.17} B_0^{0.51\pm.09} \bar{n}_e^{0.66\pm.07} P_{ECF}^{-0.55\pm.05} \iota(a)^{0.26\pm.09}$$

with τ_E in ms, $\bar{n}_e$ in 10^{14} cm^{-3}, P_{ECF} in MW, B_0 in T and a in cm, a being the minimum of effective limiter and separatrix radius. For the selected database, the experimental τ_E^{exp} versus the result of the multiple linear regression, τ_E^{mlr}, is shown in Figure 14. As a surprising result, these τ_E regression coefficients for B_0, $\bar{n}_e$ and P_{ECF} are identical to those found in Heliotron-E for ECRH discharges (Zushi, 1988). Also the energy confinement times estimated by means of the frequently used LHS-scaling (Sudo, 1990) are comparable. Furthermore, the regression coefficients for $\bar{n}_e$ and P_{ECF} are nearly identical to the LHS ones. However, the regression coefficients for B_0 and a are significantly smaller than those given by the LHS-scaling.

The relation of electron density in the bulk part of the plasma and line averaged density, $\bar{n}_e$, depends only slightly on plasma radius. Replacing $\bar{n}_e$ in the regression by the central electron density, $n_e(0)$, gives similar results. The general a dependence of τ_E in the regression is in contrast to the results shown in Figure 8 ($\tau_E \propto a^2$, see Chap. 3.1). For discharges with optimum confinement (e.g. those shown in Figure 7), the T_e profiles have nearly a triangular shape. However, for most discharges included in the database the T_e profiles are bell-shaped. For full limiter aperture at $\iota(a) \simeq 1/3$, $a > 18$ cm, the temperature gradient close to limiter is typically much smaller than for reduced limiter apertures, the edge electron densities being roughly comparable. Note that for $r \simeq 1/2$ the separatrix radius is less than 17 cm. This flattening of the T_e profile is consistent with a stronger increase of χ_e (and also $n_e \cdot \chi_e$) at the plasma edge. These findings indicate that the confinement is degraded in this region for most discharges.

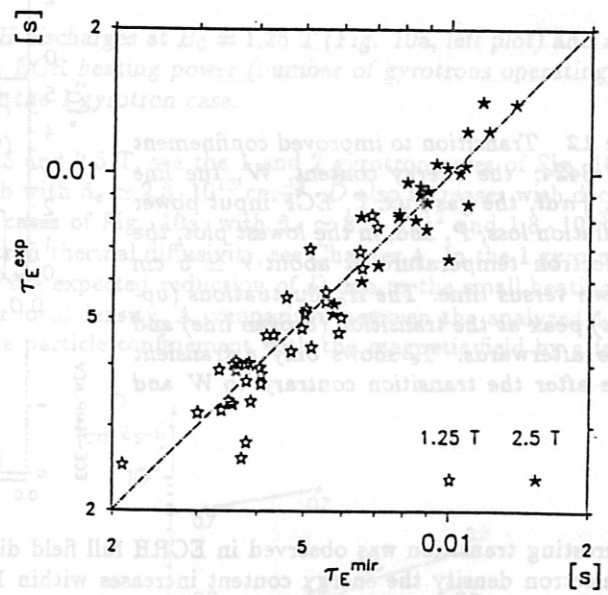

Figure 13 *Experimental energy confinement times, τ_E^{exp}, versus the values calculated by means of the multiple linear regression formula, τ_E^{mlr}.*

As the analysis of τ_E scaling laws is not very conclusive for describing the transport properties, a local χ_e regression is performed by using the χ_e profiles estimated from the electron energy balance analysis. For each χ_e profile a radial range of confidence was specified to exclude uncertainties depending on the quality of the measured profiles, especially near the plasma edge. In the central part of the plasma, the experimental χ_e can reach the neoclassical value for discharges with peaked T_e in the LMFP collisionality regime. Here, different T_e dependences must be expected. Furthermore, the χ_e profile from the electron energy balance analysis depends sensitively on the ECRH power deposition profile in the central region. Therefore, the plasma center with $r < 5$ cm was excluded from the regression analysis. For the gradient region, however, with $r > 5$ cm where the neoclassical χ_e is always small compared to the experimental one, the global regression analysis gives reasonable results.

As the experimental χ_e is roughly constant in the bulk part of the plasma and $T_e(r)$ varies strongly, a global χ_e regression must result in a very small T_e dependence of χ_e. Consequently, local regressions of χ_e (fixed plasma radius) with the local parameters B_0, n_e and T_e which are assumed to be dominant were performed. No conclusive results were found: the regression coefficients for B_0 and n_e were nearly independent of radius while the T_e dependence for $r > 8$ cm was rather small and the quality of these regressions was unacceptable. Adding a global heating power dependence leads to a significant improvement, however, the local T_e dependence remains to be rather small but is inverted: χ_e decreased with increasing T_e. Omitting the T_e dependence in local regressions has only a small effect on

the regression quality. In this case, all regression coefficients were roughly independent of radius. Contrary to what one might expect, the local $\chi_e(r)$ are better described (in sense of a best fit) by the global parameter P_{ECF} than by only local ones. Consequently, a global regression of $\chi_e(r)$ with the parameters B_0, $n_e(r)$ and P_{ECF} which were the dominant ones in local regressions was performed. An additional $\iota(a)$ dependence was allowed to be consistent with the τ_E regresssion.

$$\chi_e{}^{mlr} = (0.64 \pm .10)\, B_0{}^{-0.60\pm.05}\, n_e{}^{-0.95\pm.03}\, P_{ECF}{}^{0.76\pm.03}\, \iota(a)^{-0.49\pm.06}$$

(with χ_e in 10^4 cm^2/s, n_e in 10^{14} cm^{-3}, P_{ECF} in MW, B_0 in T). The quality of this regression becomes obvious from Figure 14 where $\chi_e{}^{exp}$ is plotted versus $\chi_e{}^{mlr}$. The global standard error of the χ_e regression defined by means of the fit variance is less than 40%. The only radial dependence in this regression ansatz is given by the electron density profile. Thus, a remaining radial dependence is checked by analyzing the ratio $\chi_e{}^{exp}(r)/\chi_e{}^{mlr}(r)$ for all selected discharges. The mean value and the standard deviation are plotted versus radius in Figure 15. Obviously, no explicit radial weighting function is neccessary for this form of χ_e regression. Furthermore, the energy balance equation was integrated with this $\chi_e{}^{mlr}$ and when the resulting energy confinement times were compared with the experimental values, very good agreement was found.

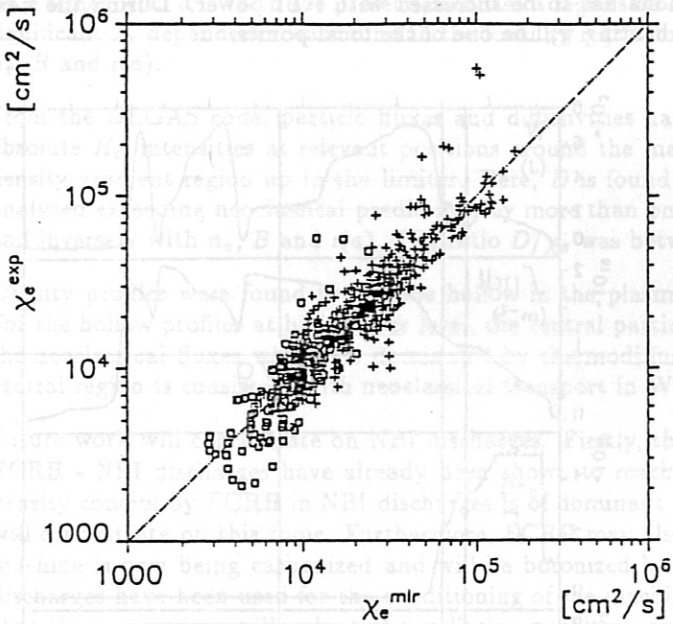

Figure 14 *Experimental electron heat conductivities, $\chi_e{}^{exp}$, versus the values calculated by means of the multiple linear regression formula, $\chi_e{}^{mlr}$.*

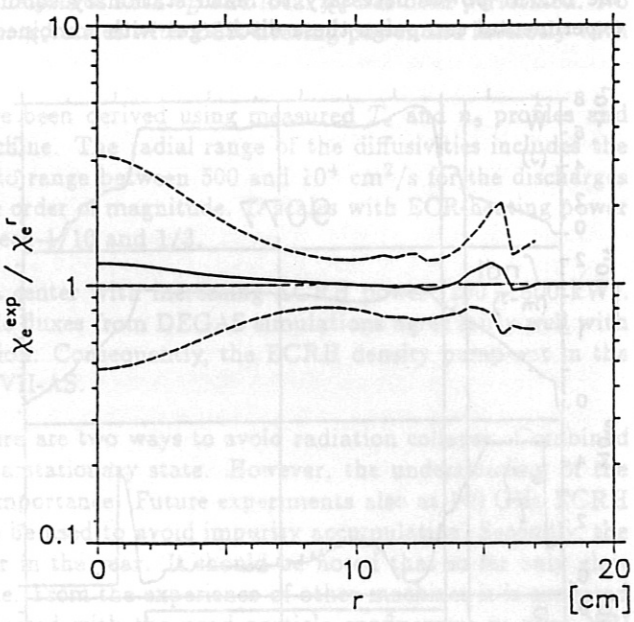

Figure 15 *Mean value (solid line) and standard deviation (broken line) of $\chi_e{}^{exp}/\chi_e{}^{mlr}$ estimated for 63 selected discharges of the database versus radius, r.*

The χ_e regression yields the analogous (inverse) parameter dependences as the τ_E regression. With a simplified integration of the electron energy balance based on $\chi_E{}^{mlr}$ a corresponding τ_E scaling formula can be derived. Thus, both the local and global transport regressions are consistent. The heating power dependence in the global χ_e regression can be qualitatively understood by means of the electron energy balance equation. Radiation losses and collisional electron-ion energy transfer can be neglected in this rough approach as the electron heat conduction is the dominant loss term. Outside of the ECRH power deposition zone ($r > 5\,cm$) the electron energy balance equations can be written in the form

$$-n_e \chi_e \frac{\partial T_e}{\partial r} \approx \frac{1}{4\pi^2 R r} P_{ECF}.$$

Typically, the density profiles are flat and very broad, and $n_e \cdot \chi_e$ is roughly constant. The shape of the T_e profiles does not change very much on variation of external plasma parameters. Within the important confinement region, the temperature gradient is only slightly affected by the heating power. These experimental findings reflect the basic physics of the electron energy transport. The parameter dependence of $\chi_e(r)$ follows directly: the strong relation of $n_e \cdot \chi_e$ to the heating power becomes obvious. The statistical significance shows this to be a general trend in all ECF heated discharges where electron heat conduction is the dominant loss channel. Consequently, on the basis of the electron energy balance the χ_e regression reflects the fact that only little variation is found in the electron temperature gradient. Furthermore, the dependences of χ_e on B_0 and $\iota(a)$ is given directly by the regression. A physical picture of this anomalous transport cannot be given by such a form of regression analysis. However, the fact that no local scaling of χ_e with T_e was found indicates two possible explanations. Firstly, the electron heat conduction cannot be treated by the specific form of regression ansatz as described in this Chapter or, secondly, the picture of transport being determined by only local plasma parameters is inadequate.

5. Combined ECRH and NBI Discharges

Most of the shots in W VII-AS have been oriented to the study of pure ECR heated plasmas. Two types of discharges have been investigated in connection with NBI.

a) NBI with ECR heated target plasma: the gyrotrons were only used to provide a target plasma and then shut off. The trapping of the neutral beams was improved in with additional pellet injection. The plasma parameters reached are $n_e(0) \simeq 10^{14}$ cm^{-3}, $T_e(0) \simeq T_i(0) \leq 0.7$ keV with an energy content $W \leq 15$ kJ and $\tau_E = 10$ ms. The discharges were always non-stationary and, due to good particle confinement, the fast density increase led to a radiative collapse.

b) Combined ECR and NBI heated plasmas leading to stationary discharges at moderate densities and radiation power levels. Similar experiments have already been reported from W VII-A (Ringler, 1986). An influence of ECRH on the time evolution of the density has been seen before (Alikaev, 1984 and Uo, 1986). Due to a reduction of the particle confinement as compared to purely NBI heated discharges, the density can even be feedback controlled by gas puffing. In Figure 16, shots are shown to illustrate this technique. Energy content, line density, gas flux and heating power are shown as a function of time. In the case of shot 9077, stationary conditions were reached using 3 gyrotrons with feedback control of the density. For shot 9079, however, one of the 3 gyrotrons failed with the result of a nonstationary discharge. The density reaches twice the ECRH cut-off without gas puffing. It turns out that the ECRH power necessary to reach stationary conditions has to be increased with NBI power. During the next experimental campaign these discharges with combined heating will be one of the focal points.

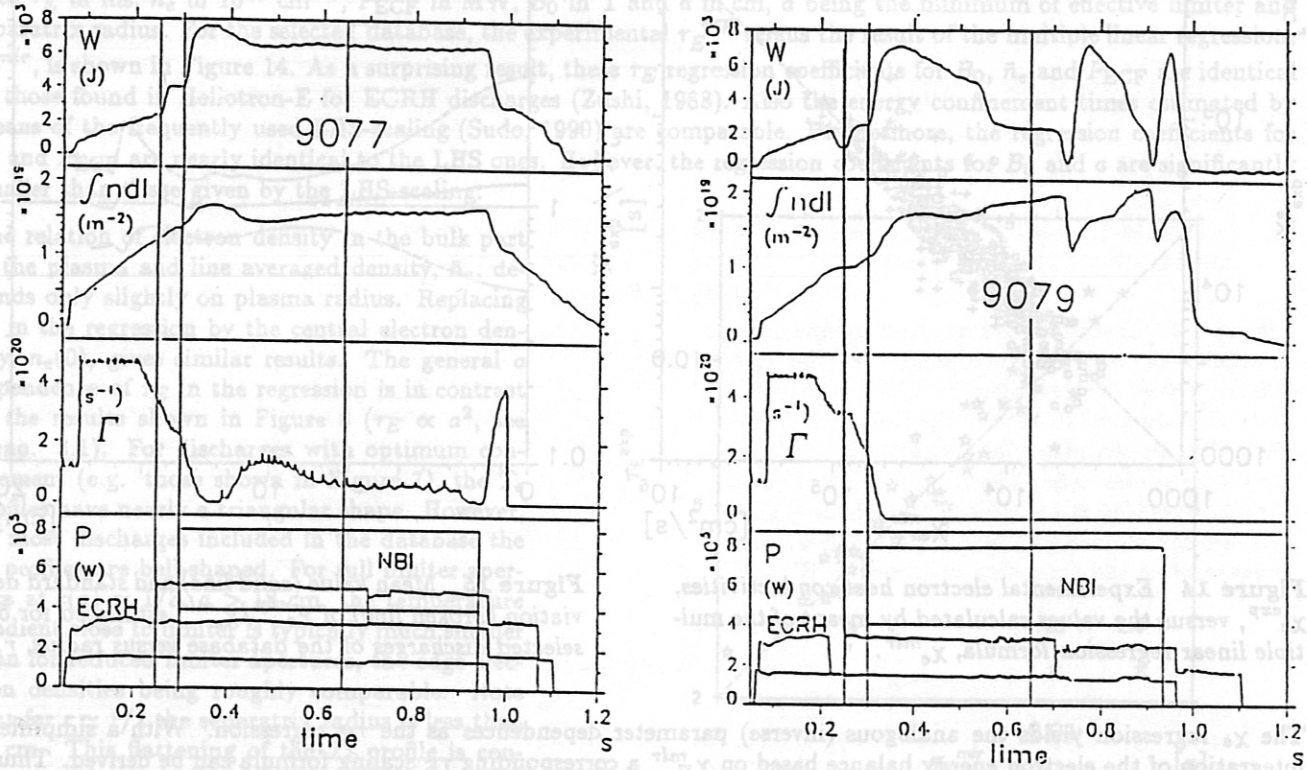

Figure 16 *Density control in combined ECRH + NBI discharges: the energy content, W, the line density, $\int n\,dl$, the gas flux, Γ, and NBI and ECF input power, P, are plotted versus time. In shot 9077 with 3 gyrotrons operating, the density reamins below cut-off and even a small gas flux was neccessary for stationary conditions. In shot 9079 with only 2 gyrotrons operating, however, the density increases to cut-off, no gas flux was applied.*

6. Summary and Conclusion

W VII-AS with its modular field system has operated routinely since January 1990 with full field parameters. From this experience one can draw the conclusion that also a large modular system can be realized, especially as the mechanical forces will not exceed values known from W VII-AS. In the 1st and 2nd experimental campaigns most of the investigations were devoted to ECR-heated plasmas (70 GHz) at 1.25 T and 2.5 T magnetic field with 2nd harmonic x-mode and fundamental o-mode launching. Maximum plasma parameters of $T_{eo} \simeq 2.5$ keV, $T_{io} \simeq 0.4$ keV, $n_{eo} \simeq 5 \cdot 10^{13}$ cm^{-3} and $\tau_E \simeq 10 - 20$ ms have been achieved with this technique. The expected reduction of the Shafranov shift by reducing the Pfirsch-Schlüter currents by a factor of two has been confirmed by the experiment.

The control of the rotational transform at the plasma edge, $\iota(a)$, works for all possible scenarios under consideration. For low internal shear operation, degraded confinement is found to be related to low order rational values of ι which indicates island formation and ergodization in the magnetic configuration. Even local flattening of the electron

temperature profile has been resolved for these conditions. Internal shear is generated by internal currents. In most discharges, the pressure driven bootstrap current which is experimentally confirmed is feedback-compensated by an Ohmic current. This scenario results in a positive shear depending on the magnitude of the bootstrap current and consequently on the energy content. The positive effect of internal shear on the energy confinement has been shown to be significant. Finally, a future task will be the study of confinement optimization by means of an appropriate shaping of the whole rotational transform profile using local ECCD.

Electron energy balance analysis based on measured T_e and n_e profiles yields the electron heat conductivity, $\chi_e(r)$. The best χ_e values which have been achieved are well below 10^4 cm^2/s which are in the range of the optimum χ_e values found in tokamaks. For all analyzed discharges, the neoclassical transport coefficients were calculated by using the DKES code and compared to the experimental values. Due to the strong T_e dependence, the neoclassical χ_e values decrease rapidly with radius and are typically about one order of magnitude smaller than the experimental value at half plasma radius. The experimental χ_e, however, are roughly constant in the bulk part of the plasma and increase close to the plasma edge. The neoclassical χ_e come up to the experimental values only for central high ECF power deposition with peaked temperatures where the neoclassical ripple losses dominate. For discharges with $n_e > 3 \cdot 10^{13}$ cm^{-3} at full field optimum confinement properties were achieved, being characterized by $T_e' \approx const$ as well as $n_e \cdot \chi_e \approx const$ in nearly the whole confinement region. For these discharges, the global energy confinement time scales with a^2. With the present database a regression analysis of both τ_E and local χ_e has been performed. No significant T_e dependence was found in the local χ_e regression. χ_e scales with ECR-heating power and inversely with n_e, B and $\iota(a)$.

From the DEGAS code, particle fluxes and diffusivities have been derived using measured T_e and n_e profiles and absolute H_α intensities at relevant positions around the machine. The radial range of the diffusivities includes the density gradient region up to the limiter. Here, D is found to range between 500 and 10^4 cm^2/s for the discharges analyzed exceeding neoclassical predictions by more than one order of magnitude. D scales with ECR-heating power and inversely with n_e, B and $\iota(a)$. The ratio D/χ_e was between 1/10 and 1/3.

Density profiles were found to become hollow in the plasma center with increasing ECRH power (200 – 800 kW). For the hollow profiles at high power level, the central particle fluxes from DEGAS simulations agree fairly well with the neoclassical fluxes which are dominated by thermodiffusion. Consequently, the ECRH density pump-out in the central region is consistent with neoclassical transport in W VII-AS.

Future work will concentrate on NBI discharges. Firstly, there are two ways to avoid radiation collapse. Combined ECRH - NBI discharges have already been shown to reach a stationary state. However, the understanding of the density control by ECRH in NBI discharges is of dominant importance. Future experiments also at 140 GHz ECRH will concentrate on this topic. Furthermore, ECRH may also be used to avoid impurity accumulation. Secondly, the machine is now being carbonized and will be boronized later in the year. It should be noted that so far only glow discharges have been used for the conditioning of the machine. From the experience of other machines it is expected that these measures will reduce the radiation problem connected with the good particle confinement in pure NBI discharges.

References

Alikaev, V.V. (1985) Plasma Physics and Contr. Nucl. Fus. Res.; 1, 419

Behringer, K. (1987) JET-R (87) 08

Erckmann, V. et al. (1990) ECA, 17th EPS Conf. on Contr. Fus. and Plasma Phys., Amsterdam, 3, 1271

Gasparino, U. et al. (1989) ECA, 16th EPS Conf. on Contr. Fus. and Plasma Phys., Venice, 2, 631

Gasparino, U. et al. (1990) ECA, 17th EPS Conf. on Contr. Fus. and Plasma Phys., Amsterdam, 3, 1275

Grieger, G. et al. (1986) Plasma Physics and Contr. Fusion, 28, 43

Heifetz, D.B. et al. (1982) J. Comput. Phys., 46, 309

Horton, W. et al. (1989) Plasma Physics and Contr. Nucl. Fus. Res.; Proc. of the 12th Conf. (Nice), 2, 211

Kaneko, H. et al. (1987) Nuclear Fusion, 27, 1075

Kasparek, W. (1988) Proc. 15th Symp. on Fusion Technology (SOFT), Utrecht, B19

Kisslinger, J. and H. Wobig (1985) ECA, 12th EPS Conf. on Contr. Fus. and Plasma Phys., Budapest, 1, 453

Motojima, O. (1989) Proc. 1st Int. Tokei Conf. on Plasma Physics and Contr. Nucl. Fus., P3

Renner, H. (1986) ECA, 13th EPS Conf. on Contr. Fus. and Plasma Phys., Schliersee, 1, 287

Renner, H. (1989) Plasma Physics and Contr. Fusion, 31, 1579

van Rij, W.I. and S.P. Hirshman (1989) Phys. Fluids B, 1, 563

Ringler, H. et al. (1987) Plasma Physics and Contr. Nucl. Fus. Res.; Proc. of the 11th Conf. (Kyoto), 2, 603

Sardei, F. et al. (1990) ECA, 17th EPS Conf. on Contr. Fus. and Plasma Phys., Amsterdam, 2, 471

Sudo, S. et al. (1990) Nuclear Fusion, 30, 11

Uo, K. et al. (1987) Plasma Physics and Contr. Nucl. Fus. Res.; Proc. of the 11th Conf. (Kyoto), 2, 355

Weller, A. et al. (1990) ECA, 17th EPS Conf. on Contr. Fus. and Plasma Phys., Amsterdam, 2, 479

Wesner, F. et al. (1988) Proc. 15th Symp. on Fusion Technology (SOFT), Utrecht

Wobig, H. et al. (1987) Plasma Physics and Contr. Nucl. Fus. Res.; Proc. of the 11th Conf. (Kyoto), 2, 369

Zushi, H. et al. (1988) Nuclear Fusion, 28, 1801

Statistical Analysis of Electron Heat Conduction on W7-AS

G.Kühner, H.Maaßberg, H.Ringler
W7-AS Team, ECRH-Group

Max-Planck Institut für Plasmaphysik
Association EURATOM-IPP, D-8046 Garching, FRG

INTRODUCTION

During the first two periods of plasma operation in the Wendelstein 7–AS stellarator most of the discharges were built up and sustained by ECRH at 70 GHz with up to 800 kW input power. Since in the earlier one the magnetic field strength was restricted to 1.25 T, 2^{nd} harmonic heating (x-mode launching) with average densities between $7 \cdot 10^{18}$ and $2 \cdot 10^{19}\ m^{-3}$ was extensively investigated. The more recent experiments were performed using 1^{st} harmonic heating at 2.5 T (o-mode) with densities up to $4 \cdot 10^{19}\ m^{-3}$.

Within the experimental range of the plasma parameters (heating power P_{ECF}, electron density n_e and temperature T_e, rotational transform ι and toroidal magnetic field B_0), a statistical description of the local electron heat conductivity, $\chi_e(r)$, resulting from the energy balance analysis is given by regression methods. Such formulae are used as a basis for model calculations, but they reveal also global parameter dependences and may give some insight into the mechanism of the enhanced electron energy transport. Additionally, these local χ_e formulae can be converted to global energy confinement times, τ_E. If a sufficient database is available, the statistical analysis of local transport is much more powerful than the usual global scaling of energy confinement times. Furthermore, for comparing present stellarator (W7-AS, ATF, Heliotron-E) and tokamak experiments of quite different size, a statistical formulation of the electron heat conductivity is very useful.

DATA ANALYSIS

About 30 series of discharges with 2^{nd} harmonic ECRH as well as about 20 series of 1^{st} harmonic ECRH are included in the database for the statistical analysis. The electron heat conduction was determined by a direct fit of the electron energy balance equation to electron temperature and density profiles measured by Thomson scattering (see Fig.1). For these discharges, electron heat conduction was the major loss channel, radiation and electron-ion coupling played only a minor role.

The χ_e, T_e, n_e profiles as well as global parameters like P_{ECF}, B_0, τ_a at the plasma edge were stored in a database system. Only discharges with central ECF power deposition which is highly localized were taken into account since the database for off-axis heating is not sufficient. For each profile a radial range of confidence was specified to avoid the influence of uncertainties at the profile boundaries. Nonlinear regression was employed for the determination of the parameter dependences. Using this method correlations between regression coefficients can be kept under control and also complicated parameter expressions can be tested.

The regression was tested for different intervals in minor radius and it turned out that a simple regression ansatz was inadequate for the central plasma interval with $r < 5\ cm$. In this region, two types of discharges were distinguished: a) discharges at very low collisionalities (with peaked T_e) which are dominated by neoclassical transport (high ripple losses in the $1/\nu$-regime), b) discharges at higher collisionalities for which no central

peaking in χ_e was found and for which the neoclassical χ_e was small compared to the experimental one over the whole plasma radius. As the neoclassical T_e-dependence is very strong, these two types of discharges could not be treated by a an unique regression ansatz indicating a quite different parameter dependence for χ_e in the central region. For the gradient region with $r > 5\ cm$ where all neoclassical χ_e are small compared to the experimental ones, the analysis gives reasonable results, therefore, the plasma center with $r < 5\ cm$ was excluded from the statistical analysis. The most significant parameters turned out to be $n_e(r)$, P_{ECF} and B_0, as the corresponding regression coefficients were large compared to their variances. This parameter combination was chosen to be the "best fit", the resulting formula is given below:

$$\chi_e^r = (0.79 \pm 0.07) \cdot P_{ECF}^{0.685\pm0.03} \cdot n_e^{-1.05\pm0.03} \cdot B_0^{-0.71\pm0.13}$$

(with T_e in keV, n_e in $10^{20}m^{-3}$, P_{ECF} in MW, B_0 in T). The quality of this regression result is demonstrated as a χ_e^r vs χ_e^{exp} plot in Figure 2. Including the electron temperature $T_e(r)$ and the edge value of the rotational transform, ι_a, improved the χ^2 of the fits only slightly. The corresponding regression coefficients were rather small and comparable to their variances while the other regression coefficients for $n_e(r)$, P_{ECF} and B_0 remain nearly unchanged.

The most remarkable effect was that $\chi_e(r)$ is better described by the global parameter P_{ECF} than by the local one, $T_e(r)$, the latter having a nearly vanishing regression coefficient. So the local heat conductivity seems to be determined by the global heating and not by only local effects.

In the same way experimental χ_e-scalings (e.g. W7-A: $\chi_e \sim n_e^{-1}T_e^{-2/3}$ for OH discharges and $\chi_e \sim n_e^{-1.7}T_e^{0.6}$ for ECRH) as well as theoretical approaches (see e.g. [1]) were tested. The results, however, were negative; none of the quoted formulae is capable of describing the electron heat conductivity found in W7-AS .

This analysis would be incomplete without a cross check of the χ_e formula for consistency with the global energy confinement time, τ_E. Therefore, τ_E was estimated by solving the electron energy balance equation for each regression ansatz, the results were related to the experimental τ_E. This cross check is shown in Figure 3 for the regression based on the combination of $n_e(r)$, P_{ECF} and B_0. The energy content based on the χ_e-regressions depends sensitively on deviations to the experimental χ_e at outer radii which may be influenced by the topology of magnetic surfaces at values of the rotational transform close to low order rational numbers. Nevertheless, the regressions excluding the heating power dependence underestimate the energy content typically by a factor of 2, while the other regressions result in a very reasonable agreement.

A similar analysis can be done by deriving analytical expressions for τ_E . Solving the energy balance equation for χ_e^r in an approximative way, one obtains:

$$\tau_E^r \approx \frac{3 \cdot a^2}{8 \cdot 0.79} < n_e >^{1.05} \cdot B_0^{0.71} \cdot P_{ECF}^{-0.685}$$

The parameter dependences are similar as in the formula of the LHS group [2] which was already anticipated by a direct comparison of the experimental τ_E to the latter relation.

DISCUSSION

The heating power dependence of χ_e can be qualitatively understood from the energy balance equation where radiation and ion heating is neglected for the discharges with

dominant electron heat conduction

$$-n_e \chi_e \left(\frac{\partial T_e}{\partial r} \right) \approx \frac{1}{r} \int_0^r S_{ECF}\, r\, dr$$

with S_{ECF} being the ECF power deposition profile. Typically, the density profiles were flat and very broad. The shape of the T_e profiles did not change very much on variation of external plasma parameters (see Figure 1), the temperature gradient was only little affected by the heating power. These experimental findings reflect the basic physics of the electron energy transport, the parameter dependence of $\chi_e(r)$ follows directly from the energy balance equation: the strong relation of $n_e \cdot \chi_e$ to the heating power becomes obvious. The statistical significance shows this to be a general trend in all ECF heated discharges where electron heat conduction is the dominant loss channel.

The observations just made can not be done by a study of the energy confinement time. As the analytical expression for τ_E above shows, the information on the temperature profile shape gets lost as only the global parameter dependencies remain.

CONCLUSIONS

Formulae of the electron heat conductivity for ECF heated discharges in W7-AS were derived based on statistical regression methods. They differ markedly from a parametrization found for W7-A for Ohmic discharges. The explicitly found ECF heating power dependence may be understood as owing to a roughly constant temperature gradient. Future work should answer the question whether this effect can also be found at higher densities using different heating methods.

The resulting energy confinement times are rather insensitive to the regression model used for the electron heat conductivity. Consequently, the statistical analysis of local electron heat conduction is much more significant than global scalings of energy confinement time.

REFERENCES

[1] W. Horton et al., IAEA-CN-50, Paper DIV-3, IAEA Conference (Nice), 1989
[2] S. Sudo et al., Nucl. Fusion 30, p. 11, 1990

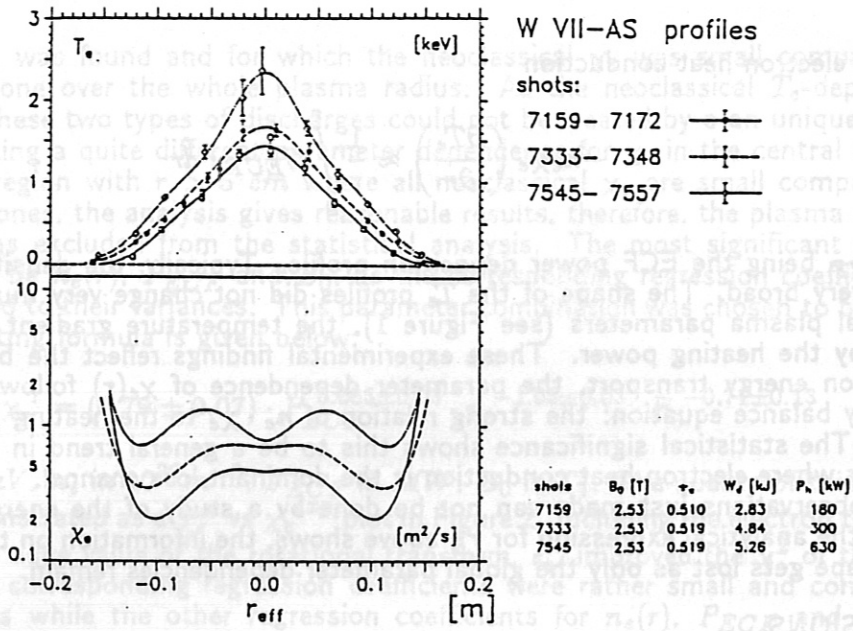

Fig. 1: Electron temperature profiles and heat conductivities, χ_e, for a power scan (1, 2 and 4 gyrotrons) at equivalent densities.

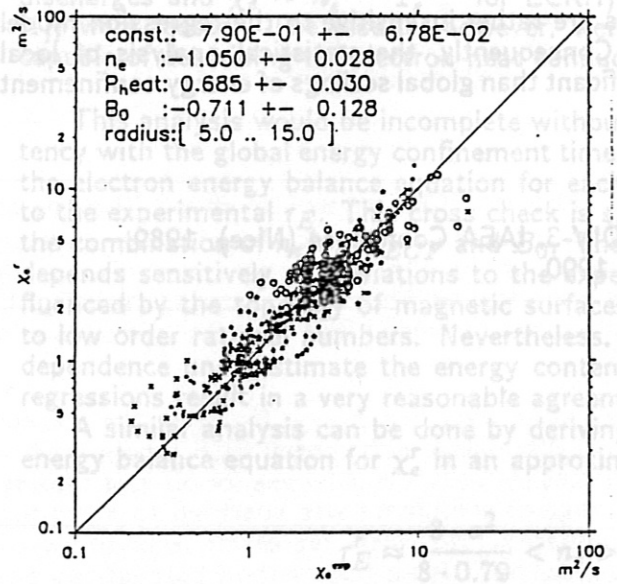

Fig. 2: $\chi_e{}^r$ vs $\chi_e{}^{exp}$ plot as a significance test of the $\chi_e{}^r$-regression ansatz with $n_e(r)$, P_{ECF} and B_0.

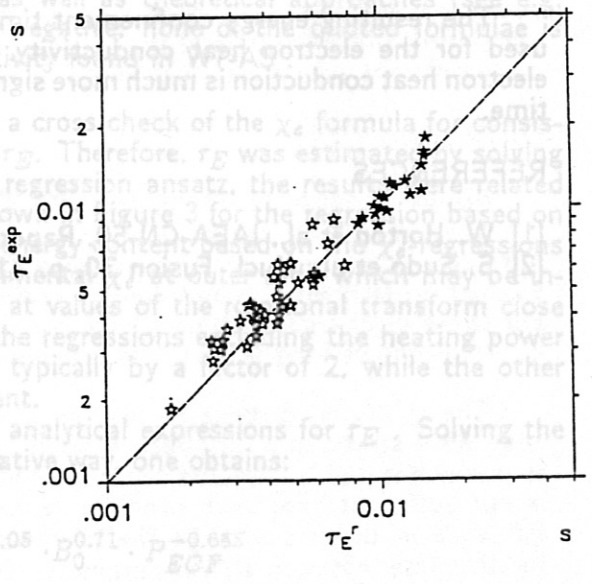

Fig. 3: Test of the global energy confinement time, τ_E^r obtained from the χ_e-regression with $n_e(r)$, P_{ECF} and B_0. Black and white symbols correspond to B_0=2.5T and 1.25T.

PARTICLE TRANSPORT AND RECYCLING STUDIES ON THE WVII-AS STELLARATOR

F. Sardei, H. Ringler, A. Dodhy, G. Kühner
and WVII-AS Team
Max-Planck-Institut für Plasmaphysik, EURATOM Ass.
Garching bei München, FRG

ECRH Group
Institut für Plasmaforschung der Universität Stuttgart,FRG

To Professor Rudolf Wienecke on his 65th Birthday

INTRODUCTION

In WVII-AS, ECRH plasmas with central deposition are characterized by peaked temperature profiles but flat or slightly hollow density profiles up to $10 - 12$ cm, which is more than half of the plasma radius (see Fig. 1). This difference is mainly due to the different radial location and extent of the energy and particle deposition zones, the first being narrow ($1 - 2$ cm) and peaked at the center, the second broad ($5 - 10$ cm) and peaked near the edge. In contrast to the energy source, the particle source strength is experimentally unknown, since it is dominated by toroidally and poloidally asymmetric recycling processes. However, the particle deposition profile can be determined by 3D neutral gas transport modelling and the source strength by calibrating the calculations with H_α measurements. Radially resolved particle fluxes and diffusivities can then be obtained from the particle sources and the measured density profiles.

RESULTS FOR 1.25 T DISCHARGES

In order to get information about ion production rates, particle confinement and neutral density distributions, several ECRH discharges at 1.25 T (2^{nd} harmonic X-mode) were analyzed by coupling DEGAS code /1/ simulations with H_α emissions obtained at different toroidal positions. For each discharge,with given Thomson temperature and density profiles at stationary conditions, three simulations were performed according to the three most relevant sources of neutrals (limiter recycling, wall recycling, external gas release). The magnetic-surface-averaged ion production rates, as obtained from the neutral densities and the Thomson profiles, were integrated to give the radially resolved ion fluxes. The electron fluxes were derived from the ion fluxes by adding estimated contributions due to the impurities, for which comparable confinement times as for the background ions were assumed. Neoclassical fluxes, as predicted by the DKES code, were used for comparison.

The radial profiles of the ion and electron fluxes and of the particle confinement time are shown in Fig. 2 for a 1.25 T discharge heated by 350 kW ECRH power (2 gyrotrons). In the central part of the plasma, the deduced electron fluxes are close to neoclassical values, whereas they become strongly anomalous towards the plasma edge. The ion particle confinement time has a maximum of 11 ms in the bulk of the plasma and drops to about 2 ms at the plasma edge, indicating strong recycling in front of the limiters. A comparison of this discharge with a similar one (same $\bar{n}$, same limiter position and comparable plasma density), but with only half of the ECRH power, shows an increase

of τ_p by a factor of two over the whole plasma radius. This is consistent with a similar ECRH power scaling of τ_E found for the same discharges.

The sensitivity of the limiter and wall recycling to the radial position of the limiters was also investigated by comparing two discharges with the limiters placed at the two extreme positions $z = 22$ and 31.5 cm from the equatorial plane (see Fig. 3). If the limiter is fully retracted to the wall, the dominant refuelling (45%) is provided by wall recycling, the limiter contribution being only 20%, which is even less than that of the external gas feed (Fig. 3b). If, however, the limiter is moved deeply into the vacuum vessel, then it accounts for 80% of the ion production (Fig. 3a). In this case, the limiter effectively screens the wall from ion impact. Impact by high energetic CX neutrals, however, is not directly affected by the limiter position. The radial range of the ion production (between 12 and 18 cm, see Fig. 3c,d) is almost the same for the three sources and for the 2 limiter positions. This indicates that the refuelling profiles are mainly affected by the electron density and temperature profiles and only slightly by the limiter position. Between the plasma edge and the wall the electron density and temperature are very small ($n_e \simeq 10^{11}\ cm^{-3}, T_e \simeq 15eV$ from probe measurements) and the ion production is negligible.

For five typical ECRH discharges with ϵ close to 0.5 and with fully retracted limiter, diffusivity profiles were calculated from particle fluxes and density gradients. D was found to range between 3×10^3 and $5\times10^4\ cm^2s^{-1}$. Fig. 4 shows diffusivities for various heating powers, with 1, 2 and 4 gyrotrons as indicated by the index. The strong increase of D towards the plasma edge is similar to that observed for χ_e. In the flat density region up to $r \simeq 10\ cm$, D is undetermined. At larger radii, the density profiles can be explained by diffusive transport only, without the need of an additional "inward drift". At moderate line averaged densities, $\bar{n} \simeq 10^{13} cm^{-3}$, there is a clear deterioration of the particle confinement with increasing ECRH power, a_2 vs. a_1. The same behaviour was found for the electron energy confinement and for the decay time of laser-ablated aluminum. If one compares diffusivities for constant heating power (4 gyrotrons) at low and high line densities ($\bar{n} = 8.5 \times 10^{12} cm^{-3}$, case b_{4low}, as compared to 1.8×10^{13}, case b_4), there is a clear decrease of D with increasing electron density. A similar improvement of the confinement was found from the decay time of laser-ablated titanium radiation, which could be simulated by diffusivities of 5×10^3 and $8 \times 10^3\ cm^2s^{-1}$ for high ($\bar{n} = 1.2 \times 10^{13} cm^{-3}$) and low ($\bar{n} = 7.3 \times 10^{12} cm^{-3}$) density, respectively.

RESULTS FOR 2.5 T DISCHARGES

The presented 1.25 T results can be compared with those obtained from recent ECRH discharges operated at the full field of 2.5 T (1^{th} harmonic O-mode). Fig.5 shows the diffusivities in the density gradient region $10 < r < 18\ cm$ for 4 Thomson series at full field, heated by 1.2.3.4 gyrotrons, respectively, with average absorbed power of 175 kW each. The bootstrap current was compensated by the OH transformer to a net current of $\simeq 200\ A$. The central electron density was $\simeq 4\times10^{13}\ cm^{-3}$ for all discharges. T_e increased with heating power from 1.4 to 2.4 keV. The density profiles were very similar, but in the 1 gyrotron case the profile was narrower by $\simeq 4\ cm$, which implies smaller densities at equivalent radial positions. As in the 1.25 T discharges, the diffusivities strongly increase from $r = 12\ cm$ up to the edge, suggesting an inverse scaling with the plasma density, as it was found for the thermal diffusivity /2/. A degradation with increasing ECRH power is also found except in the 1 gyrotron case (Fig. 5a), for which a reduction of D due to the small heating power seems to be overcompensated by an enhancement due to the smaller densities in the gradient region. The global particle confinement time at the plasma edge drops from 25 to 5 ms over the given ECRH power scan. A comparison with the 1.25 T

discharges shows a clear improvement of the particle confinement with the magnetic field throughout the gradient region, the average D being about 1/3 of the value in the half field case.

Finally, D is found to be smaller than χ_e (D/χ_e between 1/3 and 1/10) for the analyzed discharges both at 1.25 and 2.5 T.

Concerning the accuracy of the presented results, it should be noted that radially constant Z_{eff} values (increasing from 3 to 6 over the ECRH power scan), as estimated from X-ray continuum measurements, were used to determine the ion densities from the Thomson profiles. This may be a poor approximation of the actual Z_{eff} profiles. Furthermore, the wall recycling sources, as monitored by the H_α emission at the "undisturbed" triangular plasma cross section, may not represent a good average of the global recycling from the entire torus wall. Additional diagnostics are being installed to improve the experimental basis for both estimates.

REFERENCES

/1/ D.B. Heifetz et al., J. Comput. Phys. 46 (1982), 309

/2/ G.Kühner et al., see these proceedings

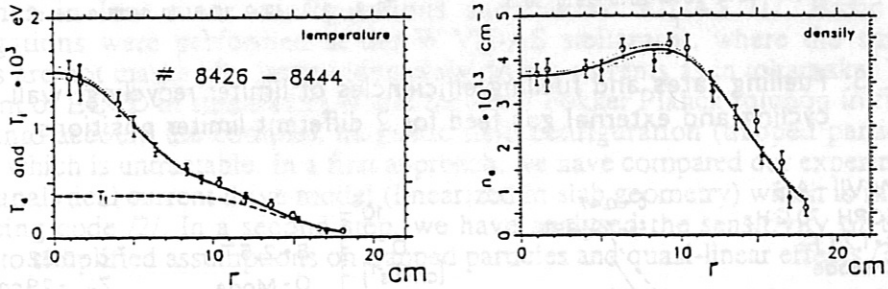

Fig. 1: Typical electron temperature and density profiles for ECRH discharges with central power deposition.

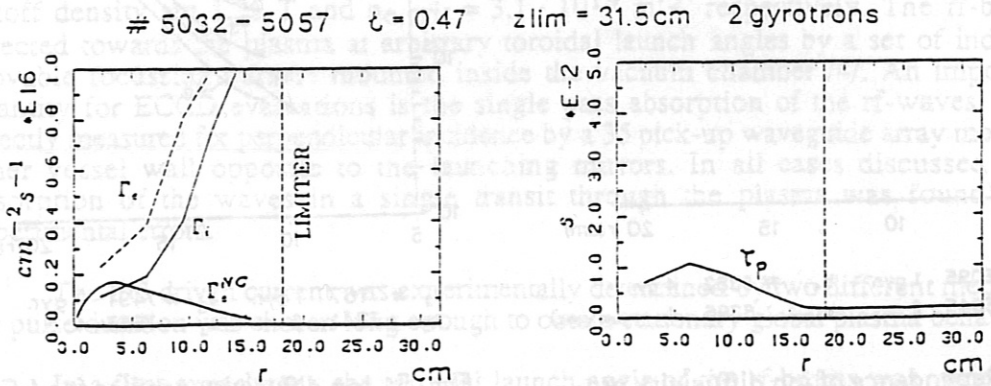

Fig. 2: Ion and electron fluxes and particle confinement time for a typical 1.25 T discharge heated by 2 gyrotrons. Γ_e^{NC}: neoclassical electron flux as obtained by DKES code.

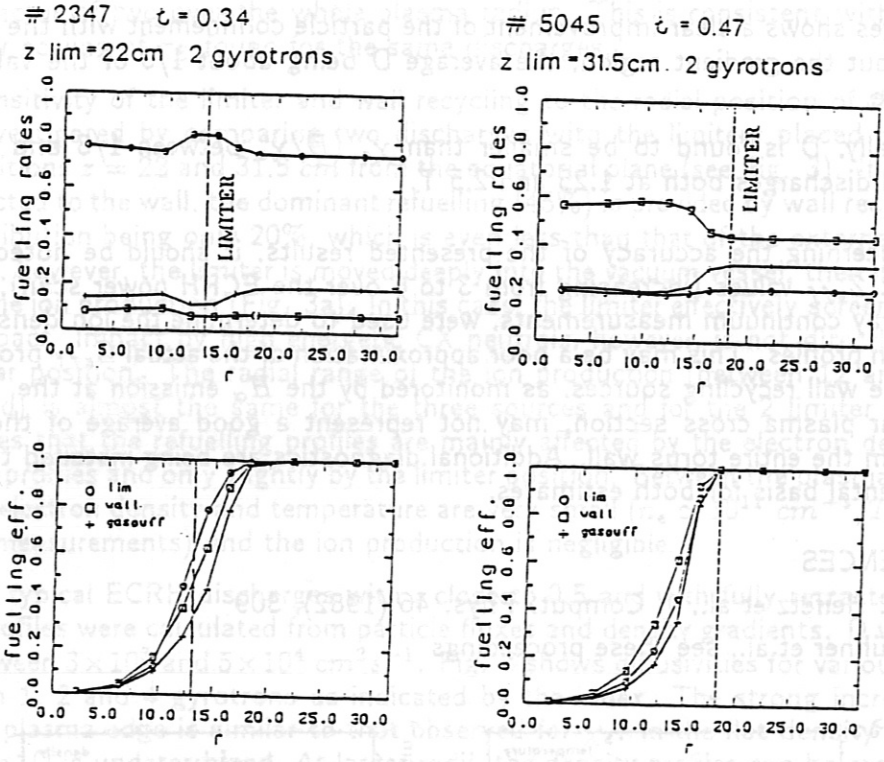

Fig. 3: Fuelling rates and fuelling efficiencies of limiter recycling, wall recycling and external gas feed for 2 different limiter positions.

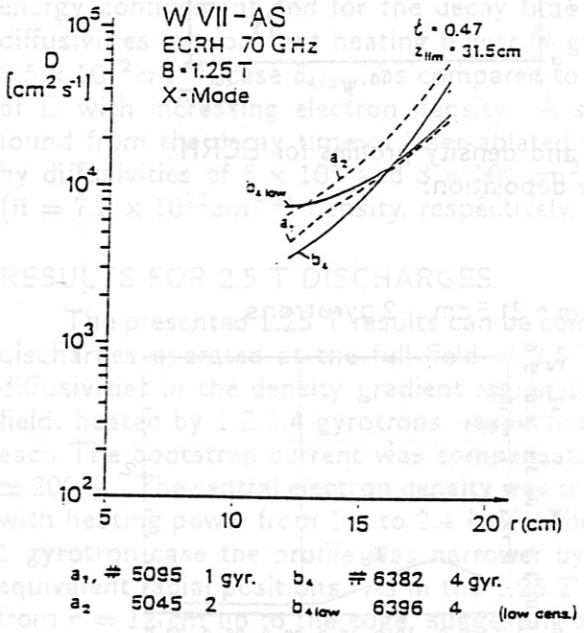

Fig. 4: Dependence of ion diffusivity profiles on ECRH power and electron density for 4 typical ECRH discharges at 1.25 T.

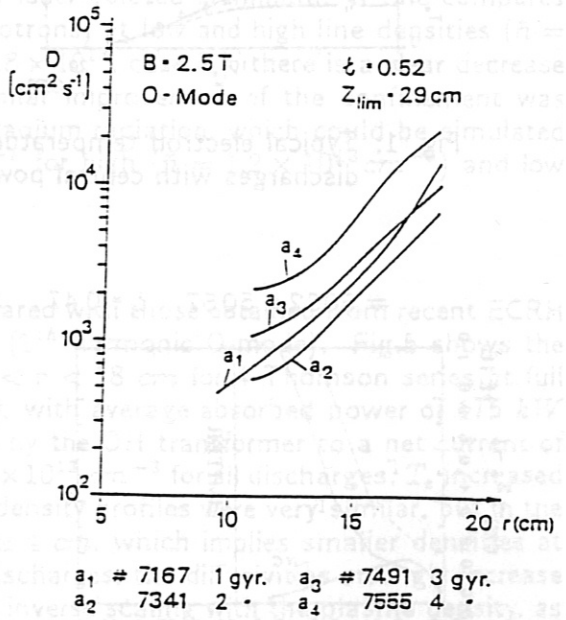

Fig. 5: Ion diffusivity profiles for 4 ECRH discharges at 2.5 T, heated by 1, 2, 3, 4 gyrotrons, respectively, with same central densities.

CURRENT DRIVE EXPERIMENTS AT THE ELECTRON CYCLOTRON FREQUENCY

V. Erckmann, U. Gasparino, H. Maaßberg, H. Renner, M. Tutter
W VII-AS Team
Max-Planck-Institut für Plasmaphysik,
EURATOM Association, D-8046 Garching, FRG

W. Kasparek, G.A. Müller, P.G. Schüller, M. Thumm
Institut für Plasmaforschung, Universität Stuttgart, FRG

1. Introduction

The experimental investigation of non-inductive current drive by electromagnetic waves in the electron cyclotron range of frequencies and the comparison with theoretical predictions attracts increasing interest in both, tokamak as well as stellarator research. In spite of the low current drive efficiency (compared to Lower Hybrid Current Drive) Electron Cyclotron Current Drive (ECCD) is a candidate for MHD-mode control and current profil shaping in tokamaks and stellarators due to the high localization of the driven currents and the capability to drive currents in the plasma centre in large machines. ECCD is an appropriate tool for the control of the pressure effects on the profile of the rotational transform, particularly the bootstrap current in stellarators. This is a crucial condition to maintain good confinement properties in low shear configurations such as W VII-AS /1/. Basic experimental investigations were performed at the W VII-AS stellarator, where the small EC-driven currents are not masked by large inductively driven currents as in tokamaks. The theoretical treatment of ECCD in stellarators would require a Fokker Planck solution in full phase space taking into account the complex magnetic field configuration (trapped particles, loss cone effects) which is untractable. In a first approach, we have compared our experimental data to a simple analytical current drive model (linearized in slab geometry) which is incorporated in a ray-tracing code /2/. In a second step, we have analysed the sensitivity of the model with respect to simplified assumptions on trapped particles and quasi-linear effects./3/.

2. ECCD Experimental Results, Comparison with Theory

The ECCD experiments were performed at the W VII-AS stellarator with up to 0.8 MW rf-power at 70 GHz. Up to four linearly polarized rf-beams were launched at the 2nd harmonic extraordinary wave polarization from the low field side. The resonant magnetic field and the cutoff density are 1.25 T and $n_{e,crit} = 3.1 \cdot 10^{19}$ m^{-3}, respectively. The rf-beams were directed towards the plasma at arbitrary toroidal launch angles by a set of independently movable focussing mirrors mounted inside the vacuum chamber /4/. An important input quantity for ECCD evaluations is the single pass absorption of the rf-waves, which was directly measured for perpendicular incidence by a 35 pick-up waveguide array mounted at the inner vessel wall opposite to the launching mirrors. In all cases discussed here, total absorption of the waves in a single transit through the plasma was found within the experimental errors.

The EC-driven current was experimentally determined by two different methods, where the pulse duration was chosen long enough to obtain stationary global plasma behaviour.

In a first experiment, the toroidal launch angle of the rf-beams was varied while the total net plasma current was kept close to zero ($I < 0.2$ kA) by feedback control with the OH-transformer. The change of the required loop voltage ΔU with respect to perpendicular launch

(no ECCD) was measured as a function of the launch angle. With the known plasma resistivity, which was measured independently, the EC-driven current was evaluated straightforward. This method is based on the assumption that the bootstrap current contribution remains constant, in other words, that the profiles of n_e and T_e do not change very much during the launch angle scan, which holds for small launch angles. Although the stored plasma energy changes from + 20 to - 40 % depending on counter- or co-current drive with respect to the bootstrap current, the energy change is < 10 % for launch angles < 10°. In Fig. 1 the loop voltage increment ΔU is plotted versus the toroidal launch angle at the resonance layer

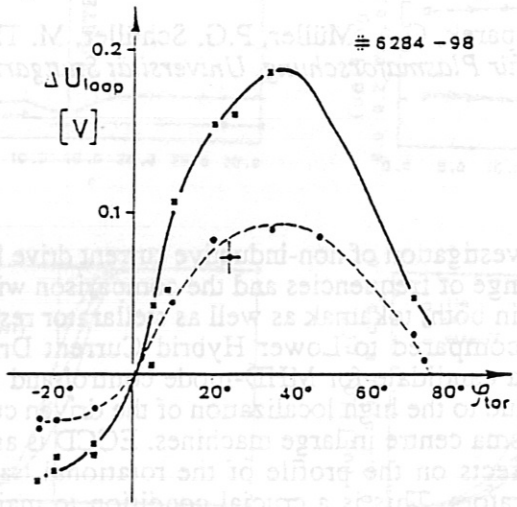

Fig. 1: Loop voltage increment ΔU_{loop} as a function of the launch angle φ_{tor} for discharges, where the net plasma current is controlled by inductive current drive (I_p < 0.2 kA). An rf-power of 0.35 MW (solid curve) and 0.17 MW (dashed curve) was applied for current drive.

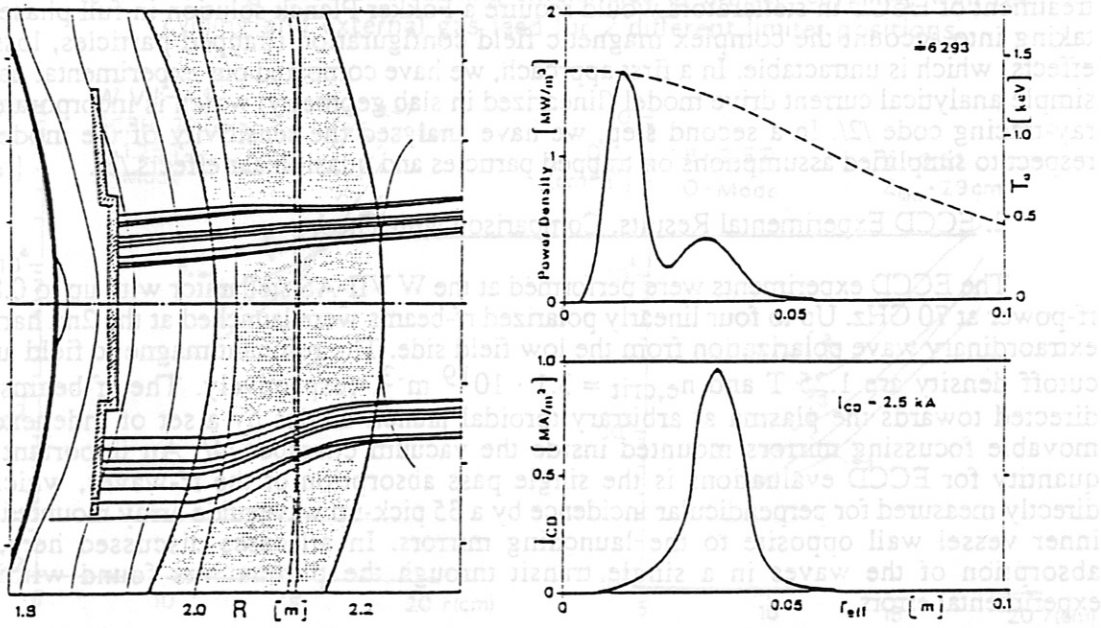

Fig. 2: LEFT: Ray-tracing geometry (horizontal cut in the z = 0 plane). The shady region indicates the plasma column. Two rf-beams are launched from the right (low field side), the upper one in perpendicular direction, the lower one with an oblique angle of 10°.
RIGHT TOP: EC-power deposition profile (solid curve), and electron temperature from Thomson scattering diagnostics (dashed curve).
RIGHT BOTTOM: Current density distribution as a function of the average minor radius.

including refractive effects for a total rf-power of 0.35 MW. The central plasma density and electron temperature measured by Thomson scattering was $n_{eo} = 2.2 \cdot 10^{19}$ m^{-3} and $T_{eo} = 1.6$ keV, respectively. Equivalent scans at lower densities show an increased contribution of suprathermal electrons, which is beyond the simplified Fokker-Planck model used here. The dashed curve is obtained for a scenario, where one rf-beam (0.17 MW) was launched perpendicularly and the launch angle of the second beam was scanned, the solid curve is obtained if the launch angle of both rf-beams is scanned together.

The result of a 3-D ray tracing simulation of the experiment based on the measured profiles of n_e and T_e is given in Fig. 2. In this example, one rf-beam is launched perpendicularly from the right (low field) side and a second beam is launched at 10° with respect to perpendicular, which finally results in 27° launch angle at the resonance layer due to beam deflection. The power deposition profiles as well as the driven current density distribution is also given as a function of the average minor radius. The perpendicular beam does not contribute to current drive. The EC-wave driven current is evaluated by an analytical model /4/ incorporated in the ray tracing code which gives an upper limit for ECCD because trapped particle effects are neglected. $Z_{eff} = 4$ was assumed. As seen from Fig. 3 (left), where the calculated total driven current is plotted versus the launch angle for one (0.17 MW, dotted line) and two rf-beams (0.35 MW, solid line), respectively, the experimental results are qualitatively well described. In particular, the launch angle for maximum current drive and the linear increase of ECCD with rf-power agree well. The absorption layer is shifted radially outward with increasing launch angle which is responsible for the decrease of the driven current at large launch angles, where T_e decreases, the fraction of trapped particles increases and the mismatch of the linear polarized wave increases.

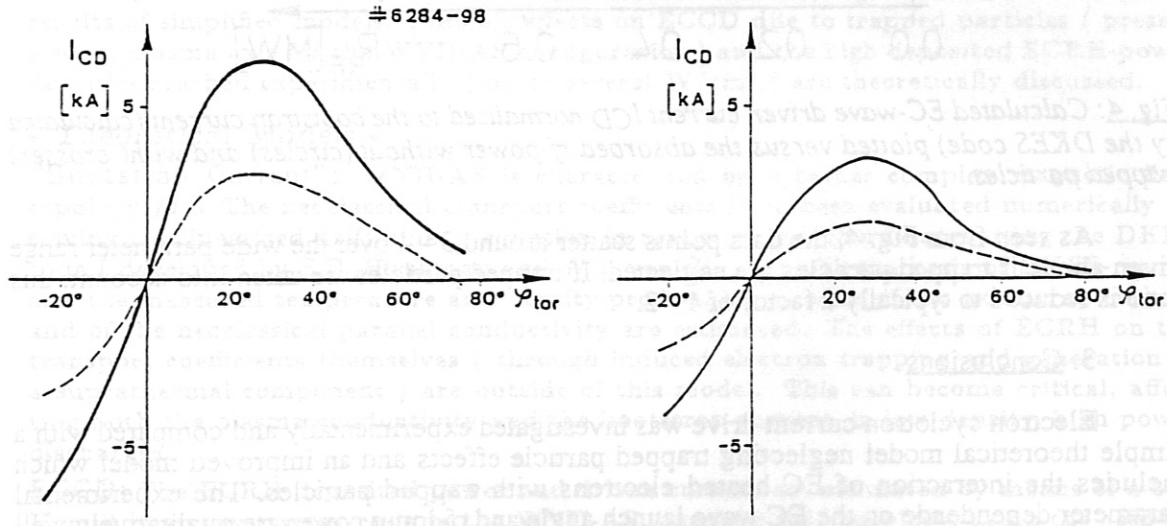

Fig. 3: Calculated EC-driven current for an rf-power of 0.17 MW (dashed curve) and 0.35 MW (solid curve) as a function of the rf-wave launch angle, where trapped particles are neglected (LEFT) and included (RIGHT) Both simulations are based on the measured profiles of n_e and T_e which are the same as in Fig. 1.

This simple ECCD model, however, overestimates the ECCD efficiency by typically a factor of 3 compared to the experimental findings, indicating that trapped particle effects can not be neglected. An improved version of the model /3, 5/ includes the interaction with a trapped particle population in the long mean free path regime of ~ 20 % on axis and ~ 40 % in the outer plasma region which is evaluated for the magnetic field topology in W VII-AS. As a result, the driven current is reduced to 60 % (Fig. 3 right).

In a second experiment, the launch angle of up to 4 rf-beams was adjusted to balance the bootstrap current without making use of the OH-transformer (counter current drive). Scanning the rf-power from 0.17 - 0.75 MW, the electron temperature from $0.8 < T_e < 1$ keV and the electron density from $1.1 < n_{eo} < 2.8 \cdot 10^{19}$ m^{-3}, the bootstrap current varies from $0.8 < I_{Boot} < 4.3$ kA

The total EC-wave driven current I_{CD} was again simulated as described previously. For the measured radial profiles of n_e and T_e, I_{CD} normalized to the bootstrap current I_{boot} is plotted versus the absorbed rf-power in Fig. 4. The dominant electron component of the bootstrap current ($T_e >> T_i$) was calculated by the DKES code which tends to underestimate the measurements /3/.

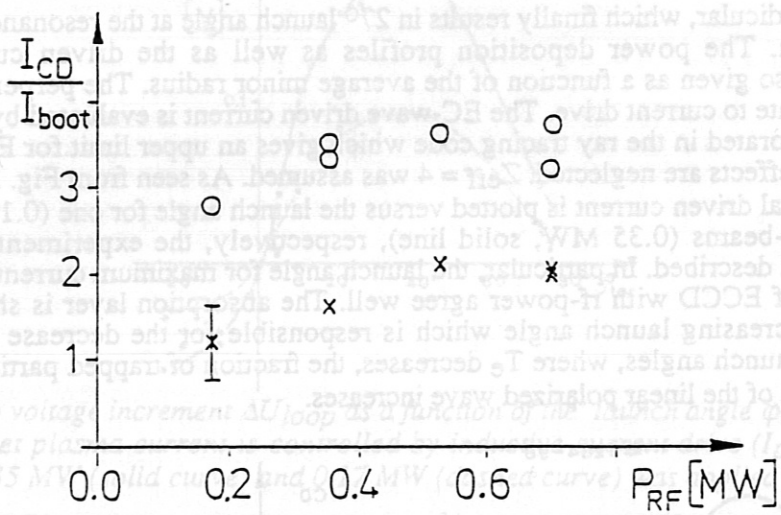

Fig. 4: Calculated EC-wave driven current I_{CD} normalized to the bootstrap current (calculated by the DKES code) plotted versus the absorbed rf-power without (circles) and with(crosses) trapped particles.

As seen from Fig. 4, the data points scatter around 3 - 4 over the wide parameter range given above if trapped particles are neglected. If trapped particles are taken into account, this ratio is reduced to typically a factor of 1 - 2.

3. Conclusions

Electron cyclotron current drive was investigated experimentally and compared with a simple theoretical model neglecting trapped particle effects and an improved model which includes the interaction of EC heated electrons with trapped particles. The experimental parameter dependende on the EC wave launch angle and rf-input power are qualitatively well described by both models. Quantitatively, however, the simple model neglecting trapped particles results in ECCD efficiencies which are typically a factor of 3 to 4 higher than the experimental data. This discrepency is reduced to values around 2 if a realistic population of trapped particles is included in the model. The sssremaining discrepency for both experimental scenarios is within the experimental uncertainties and the simplified assumption of the theory.

References

/1/ H. Renner et al., Plasma Physics and Contr. Fusion, 31, (1989), 1579-1596
/2/ U. Gasparino et al., Proc. 16th Europ. Conf. on Plasma Physics and Contr. Fusion, Venice, Italy, Vol. II, 631
/3/ U. Gasparino et al., this conference
/4/ V. Erckmann et al., Fusion Technology, Vol. 17, (1990), 76
/5/ M. Taguchi, Plasma Physics and Contr. Fusion 31 (1989), 241

NON-INDUCTIVE CURRENTS IN W VII-AS:
experimental results and theoretical modelling

U. Gasparino, V. Erckmann, H. Maaßberg, W VII-AS Team
Max-Planck Institut für Plasmaphysik
Association EURATOM-IPP, D-8046 Garching, FRG

ECRH Group
Institut für Plasmaforschung der Universität Stuttgart
D-7000 Stuttgart, FRG

• *Introduction* •

Stellarator-devices offer the possibility of studying non-inductive currents without the presence of a strong "obscuring" ohmic component. The net toroidal current (of the order of a few kA) observed during ECRH-discharges in W VII-AS (major radius R= 2 m, average minor radius $< a > = 0.2$ m) is modelled as the superposition of a neoclassical ("bootstrap") component and a component directly driven by the heating mechanism (ECCD: Electron Cyclotron Current Drive).
The boostrap current determined experimentally is (up to a factor of two) larger than the neoclassical predictions (for the electron contribution alone) based on the DKES code. The experimental dependence of ECCD on the toroidal injection angle of the waves is as expected theoretically and the experimental efficiency agrees fairly well with the results of simplified models. Possible effects on ECCD due to trapped particles (present also on plasma axis for the WVII-AS configuration) and the high deposited ECRH-power densities reached experimentally (up to several W/cm^3) are theoretically discussed.

• *Theoretical Models* •

"Bootstrap Current": WVII-AS is characterized by a rather complex magnetic field topology /1/. The neoclassical transport coefficients have been evaluated numerically by solving the linearized drift kinetic equation in magnetic flux coordinates using the DKES code (developed by S.P. Hirshman and W.I. van Rij /2/). On the basis of DKES-results and the measured temperature and density profiles, the profiles of the bootstrap current and of the neoclassical parallel conductivity are estimated. The effects of ECRH on the transport coefficients themselves (through induced electron trapping and generation of a suprathermal component) are outside of this model. This can become critical, affecting both the plasma conductivity and the bootstrap current, in low density, high power discharges.

ECCD: The ECRH deposited power and driven current are estimated by means of a 3-D Hamiltonian ray tracing code in the WVII-AS magnetic field topology, using the cold dispersion relation and an absorption coefficient for general angle of propagation (relativistic Doppler shifted resonance condition) based on a Maxwellian distribution function. Using the "adjoint property" of the linearized collisional operator, in the case of homogeneous plasma (no trapped particle effects) the evaluation of the driven current reduces to a convolution with the classical Spitzer function for the electric conductivity. This function can be evaluated very rapidly (in dependence of the effective charge Z_{eff}) using a sufficiently accurate energy polynomial expansion, the coefficients being determined through a variational principle /3/. This approach can be extented to include trapped particle effects in long mean free path regime (in this case a convolution with the neoclassical solution of the conductivity problem would appear). Introducing an approximate collision operator, the problem has been recently reduced to the solution of an ordinary differential equation in dependence of two parameters (Z_{eff} and f_t, the "fraction of trapped particles") /4/. While in /4/ the differential equation was solved through an expansion in Sonine polynomials (and evaluating the expansion coefficients from an infinite system of coupled

equations), we have used a generalization of the variational principle already used for the homogeneous case. In this way the driven current can be directly estimated by the ray-tracing with a minimum amount of computing time for both the case with and without trapped particle effects.
With the aim of investigating quasi-linear effects on the ECRH absorption and current drive, the non-linear Fokker-Planck equation solver /5/ has been implemented. The analyzed equation is of the type:

$$(\frac{\partial f_e}{\partial t})_{coll} + (\frac{\partial f_e}{\partial t})_{ECRH} + (\frac{\partial f_e}{\partial t})_{trap} + (\frac{\partial f_e}{\partial t})_{loss} = 0$$

where $(\partial f_e/\partial t)_{coll}$ is the collision operator, $(\partial f_e/\partial t)_{ECRH}$ the quasi-linear operator, the quasi-linear tensor component $D_{\perp\perp}(v_\parallel, v_\perp)$ being obtained by the ray-tracing, for a specific magnetic surface:

$$(\frac{\partial f_e}{\partial t})_{ECRH} = \frac{1}{v_\perp}\frac{\partial}{\partial v_\perp}[\, v_\perp D_{\perp\perp}(v_\parallel, v_\perp)\frac{\partial f_e}{\partial v_\perp}\,]$$

$(\partial f_e/\partial t)_{trap}$ an increment of pitch angle scattering in the loss-cone region of velocity space to force the fast isotropization of the bouncing trapped particles /6/:

$$(\frac{\partial f_e}{\partial t})_{trap} = \frac{1}{sin(\vartheta)}\frac{\partial}{\partial \vartheta}[\, \nu_{trap}(v,\vartheta)sin(\vartheta)\frac{\partial f_e}{\partial \vartheta}\,] \qquad (\ \vartheta \text{ being the pitch angle})$$

and $(\partial f_e/\partial t)_{loss}$, a model operator describing the energy loss (related to radial transport) in velocity space (necessary to reach a steady state in high power density conditions). Different models for the loss term have been analyzed: an isotropic convective term of the form $(\partial f_e/\partial t)_{loss} \propto (\, v^2 - < v^2 >) \cdot f_e$ (in case of an anisotropic distribution function also parallel momentum can be lost), the extension conserving parallel momentum and a loss term limited in the loss-cone region of velocity space (to simulate loss of electrons trapped in local magnetic mirrors).

• *Experimental Conditions* •

"Bootstrap Current": In ECRH-experiment a plasma is built up and heated, starting from a neutral gas target. Associated to finite plasma energy a net current is experimentally observed. This current reverses its sign by a reversal of the direction of the magnetic field and is interpreted as bootstrap current. Due to the strong correlation between the global energy confinement properties and the edge value of the rotational transform found in low-shear devices /7/, operation in the narrow ι regimes with optimum confinement during the whole duration of the discharge required external current control, in most cases by a small loop voltage.

ECCD: Two main ECCD-scenarios have been analyzed experimentally /8/. In the first case the ECCD was used to counterbalance the bootstrap current, the ECCD-efficiency being obtained in unit of bootstrap current. In the second scenario, the ECRH-beams with perpendicular launching were replaced by other ECRH-beams with oblique launching and equivalent power, the toroidal launch angle ($k_\parallel$-spectrum) was changed shot by shot. Due to the strong relation between confinement properties and boundary value of the rotational transform, the total plasma current was controlled by the Ohmic-transformer. Nevertheless, changes in the current profiles affected the global confinement properties and macroscopic consequences could be observed in the plasma energy content ($\Delta W_p/W_p$ up to $-40 \div +20\%$ for ECCD co- and counter-bootstrap, respectively).

• *Theory vs. Experiment* •

"Bootstrap Current": Fig. 1 shows the result of the analysis of the current behaviour for series where temperature and density profiles have been measured by Thomson scattering ($0.9 \cdot 10^{13} < n_{e,0} < 4.5 \cdot 10^{13}$ cm^{-3} ; $0.4 < T_{e,0} < 2.5$ keV). The EC-waves were injected perpendicularly (with respect to the magnetic field direction) so that the contribution of ECCD should be minimized. In the figure, I_{pi} and V_{loop} correspond to the measured

net current and loop voltage respectively, while $I_{boot,DKES}$ and R_{DKES} are the predicted bootstrap current and plasma resistance. The sign of the current reverses, reversing the magnetic field, only the absolute value is reported in the figure. The observed deviation from the expected one to one proportionality can be compensated only partially by the ion bootstrap component (not included in the present theoretical analysis due to the experimental uncertainty in the ion temperature profiles, but estimated to be less than 30% of the electron contribution), whereas at low density the ECRH-induced suprathermal component (experimentally observed), decreases the plasma resistance and increases the discrepancy. Uncertainty in Z_{eff} plays a minor role (I_{boot} and V_{loop}/R show a quite similar Z_{eff} dependence).

ECCD: In (X)-mode, 2^{nd}-harmonic, resonance on axis ECCD-experiments the r.f. power is expected to be absorbed by thermal electrons and the central plasma region is in long mean free path regime. In WVII-AS a non-negligible amount of trapped electrons is present also on plasma axis. The "fraction of trapped particles" f_t on axis is $\approx 20\%$, around $\epsilon = 1/3$ and $\approx 25\%$ for $\epsilon \approx 1/2$. At the plasma edge f_t reaches values of $\approx 40 \div 50\%$. The presence of these trapped electrons would tend to decrease the ECCD-efficiency: power directly absorbed by them doesn't contribute to ECCD; trapping (ECRH increases the perpendicular energy) of passing particles causes a contribution opposite to the Fisch-Boozer one; the parallel momentum collisionally transferred from passing to trapped particles is lost. While the first two mechanisms strongly depends on the position of the resonance and can be minimized moving the resonance close to the maximum of the magnetic field, the third one would always be present. In the WVII-AS experimental conditions these effects reduce the ECCD-efficiency typically $30 \div 40\%$. Up to an angle of $\approx 30°$ from perpendicular this reducing factor is nearly independent of the launching angle itself. For bigger injection angles the current evaluated with trapped particles shows a steepler decay and it can even slightly reverse its sign (trapping effect overcompensating the Fisch-Boozer mechanism). The very good qualitative agreement found between the experimental and the theoretical dependence of ECCD on launching angle /9/ is valid for both approaches. At the large injection angles, where the efficiency with trapped particles decays more steeply, the ECCD-efficiency is low and the uncertainty (profile effects, deposition profile, percentage of the power coupled as X-mode) is too large to permit a discrimination /8/.
By means of the model Fokker-Planck equation the dependence of the ECCD-efficiency on input power was analyzed. The results related to a discharge where the EC-driven current was counterbalancing the bootstrap component are shown in Fig. 2 for the effective radius where the maximum deposition occurs ($r_{eff} = 1.5$ cm). At power densities greater than 5 W/cm^3 the efficiency starts to degrade. The case with and without trapped particles shows a very similar qualitative behaviour. The dependence on the energy loss model is analyzed for the case corresponding to 10 W/cm^3. The full points above the curves correspond to the ripple loss model, the ones below to the isotropic convective loss model while the two curves were obtained using the parallel momentum conserving convective loss model. For low power density the dependence on the loss model vanishes.
The quantitative analysis of the ECCD-efficiency has brought to quite similar results for all the cases analyzed up to now. As a representative example, we report on the results relative to the series of Fig. 2. Here the EC-driven current (four gyrotrons) counterbalances (within few hundreds A) the bootstrap component. No loop voltage being applied (so that in the analysis the uncertainty in the plasma conductivity could be avoided). For $Z_{eff} = 4$ the bootstrap current evaluated by DKES is $I_{boot,DKES} = 2.7$ kA, the ECCD-driven current evaluated by the ray-tracing is $I_{ECCD,hom} = 8.5$ kA neglecting trapped particles, while with trapped particles it is reduced to $I_{ECCD,t.p.} = 5.2$ kA. Recalling that $I_{boot,DKES}$ represents probably an underestimation (recall Fig. 1), the efficiency with trapped particles is within the rather large "error bars" of the analysis. This conclusion is only slightly dependent on the assumed value for Z_{eff}. Although deposited power densities up to 50 W/cm^3 are evaluated by the linear ray-tracing in case of high input power and peaked on-axis deposition, there is no experimental evidence for a degradation of the ECCD-efficiency, X-mode, 2^{nd} harmonic launching, so far.

• *Conclusions* •

A simplified theoretical approach describing the plasma current as the superposition of a bootstrap and a ECCD-component, independently evaluated, agrees fairly well with the experimental findings. Considering the complexity of the problem, where transport, quasi-linear and trapped particle effects are strongly linked together in the magnetic topology of WVII-AS stellarator this result is fairly satisfactory. More definite conclusions on the role played by trapped particles and high power densities on the ECCD-efficiency will be obtained by more appropriate experimental investigations (e.g. ECCD in local minima of the magnetic field and highly localized input power).

• *References* •

/1/ J. Kisslinger et al., Fusion Tech. (Proc. 12th Symp. 1982), Pergamon (1983), 1051
/2/ S.P. Hirshman et al., Phys. Fluids 29 (1986), 2951
/3/ S.P. Hirshman, Phys. Fluids 23 (1980), 1238
/4/ M. Taguchi, Plasma Phys. and Contr. Fus. 31 (1989), 241
/5/ A.A. Mirin et al., Comp. Phys Comm. 51 (1988) 373
/6/ Yu.N. Dnestrovskij et al., Nucl. Fus. 28 (1988),267
/7/ H. Renner et. al., Plasma Phys. and Contr. Fus. 31 (1989), 1579
/8/ V. Erckmann et al., this conference
/9/ U. Gasparino et al., (Proc. 16th EPS, Venice 1989), Vol. II, 631

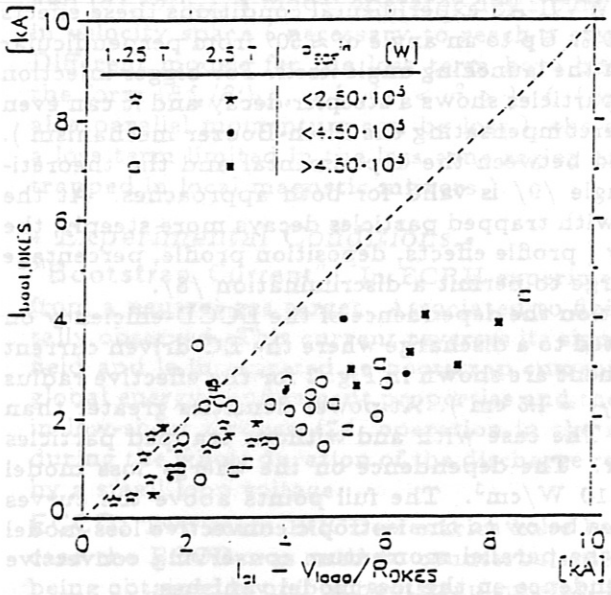

Fig. 1

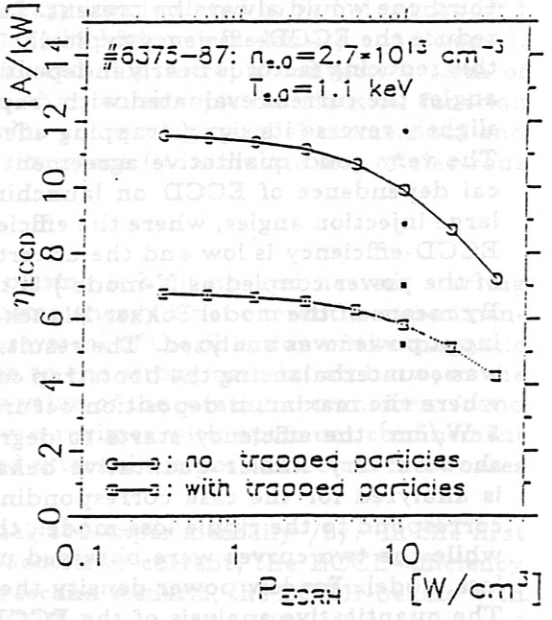

Fig. 2

• *Figure Captions* •

Fig. 1: Current components for the shots where density and temperature profiles have been measured by Thomson scattering. I_{pl} and V_{loop} corresponds to the measured net current and loop voltage, $I_{boot.DKES}$ and R_{DKES} are the predicted bootstrap current (only electron contribution) and plasma resistence. A one to one proportionality should be expected.

Fig. 2: ECCD-efficiency as a function of the absorbed power density. The full points corresponding to P_{ECRH} = 10 W/cm³ show the dependence on the model used for the energy loss term. At low power densities this dependence becomes negligible.

LIMITER LOAD AND REDISTRIBUTION OF MATERIALS DURING THE FIRST OPERATIONAL PERIOD OF THE WENDELSTEIN VII-AS STELLARATOR

P. Grigull, R. Behrisch, R. Brakel, I. Lakicevic,
V. Prozesky, H. Renner, J. Roth, WVII-AS Team[a)]
MPI Plasmaphysik, EURATOM Ass., Garching

Results of the phaseI limiter calorimetry and a long-term collector probe analysis of the Wendelstein VII-AS stellarator are reported. Limiter loads are related to the magnetic field parameters, heating schemes, and, as far as available from phaseI diagnostics, to SOL data. The distribution of deposited materials is phenomenologically discussed, considering the machine history as well as some tendencies which are obvious from spectroscopy.

Up to 40% (ECH, NBI) or 80% (OH), respectively, of the heating energy are deposited to the top and bottom movable main limiters (TiC-coated graphite, $0.25m^2$ each). For ECH this portion seems to depend on the geometry of the heating power deposition. In all cases a strong top-to-bottom asymmetry is observed which corresponds to the $\nabla B \times B$ direction.

Maximum limiter surface temperatures are estimated to be in ranges where excessive chemical sputtering has not to be expected.

The collector probe analysis indicates that mainly stainless steel components (originating from the torus wall and/or some installations), Titanium and Carbon (from limiters and shieldings) are redistributed. In the limiter plane, deposited steel components and Ti are strongly peaked at the probe nearest to the limiter. In a corresponding poloidal plane away from the limiters Fe, Cr, and Ni are peaked at the top and bottom but Ti is nearly absent. A probable scenario is that steel components are deposited to the limiters during He-glow discharges (standard cleaning procedure) and then released and redistributed by the plasma shots. This is supported also by spectroscopic data.

[a)] R. Brakel, R. Burhenn, G. Cattanei, A. Dodhy, D. Dorst, A. Elsner, K. Engelhardt, V. Erckmann, U. Gasparino, G. Grieger, P. Grigull, H. Hacker, H.J. Hartfuß, H. Jäckel, R. Jaenicke, S. Jiang[1)], J. Junker, M. Kick, H. Kroiss, G. Kuehner, I. Lakicevic, H. Maaßberg, C. Mahn, T. Mizuuchi[2)], W. Ohlendorf, F. Rau, H. Renner, H. Ringler, J. Saffert, J. Sanchez[3)], F. Sardei, M. Tutter, A. Weller, H. Wobig, E. Würsching, M. Zippe.

[1)] *Southwestern Inst. of Physics, Leshan, China*
[2)] *Plasma Phys. Lab., Kyoto University, Japan*
[3)] *CIEMAT, Madrid, Spain*

RESULTS FROM X-RAY MEASUREMENTS ON THE WENDELSTEIN W7-AS STELLARATOR

A. Weller, R. Brakel, R. Burhenn, H. Hacker, A. Lazaros
W7-AS Team, ECRH Group, ICRH Group, NI Group, Pellet Injection Group

Max-Planck-Institut für Plasmaphysik, EURATOM Ass.
Garching bei München, FRG

Introduction - X-ray imaging measurements have contributed to studies of the plasma equilibrium, plasma fluctuations, impurity radiation and impurity transport effects in the advanced stellarator WENDELSTEIN W7-AS (R = 2 m, a = 17 cm). In addition, time resolved electron temperature profiles are deduced from X-ray intensity ratios according to the two absorber foil method. The plasma is generated and heated by fundamental and 2nd harmonic ECRH ($P \leq 800\ kW$ at 70 GHz). Neutral beam injection heating ($P \leq 1.5\ MW$) was applied also, assisted by D_2 pellet injection.

X-ray measurements - Two X-ray imaging arrays are installed at the toroidal location of "triangular" flux surfaces. They are inclined by an angle of $\pm 37.4^o$ with respect to the horizontal midplane. Each of the X-ray cameras is viewing the entire plasma along 36 equally spaced lines of sight. A variety of X-ray absorber foils (Be) can be used to suppress radiation below the filter cut off energies or outside the hot central core of the plasma, respectively. An illustration of X-ray intensity profiles and the effect of the absorber foils is given in fig. 1 (data from upper camera).

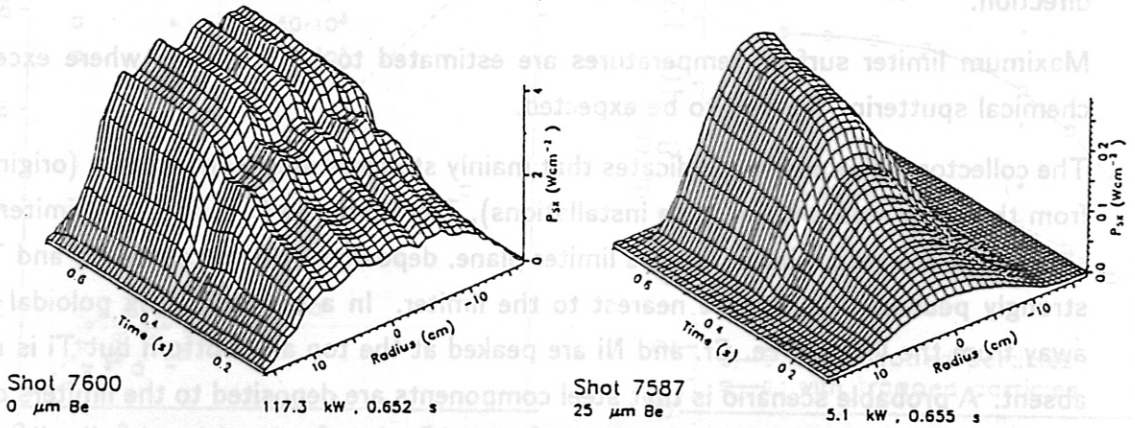

Fig. 1 : *Comparison of X-ray intensity profiles obtained without filter (left) and with 25 μm Be-foil (ECRH at $B_T = 2.5\ T$, $\iota \simeq 0.52$).*

For the electron temperature evaluation another soft X-ray camera system is used, which views the plasma at a toroidal location, where the flux surfaces are elongated in the direction of the observation (almost vertical). The measurements are made at 12 radial positions by a set of 24 large detectors arranged in pairs for intensity ratio determination with foils of different thicknesses.

Equilibrium studies - Generally the X-Ray profiles are consistent with equilibrium calculations based on the GOURDON -, KW - and TRANS - Codes [1.2], if the emissivity is assumed to be constant on magnetic surfaces. Smooth triangular flux surfaces are predicted for the low ι case, whereas at higher ι a clear ripple structure appears on the outer flux surfaces with the formation of a separatrix. This structure is observed in the steady state profiles, if no filter for the radiation is used and most of the intensity is due to very soft radiation ($300\ eV \lesssim E \lesssim 800\ eV$) from the outer part of the plasma. Figure 2 illustrates the agreement between the observed line integrated X-ray intensity profiles

and simulations by assuming constant emissivity profiles on the calculated flux surfaces (fig. 2, right).

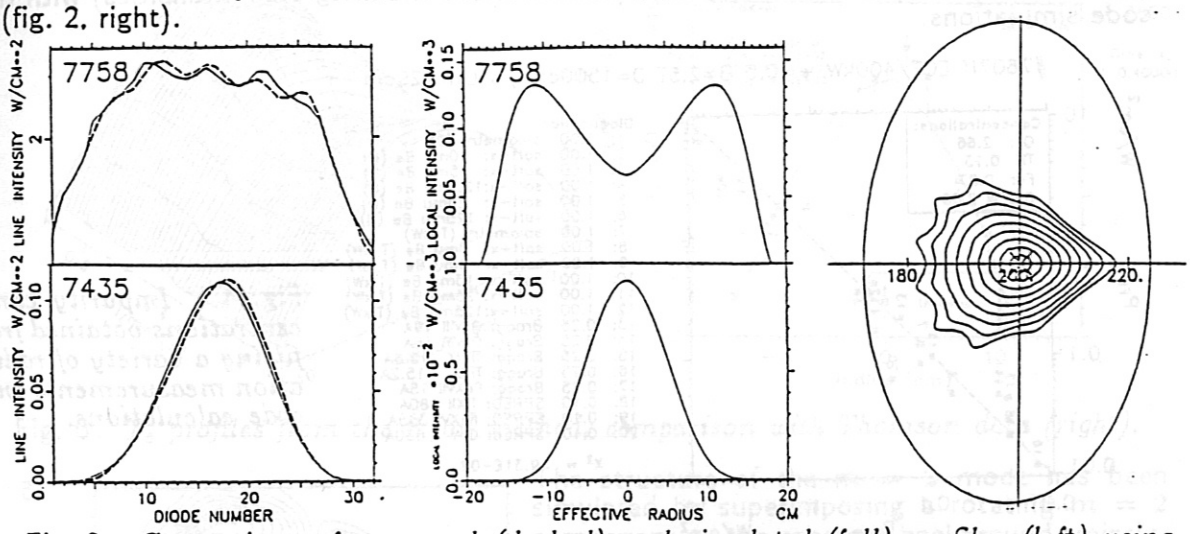

Fig. 2 : *Comparison of measured (dashed) and simulated (full) profiles (left) using a hollow (no filter, top) and a peaked (50 μm Be-filter, bottom) emissivity (middle), constant on flux surfaces (right); ECRH, $\iota(a) = 0.52$.*

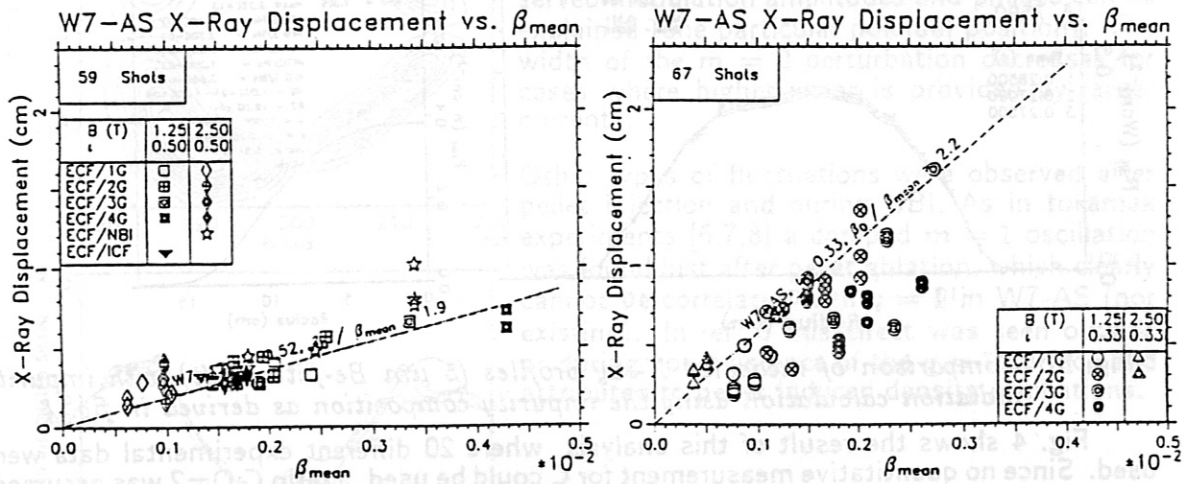

Fig. 3 : *Displacement of X-ray profiles (T_e camera, 125 μm Be-filter) due to the Shafranov shift as a function of $\langle\beta\rangle$. Left: data with $\iota \simeq 0.5$, right: $\iota \simeq 0.33$. Comparison with predictions for W7-AS.*

For W7-AS a reduced Shafranov shift is expected (factor $\simeq$ 2) compared with a conventional l=2 stellarator [3]. In agreement with first magnetic measurements a shift of the X-ray profiles depending on β and ι was found as can be seen from fig. 3. The statistical analysis was done using the X-ray temperature camera (125 μm Be filter data) and selecting series of shots for which Thomson profiles were available. The displacement was determined by taking the 1^{st} moment of the profile data at the time of the Thomson measurements subtracting the value obtained at very low plasma energy in the same shot. Fig. 3 also contains the predicted curves for the axis shift for W7-AS.

Impurity studies - X-ray intensity profiles obtained using various absorber foils have been incorporated in the impurity analysis. The code IONEQ [4] calculates the radiation of the main impurities C,O,Fe,Ti including transport, which was modelled based on the STRAHL code [5]. The diffusion coefficients were determined by Al-injection ($D = 1000-2000\, cm^2 s^{-1}$ for ECRH at 2.5 T). The impurity concentrations were evaluated finally by a

least square fit of individual line intensities (SPRED-,Bragg-spectrometers), total radiation (bolometer system) and the X-ray data (central chord and integrated intensities) with the code simulations.

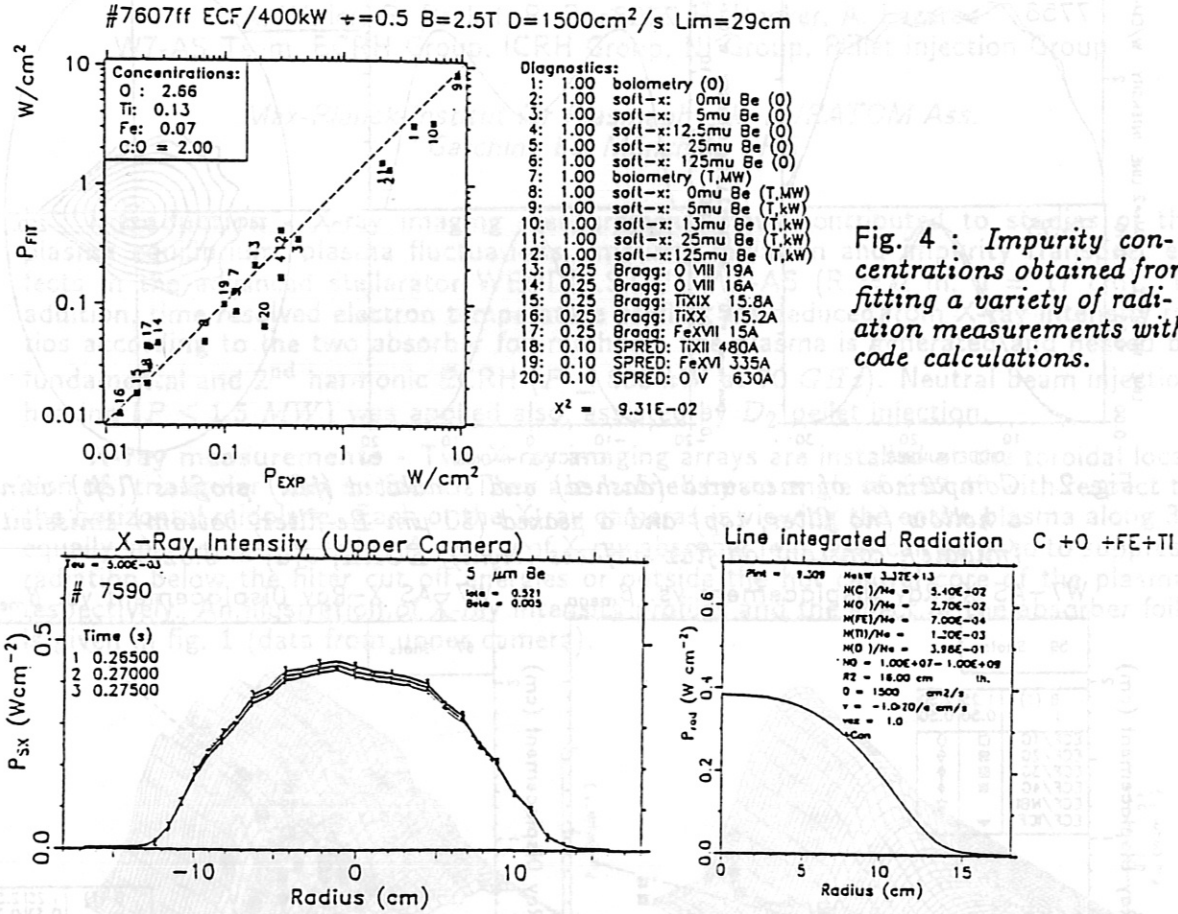

Fig. 4 : *Impurity concentrations obtained from fitting a variety of radiation measurements with code calculations.*

Fig. 5 : *Comparison of measured X-ray profiles (5 μm Be-filter, left) with impurity radiation calculation using the impurity composition as derived in fig. 4.*

Fig. 4 shows the result of this analysis, where 20 different experimental data were used. Since no quantitative measurement for C could be used, a ratio C:O=2 was assumed. A measured X-ray profile is compared in fig. 5 with a simulation taking the fitted impurity composition, which corresponds to $Z_{eff} \simeq 5$. The impurity level increases with the applied heating power and decreases with density. The radiated power is well below the heating power in ECRH plasmas but in high density NBI discharges radiation cooling effects are observed.

Temperature analysis - The electron temperature is derived from comparing the observed intensity ratios (2 different Be-filters) with values calculated by IONEQ. Impurity radiation of C,O,Fe and Ti (including line radiation) are taken into account. At $T_e \gtrsim 1\,keV$ the relative contribution of metals has to be known, since high energy lines become important. Fig. 6 shows the evolution of the T_e profile, which agrees well with the Thomson data, if the metals are included in the calculation.

Fluctuations - Optimized discharges are very quiescent due to the absence of large currents, but mode activity was observed, when the net toroidal current exceeds $\simeq 2\,kA$ and rational surfaces are created inside the plasma.

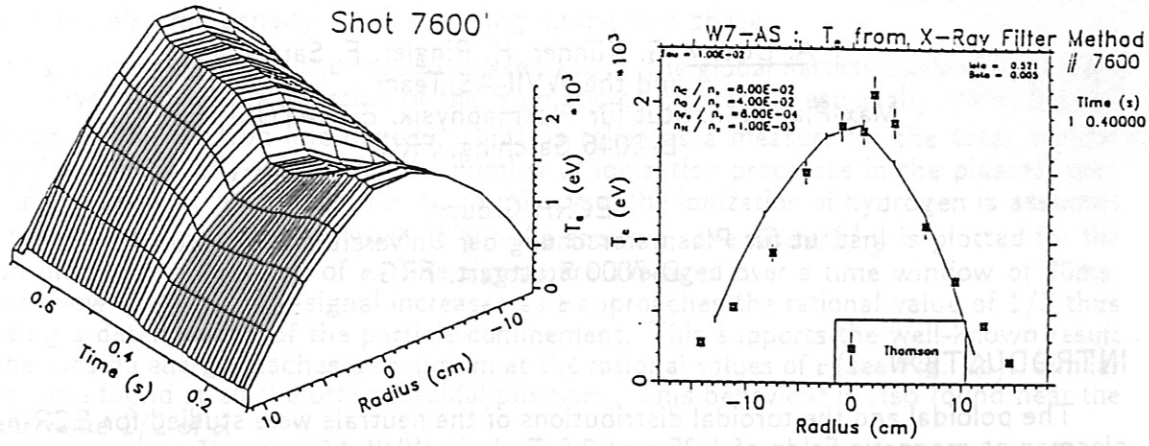

Fig. 6 : *T_e profiles from the 2 foil method, comparison with Thomson data (right).*

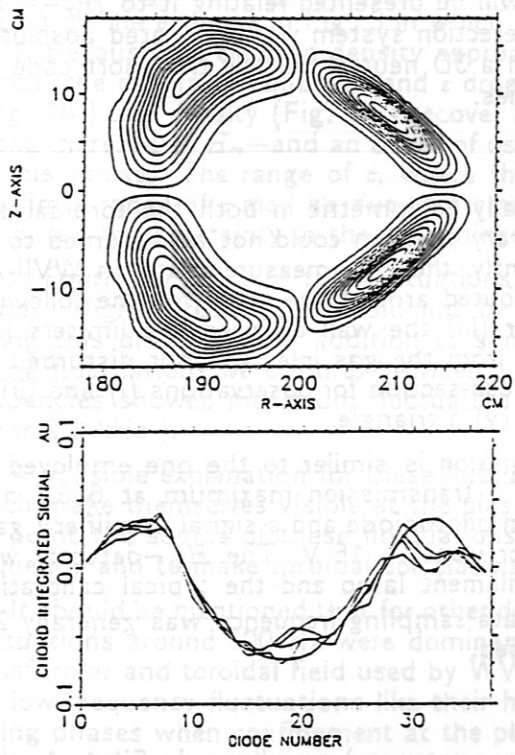

The structure of the $m = 2$ mode has been simulated by superimposing a rotating $m = 2$ component on the constant background emissivity following the flux surfaces. Fig. 7 shows the rotating part of the emissivity, by which the observed modulation amplitudes and phases can be explained (one particular poloidal position). The width of the $m = 2$ perturbation decreases for cases where higher shear is provided by larger currents.

Other types of fluctuations were observed after pellet injection and during NBI. As in tokamak experiments [6,7,8] a damped $m = 1$ oscillation was found just after pellet ablation, which clearly cannot be correlated with $q = 1$ in W7-AS (not existing). In ref. 6 this effect was seen outside or during non-existence of the $q = 1$ surface and attributed to pellet induced density oscillations.

Fig. 7 : *$m = 2$ mode simulation (fluctuating part of profile). Simulated and measured line integrated profiles (bottom).*

References

[1] Kisslinger, J., Wobig, H., in Controlled Fusion and Plasma Physics (Proc. 12th Europ. Conf. Budapest, 1985), Part I (1985) 453.
[2] Sardei, F., Richter-Gloetzl, M., private communication.
[3] Herrnegger, F., 5th Intern. Workshop on Stellarators, (Proc. of the IAEA Technical Committee Meeting on Plasma Confinement and Heating in Stellarators, Schloss Ringberg (FRG), 1984), Vol. 1, CEC, Brussels (1984) 401.
[4] Weller, A. et al., JET-IR-(87)10 (1987).
[5] Behringer, K., JET-R-(87)08 (1987).
[6] Parker, R. et al., Nucl. Fus. 27 (1987) 853.
[7] Kornherr et al., in Controlled Fusion and Plasma Physics (Proc. 14th Europ. Conf. Madrid, 1987), Part I (1987) 323.
[8] Weller, A. et al., Phys. Rev. Lett. 59 (1987) 2303.

H_α–SPECTROSCOPY ON WVII-AS

A. Dodhy, G. Kühner, H. Ringler, F. Sardei
and the WVII-AS Team
Max-Planck-Institut für Plasmaphysik, EURATOM Ass.
D-8046 Garching, FRG

ECRH Group
Institut für Plasmaforschung der Universität Stuttgart
D-7000 Stuttgart, FRG

INTRODUCTION

The poloidal and the toroidal distributions of the neutrals were studied for ECR-heated plasmas at magnetic fields of 1.25 and 2.5 Tesla in WVII-AS using H_α–spectroscopy. In this paper the dependence of the plasma confinement on various plasma parameters such as magnetic configuration, heating and density will be presented relating it to H_α–fluxes and fluctuations of the H_α–signal. The H_α–detection system was calibrated absolutely so that the H_α–fluxes could be used directly in a 3D neutral particle transport code for evaluation of the absolute neutral particle densities.

EXPERIMENTAL

As the distribution of the neutrals is generally asymmetric in both the toroidal and the poloidal directions, observations at an arbitrary position could not be assumed to be representative of the entire machine. Consequently, the H_α–measurements on WVII-AS were initially carried out at five positions distributed around the torus for the following observations: (i) top limiter (ii) bottom limiter (iii) the wall between the limiters (iv) the wall near the gas inlet and (v) the wall far from the gas inlet and not disturbed by components built in the machine. The plasma cross-section for observations (i) and (ii) is elliptical, for (iii) a tilted ellipse and for (iv) and (v) a triangle.

The detection system used for the H_α–emission is similar to the one employed at TEXTOR [1]. It consists of the light filtering (transmission maximum at 656.3 nm, bandwidth = 4 nm) and imaging optics, a silicon photodiode and a signal amplifier (gain factor 10). The dynamic range of the detector was 0 - 15 V. The H_α–detector was absolutely calibrated by means of a tungsten filament lamp and the typical calibration factors were $1.0 \cdot 10^{12}$ photons/Volt-sec. The data sampling frequency was generally 2.5 or 5.0 kHz. For several cases 25 kHz was also used.

RESULTS AND DISCUSSION

H_α–signals for an ECR-heated plasma (two gyrotrons) are shown in Fig.1. In this case the total rotational transform, ι, was 0.48, the electron line density was controlled by a feedback mechanism to the gas puffing and the plasma current was kept constant using the Ohmic transformer. From these signals, it is seen that the H_α–fluxes from the limiters are significantly larger than those from the torus wall. Furthermore, the asymmetry of the limiter signals grows as a function of time. With a few exceptions, these asymmetries were almost always present and were dependent on the discharge conditions such as the absolute value of the gas flux. The limiter asymmetries seen in the H_α–signals were also observed in limiter calorimetry measurements [2]. Note, that the difference in the signals between the wall (undisturbed) and those from the wall near the gas puff gives the contribution of the external gasflux to the H_α–signal. Finally, the increase in the H_α–signal at 610 ms at all toroidal positions corresponds to the switching-on of the second gyrotron. As

the H_α—emission is sensitive to fast changes in the particle confinement, this increase is an indication of the deterioration of the particle confinement with increasing heating power although the electron density was decreasing during this phase.

Using signals similar to the ones discussed above, the global particle confinement time, τ_p , was investigated as a function of the magnetic configuration, especially the rotational transform. If the electron line density, $\int ndl$, is taken as a measure for the total number of particles and the H_α—signal for the number of ionization processes in the plasma, then $\int ndl/H_\alpha$—is a relative measure for τ_p. In this case, the ionization of hydrogen is assumed to be the dominating particle source. Figure 2a shows a case where $1/\tau_p$ is plotted for the bottom limiter as a function of ι. The signals are averaged over a time window of 30ms. Results show that the H_α—signal increases as ι approaches the rational value of 1/3 thus indicating a deterioration of the particle confinement. This supports the well-known result that the plasma energy reaches a minimum at the rational values of ι (see Fig. 2b). Similar results were found at all the other toroidal positions. This behaviour is also found near the rational value 1/2 of ι.

Another indication for the poor particle confinement was the increase in the fluctuations of the H_α—signal during the transition through the rational values of ι. This is demonstrated by the example in Fig. 3 in which the plasma was heated using one gyrotron (200 kW). Because the electron density approaches the cut-off density for X-mode ECR power launch, the discharge collapses and ι drops very fast below 1/2 (Fig. 3a). Total energy (Fig. 3b) and density (Fig. 3c) recover again after a slow transition through $\iota = 1/2$. A strong increase of H_α—and an onset of oscillations of the H_α—signal (Fig. 3d) is typical for this phase. The range of ι, where this transition takes place is indicated in Fig. 3. The finite range of ι may be due to a small shear and the apparent shift of the ι scale is attributed to uncertainty in the determination of the absolute ι values.

A Fourier analysis of the fluctuations was made and frequencies up to 2.5 kHz were found. Higher frequencies could not be analyzed due to the sampling frequency used during this discharge. In addition to some low frequency fluctuations (50 - 400 Hz), strong fluctuations were found between 1.8 - 2.5 kHz. Time dependence of the individual frequencies showed maximum fluctuation amplitudes during poor confinement (see Fig. 3e for 2.3 kHz).

A possible explanation for these fluctuations are MHD activities present in the plasma which make themselves visible at the plasma edge when the latter is unstable. In order to pin point the source of these fluctuations, efforts are underway to increase the sampling frequency and to make toroidal correlations.

It should be mentioned that for other discharges investigated in WVII-AS, low frequency fluctuations around 300 Hz were dominant. These are attributed to the ripple on Ohmic transformer and toroidal field used by WVII-AS. Interestingly enough it was observed that the low frequency fluctuations like their high frequency counterparts were also maximum during phases when confinement at the plasma edge was poor owing to the presence of a rational surface.

Other studies included the dependence of the global particle confinement time on the ECR-heating power for various discharge conditions. For all cases, it was seen that τ_p decreases with increasing heating power. Calculations performed for the ion diffusion rates [3] and for the energy confinement times [4] support this result.

Furthermore, the global particle confinement time increases as a function of the electron density. This was investigated for an ECR-heated plasma (750 kW) at 1.25 Tesla and $\iota = 0.31$. As $\int ndl$ was increased from $3.5 \cdot 10^{18}$ to $7.5 \cdot 10^{18}/m^2$, τ_p increased at least by a factor 1.5 at all the toroidal positions of H_α—observation.

REFERENCES

[1] T.Uckan, ORNL Report, TM-10698, May 1988.

[2] P. Grigull et al., To be published in the Proceedings of the ninth PSI Conference, 21.-25. May, 1990, in Bournemouth, U. K.

[3] F.Sardei et al., see these proceedings.

[4] G.Kühner et al., see these proceedings.

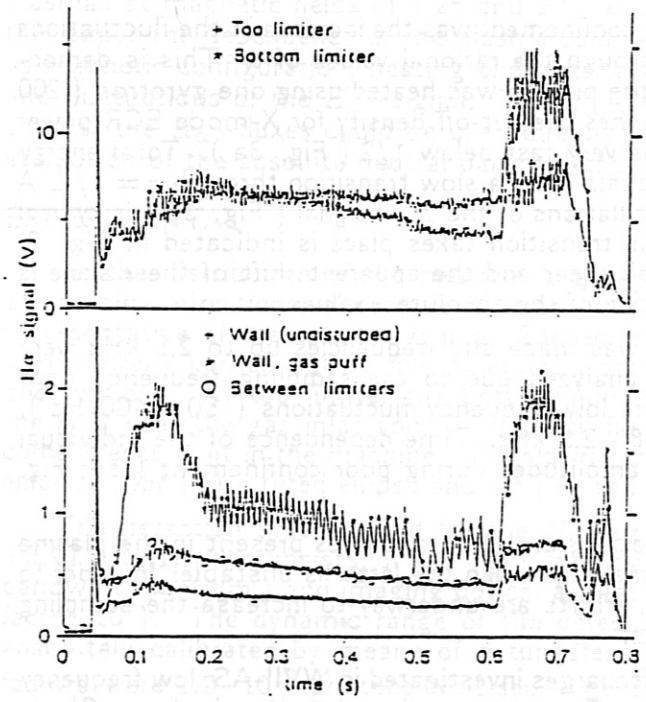

Fig. 1. H_α—signals at five toroidal positions for an ECR- heated plasma. The second gyrotron was switched on at 610 ms.

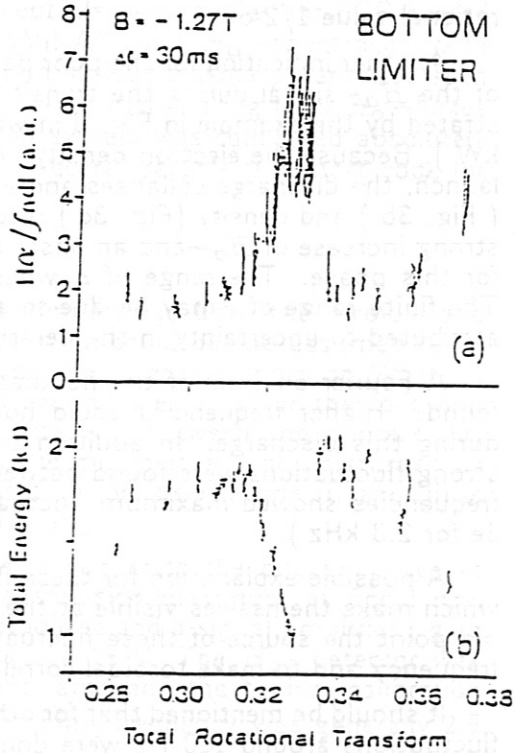

Fig. 2. a) H_α—signal normalized to the electron line density for the bottom limiter as a function of the total rotational transform. The H_α—signal increases as the rotational transform approaches the rational value 1/3, indicating a deterioration of the particle confinement. b) The corresponding deterioration of the energy confinement.

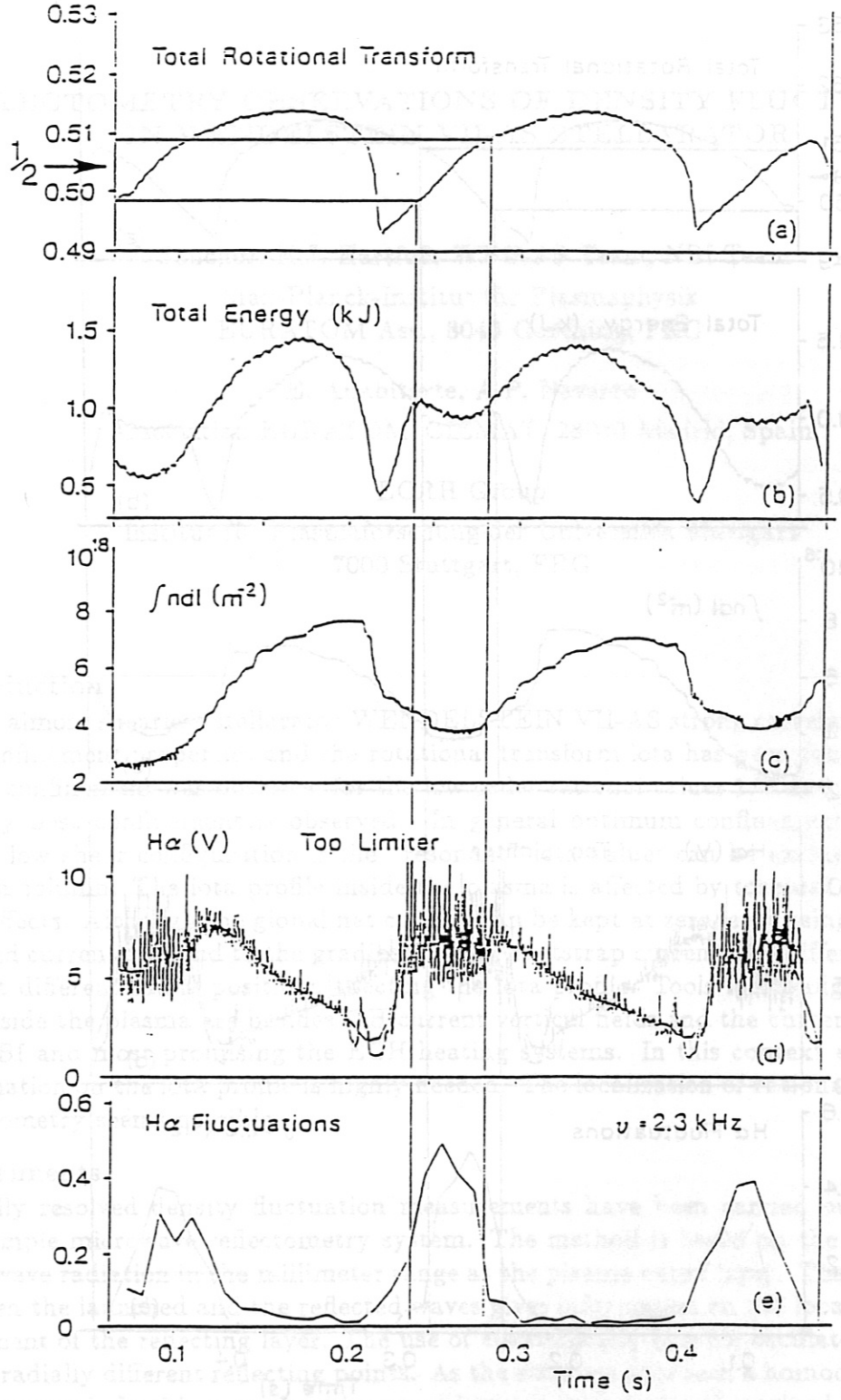

Fig. 3. Global plasma parameters and the H_α—signal as a function of time for an ECR-heated plasma. a) Total rotational transform b) the plasma energy c) the electron line density d) the H_α—signal for the top limiter e) the fluctuations at a frequency of 2.3 kHz.

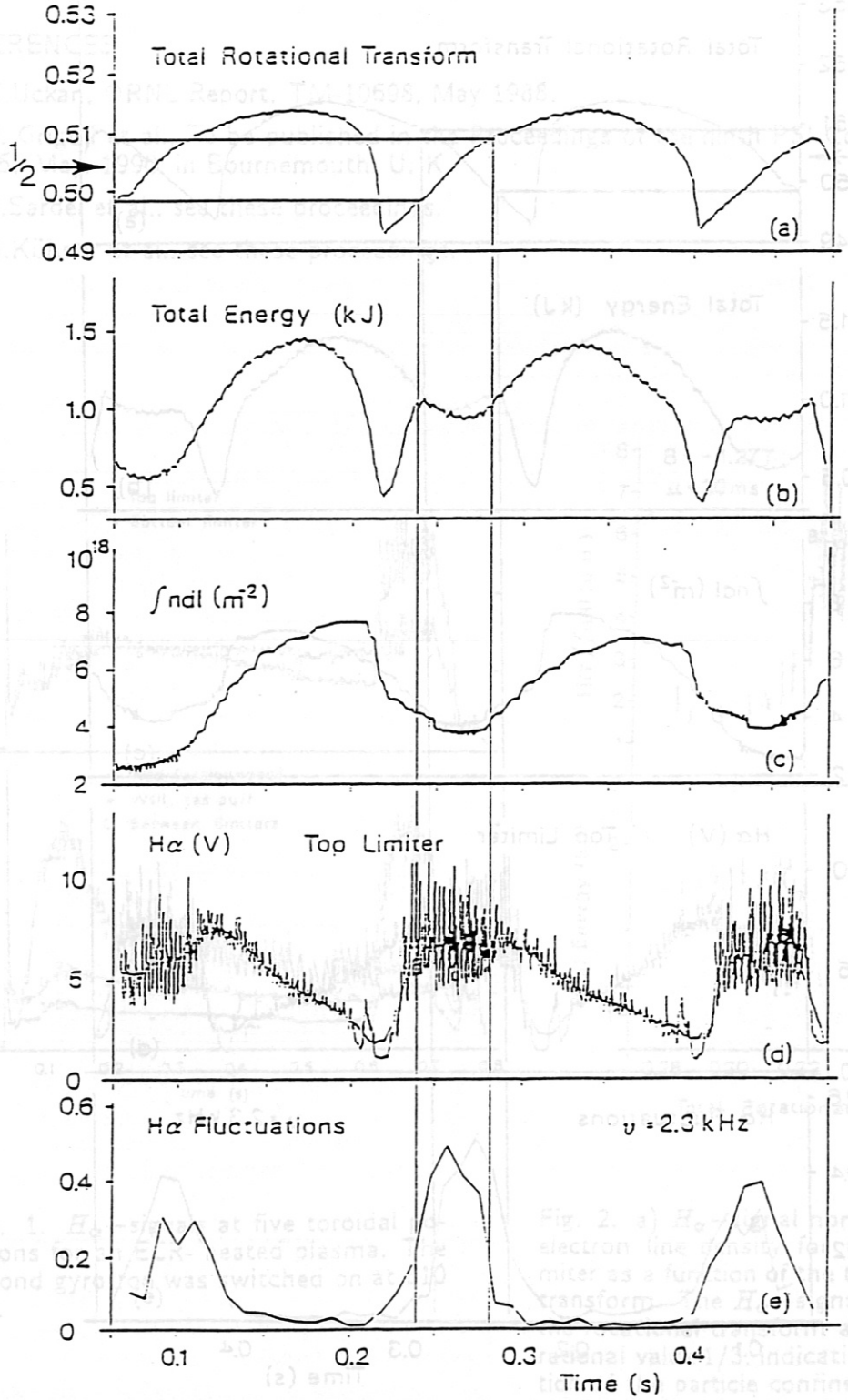

Fig. 3. Global plasma parameters and the H_α–signal as a function of time for an ECR-heated plasma. a) Total rotational transform b) the plasma energy c) the electron line density d) the H_α–signal for the top limiter e) the fluctuations at a frequency of 2.3 kHz.

REFLECTOMETRY OBSERVATIONS OF DENSITY FLUCTUATIONS IN WENDELSTEIN VII-AS STELLARATOR

J. Sanchez, H.J. Hartfuß, WVII-AS Team, NBI Team
Max-Planck-Institut für Plasmaphysik
EURATOM Ass., 8046 Garching, FRG

E. Anabitarte, A.P. Navarro
Association EURATOM/CIEMAT, 28040 Madrid, Spain

ECRH Group
Institut für Plasmaforschung der Universität Stuttgart
7000 Stuttgart, FRG

Introduction

In the almost shearless stellarator WENDELSTEIN VII-AS strong correlation between the confinement properties and the rotational transform iota has been found [1,2]. Reduced confinement was observed for the low order rational values 1/2 and 1/3. In their vicinity best confinement is observed. In general optimum confinement is obtained in the low shear configuration if the "resonant" iota values can be excluded from the plasma column. The iota profile inside the plasma is affected by toroidal currents and beta effects. Although the global net current can be kept at zero level using a small OH induced current opposed to the gradient driven bootstrap current, the different currents flow at different radial positions affecting the iota profile. Tools for configuration control inside the plasma are besides OH current vertical fields and the currents driven by the NBI and most promising the ECH heating systems. In this context experimental information on the iota profile is highly needed. The localization of rational surfaces by reflectometry seems possible.

Experiments

Radially resolved density fluctuation measurements have been carried out by means of a simple microwave reflectometry system. The method is based on the reflection of microwave radiation in the millimeter range at the plasma cutoff layer. The phase delay between the launched and the reflected waves gives information on the location and the movement of the reflecting layer. The use of electronically tunable oscillators allows to probe radially different reflecting points. As the simplest approach a homodyne receiver has been used. In this case the microwave beam is launched and received by using the same antenna. The wave reflected at the plasma and that reflected at some reference (the vacuum window) are mixed in a square law detector diode.The output voltage at the detector is:

$$v(t) = p_0 + p_1 + 2\sqrt{p_0 p_1}\cos[\delta(t)]$$

p_0 is the power coming from the reference, p_1 that one coming from reflection at the

plasma cutoff layer and $\delta(t)$ is the phase delay of interest. The variation in the output of the diode responds to changes both in the phase δ and in the amplitude p_1 of the signal coupled from the plasma. If no coherent MHD activity is present, $v(t)$ shows a broadband spectrum. When a density fluctuation with a well defined frequency Ω exists, the reflecting layer will have an oscillating movement too. So the phase shift can be written as:

$$\delta(t) = \delta_0 + \Delta\Phi \sin \Omega t$$

Thus the amplitude spectrum of the signal shows harmonics of the density fluctuation frequency Ω. The number of harmonics with significant amplitude is the higher the bigger $\Delta\Phi$ is. An analysis of the ratio of amplitudes for the harmonics of the same parity leads to a determination of $\Delta\Phi$. For 1.25 T operation the relevant cutoff frequencies for the X-mode wave lie in the range 40 - 85 GHz. A system in the microwave V-band has been used covering the range 47 - 80 GHz. The accessible density range is: $7\text{x}10^{18}$ - $4\text{x}10^{19}$ m^{-3}. This gives access to the whole gradient region up to the separatrix. The measurements were performed in a special NBI heated discharge with pellet injection at 1.25 T. Currentless plasma was produced by applying a 10 ms ECH pulse of 200 kW power that gives place to a 1.5 MW NBI (45 keV) heating period with tangential injection. The two neutral beams used are balanced to minimize the driven Ohkawa currents. The rotational transform at the edge, ι(a), is kept constant slightly above 0.5. A series of reproducible shots has been produced under these conditions. During this series the beam frequency of the reflectometer was changed shot by shot to reflect at different radial positions. Six different frequencies were chosen to cover the density range of interest. Electron density and temperature profiles have been measured by Thomson scattering. Fig. 1 gives the density profile and the location of the 6 reflection points. The accessible range is between about 0.17 m and 0.09 m. For each of the 6 different frequencies, reflectometry data where taken during 3 - 4 shots. The output voltage from the detector was digitized with a sampling rate of 1 MHz during the time interval 0.11 - 0.16 s ($5\text{x}10^4$ points are taken).

Results And Discussion

The amplitude spectrum of the reflectometer signal which is obtained by fast Fourier transform technique is given in fig.2 for channel 5 as an example. In the spectrum a monochromatic density perturbation with a frequency of 22 kHz is observed. The harmonic structure agrees with what is expected. The determination of the phase oscillation amplitude can be achieved by the analysis of amplitudes at different harmonics. Fig.3 shows the radial distribution of the phase oscillation amplitude $\Delta\Phi$ along the radius for 0.122 s, the time of maximum activity. A well defined mode is observed located at 0.105 m. In addition strong oscillation at the plasma edge outside the separatrix is present. An estimation of the amplitude of the density fluctuation can be done using the expression:

$$\delta n/n = (\Delta\Phi/2\pi)\lambda_0 \nabla n/n$$

resulting in about 3 per cent relative fluctuation level at 0.105 m. In the following we only concentrate on the instability at r = 0.105 m and its configurational implications: The vacuum iota profile of WENDELSTEIN VII-AS for this series of discharges shows a low positive shear which brings iota close to 0.5 at the plasma center. As mentioned

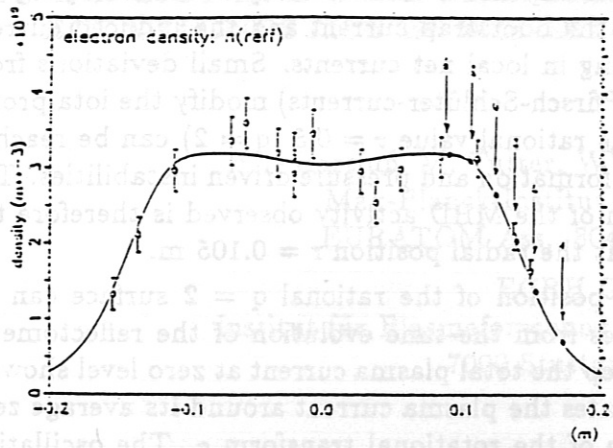

Fig.1: Density profile as measured by Thomson scattering. Reflection points for the different frequencies used are marked.

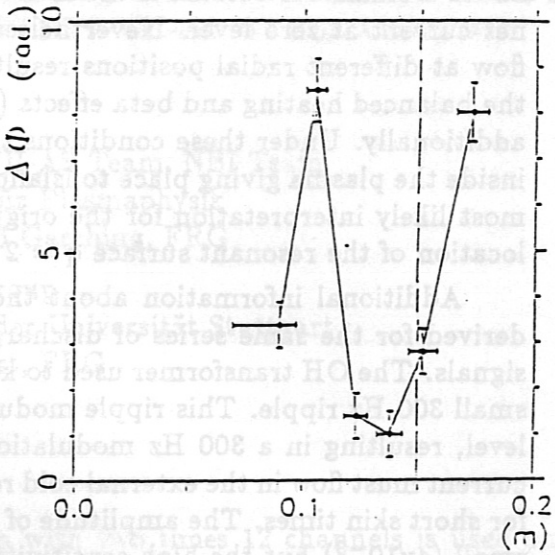

Fig.3: Radial distribution of the phase oscillation amplitude $\Delta\Phi$ for the coherent fluctuation at 22 kHz, taken at 0.122 s.

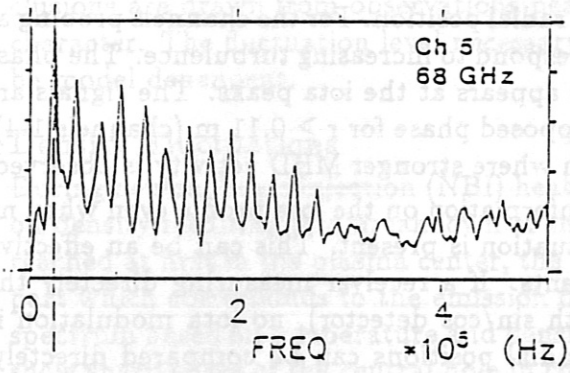

Fig.2: Normalized amplitude spectra of the reflectometer signal for the different incident frequencies showing a dominant perturbation at 22 kHz with harmonic structure at 0.122 s.

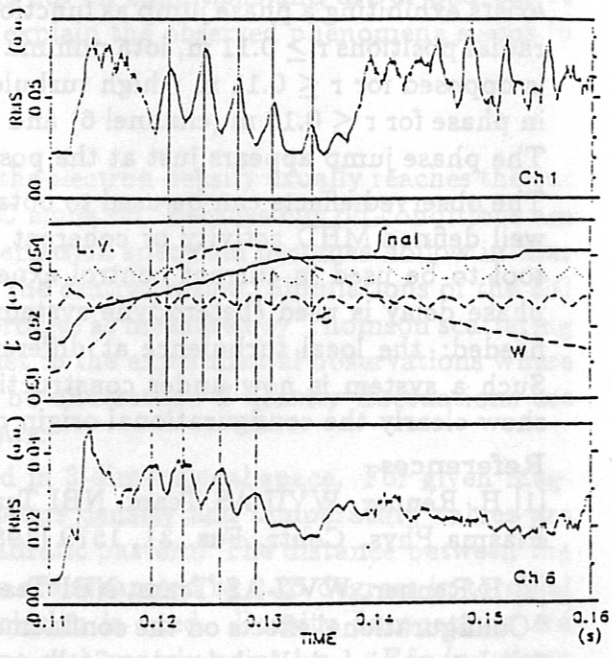

Fig.4: Modulation of the rms reflectometer signal and synchronization with the iota modulation. Upper frame: outermost, lower frame: innermost channel.

above a small OH current is induced to compensate the bootstrap current keeping the net current at zero level. Nevertheless the bootstrap current and the induced current flow at different radial positions resulting in local net currents. Small deviations from the balanced heating and beta effects (Pfirsch-Schlüter-currents) modify the iota profile additionally. Under these conditions the rational value $\iota = 0.5$ (q = 2) can be reached inside the plasma giving place to island formation and pressure driven instabilities. The most likely interpretation for the origin of the MHD activity observed is therefore the location of the resonant surface q = 2 at the radial position r = 0.105 m.

Additional information about the position of the rational q = 2 surface can be derived for the same series of discharges from the time evolution of the reflectometer signals. The OH transformer used to keep the total plasma current at zero level shows a small 300 Hz ripple. This ripple modulates the plasma current around its average zero level, resulting in a 300 Hz modulation of the rotational transform ι. The oscillating current must flow in the external cold region where the resistivity is high enough to allow for short skin times. The amplitude of the iota oscillation around the controlled value is small (4×10^{-3}) but the high sensitivity of the plasma properties to iota changes in the vicinity of rational values generates 300 Hz modulation in different plasma parameters. In fig.4 the time evolution of the rms value of the reflectometer signal is shown for two extreme radial points. The rms signal of the detector output gives information about its ac components. The 300 Hz component is a modulation of the amplitude of the broadband turbulence. A clear synchronization between iota and reflectometer signals exists exhibiting a phase jump as function of radial position. For the channels probing at radial positions $r \geq 0.11$ m, iota minima correspond to increasing turbulence. The phase is opposed for $r \leq 0.11$ m : high turbulence appears at the iota peaks. The signals are in phase for $r \leq 0.10$ m (channel 6) and in opposed phase for $r \geq 0.11$ m (channels 1-4). The phase jump appears just at the position where stronger MHD activity is observed. The observed effects can be used to obtain information on the iota profile even when no well defined MHD activity or coherent fluctuation is present. This can be an effective tool to be used in current control experiments. If a receiver measuring directely the phase delay is used (heterodyne system with sin/cos detector), no iota modulation is needed: the local turbulence at different radial positions can be compared directely. Such a system is now under construction. In any case the iota modulation helps to show clearly the configurational origin of the local enhanced turbulence.

References

[1] H. Renner, WVII-AS Team, NBI Team, ECRH Group, ICRH Group, Plasma Phys. Contr. Fus. 31, 1579 (1989)

[2] H.Renner, WVII-AS Team, NBI Team, ICRH Group, ECRH Group, "Configurational effects on the confinement in the stellarator WENDELSTEIN VII-AS". 7th International Workshop on Stellarators, April 10 - 14, Oak Ridge, TN, 1989

ON DENSITY AND TEMPERATURE FLUCTUATIONS OBSERVED BY ECE DIAGNOSTICS IN WENDELSTEIN VII-AS STELLARATOR

H.J. Hartfuß, M. Tutter, WVII-AS Team, NBI Team
Max-Planck-Institut für Plasmaphysik
EURATOM Ass., 8046 Garching, FRG

ECRH Group
Institut für Plasmaforschung der Universität Stuttgart
7000 Stuttgart, FRG

Introduction

A multichannel heterodyne radiometer system with two times 12 channels is used on WVII-AS to measure the electron cyclotron emission (ECE) both time and space resolved [1]. In this paper we report about sporadic observations of density and temperature fluctuations using this system. The observations are made under different operation conditions concerning field, rotational transform, and heating scenario. In the case of density fluctuations no direct measurement is possible using ECE diagnostics. The conclusions are drawn from observations near the cut off conditions and are of qualitative character. The fluctuation level necessary to explain the observed phenomena seems to be model dependent.

Density Fluctuations

During neutral beam injection (NBI) heating the electron density usually reaches the cut off density resulting in a breakdown of the EC emission. Because cut off conditions are reached at first in the plasma center, the EC emission spectrum becomes hollow in that part which corresponds to the emission from the central region. Simulations of the EC spectrum based on temperature and density profiles as measured by Thomson scattering show sharp edges of the central hole in contrast to the experimental observations where flat slopes are found. The observations can be understood if density fluctuations are taken into account, which are treated as follows:

Plasma density and temperature are specified in 3-dimensional space. For given magnetic coil currents and plasma profile parameters density and temperature values are calculated at meridional torus planes in a quadratic pattern. The distance between the matrix points is 1.5 cm, the meridional planes are separated by 2.25 degrees in toroidal direction. Between the points linear interpolation is used. Density fluctuations are included by multiplying the density value n at each matrix point by $1+F\delta n/n$, where F is a random function varying between -1 and +1. Fig.1 gives a density distribution generated in this way which is a momentary picture of the fluctuating plasma. After running the ray tracing code about 30 times the results are averaged.

Fig.2 gives an example of the result obtained during 1.25 T operation. As can be seen the simulated "profile" clearly shows the flat slope of the central hole as indicated by the 7 channel ECE data. At 1.25 T only 7 channels are available. They all correspond

to the high field side of the profile and monitor the 2nd harmonic X mode ECE. The absolutely calibrated spectral data have been converted to radiation temperatures as function of plasma radius in the usual way. Thomson scattering data are included for comparison.
The concept of fluctuating density can also serve to explain the power deposition profiles during electron cyclotron heating (ECH). They are found to be broader at densities near cut off than obtained by ray tracing calculations for given non fluctuating stationary profile. Fig.3 gives an example.
A further case which confirms the concept is its application to the spatial power distribution of ECH power after passing the plasma. With an antenna array which is mounted opposite to the launching antenna rather high power levels have been observed at large angles which cannot be understood assuming an unperturbed static plasma. Simulations on the basis of scattering in the presence of density fluctuations lead to good agreement with the observations.
It should be mentioned that the fluctuation level $\delta n/n$ necessary to explain the data must be of the order of 10 per cent. This high level is not confirmed by other diagnostics. Investigations on the influence of the pattern used in the simulation code are being carried out.

Temperature Fluctuations

Two examples may demonstrate in which way temperature fluctuations reflect the confinement properties of WENDELSTEIN VII-AS. In general good confinement is obtained if the edge value ι(a) of the rotational transform is slightly above or below the low order rationals 1/2 and 1/3. Confinement is strongly reduced in the shearless configuration when ι(a) reaches these values [2].
Strong temperature fluctuations were observed during EC heated transient plasma discharges conducted at 2.5 T which cross ι(a)=1/3 due to the monotonic development of a bootstrap current.
The low field side of the electron temperature profile was monitored with the ECE radiometer system at 12 different radii. When the resonant iota value is reached, the confinement time collapses to about 15 per cent, accompanied by a shrinking of the hot core of the plasma column. It takes about 100 ms until the regime of poor confinement is crossed. This interval was analyzed by applying autocorrelation techniques to determine the relative level $\delta T_e/T_e$ of the temperature fluctuations. Fig.4 gives the result as a function of the plasma radius. About 3 per cent are found in the central confinement region of the plasma with a strong increase towards the plasma edge.
After the ι range of poor confinement is crossed, the high fluctuation level almost completely disappears: Fig.4 for comparison gives $\delta T_e/T_e$ as determined from the same discharge about 150 ms later. The central value is reduced by about a factor of 3, while the edge value drops to at least 1/15.
The whole phenomenon can be suppressed by controlling the plasma current to zero level with the aid of a small counterdirected OH current. The results obtained in a different shot conducted under these conditions are included in the figure too. Within the estimated experimental errors they are identical to results obtained in the unperturbed phase of the discharge discussed before.
Two fundamental difficulties in the measurement of temperature fluctuations with ECE

diagnostics should be mentioned. A fundamental fluctuation level always exists observing an incoherent, thermal light source. The level observed depends on the detection method applied i.e. coherent or incoherent detection, and the input and video bandwidth of the radiometer involved [3]. Below this fundamental lower limit of temperature fluctuations no source fluctuation can be detected. The fluctuation level of 1 per cent which is reached in the plasma center corresponds to this limit for the parameters of the ECE radiometer in use. Therefore the true temperature fluctuation in the plasma center cannot be measured in this case. Crossed sightline correlation techniques may overcome the fundamental difficulties.
The second difficulty deals with the optical depth of the plasma at its edge. It depends both on the electron temperature and density. Because the radiation temperature depends on the optical depth, the measured ECE signal is not only determined by the electron temperature but becomes dependent on the electron density at the plasma edge too. In this way density fluctuations can be converted to apparent temperature fluctuations. The total fluctuations observed are a combination of density and temperature fluctuations and are always higher than the temperature fluctuations alone.

Cross correlation between channels monitoring at different radial positions shows that the strong fluctuations as found during the ι=1/3 crossing are coherent over a large part of the profile whereas in the current controlled case spatial coherence is clearly below 1 cm.
The dominating part of the fluctuation spectrum is restricted to below about 3 kHz, reflecting the timescale of rearrangement of the bootstrap current in the plasma column.

In a second example the relative fluctuation level has been measured near the plasma center (1 ECE channel evaluated only) during a series of shots in which ι(a) has been scanned around 1/2. As mentioned above confinement maxima are found in close vicinity to the sharp confinement minimum at 1/2. In this series of shots the line density has been kept constant. No stationary discharge could be established at the resonant iota value 1/2.
Fig.5 shows $\delta T_e/T_e$ as function of ι(a). A broad minimum in the fluctuation level is observed which corresponds to the maxima of confinement near ι=1/2 and its flat decrease with increasing distance to this value. Because no stationary discharge was possible at ι=1/2 the expected sharp peak in the fluctuation level cannot be observed. Again the central fluctuation level at optimum confinement is about 1 per cent identical to the radiometric fundamental level. At poor confinement in the wings of the curve about 3 per cent are found as before in the transient discharge.

References

[1] H.J. Hartfuß et al.,"ECE Diagnostic for the new Stellarator Wendelstein VII-AS", Proc. of EC-6, Joint Workshop on ECE and ECRH, September 16-17, Oxford, 1987

[2] H. Renner, WVII-AS Team, NBI Team, ICRH Group, ECRH Group,
"Configurational effects on the confinement in the stellarator WENDELSTEIN VII-AS". 7th International Workshop on Stellarators, April 10 - 14, Oak Ridge, TN, 1989

[3] H.J. Hartfuß, "Coherent Versus Incoherent Detection Schemes", Proc. Joint IAEA Technical Committee Meeting On ECE and EC-7 Meeting, May 8-11, Hefei PR China, 1989

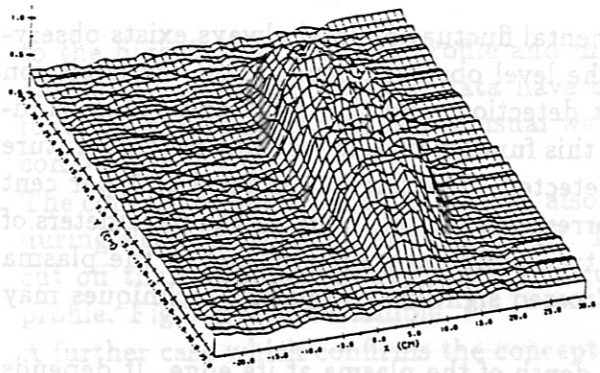

Fig.1 Snapshot of the fluctuating plasma as used for the ray tracing calculation.

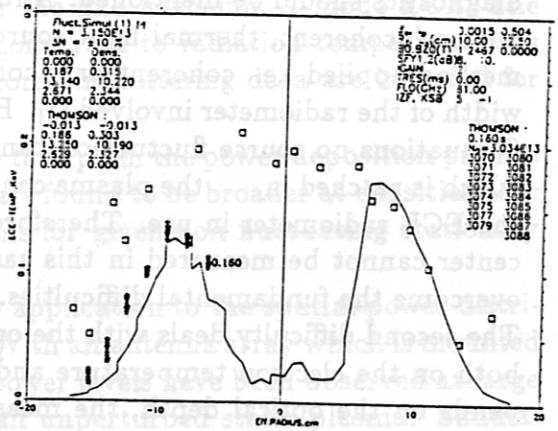

Fig.2 Breakdown of the experimental ECE "profile" (dots) at plasma density near cut off. The line is the result of a simulation, squares give the temperature profile as measured by Thomson scattering.

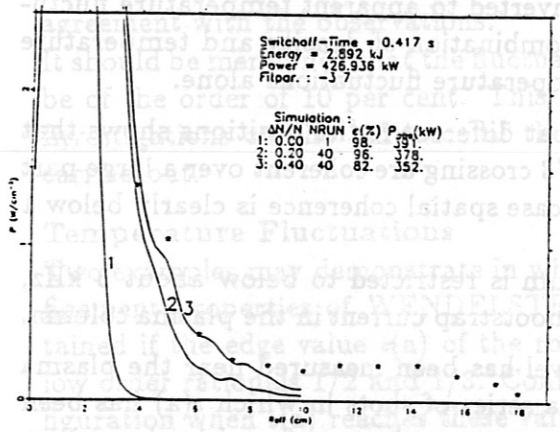

Fig.3 Power deposition profiles: Dots are derived from the slope of ECE temperature signals at ECH switch off. Lines are from simulations using $\delta n/n = 0$, 0.2 and 0.4 resp.

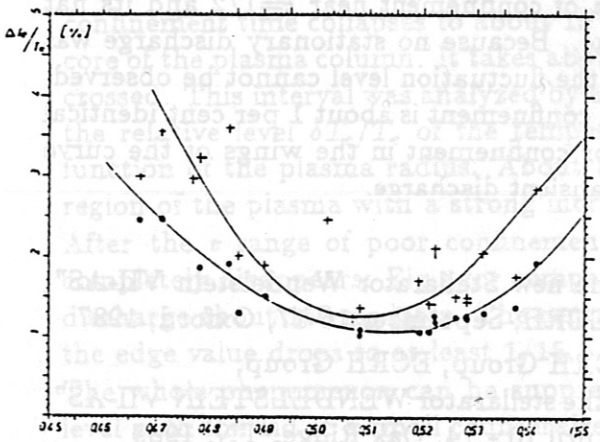

Fig. 5 Temperature fluctuations of central temperature as function of the edge value of the rotational transform.

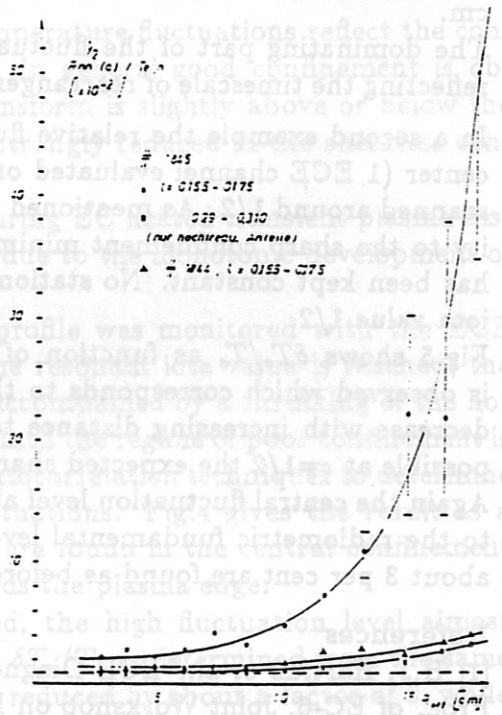

Fig. 4 Temperature fluctuations as function of plasma radius as derived from ECE data during the crossing of ι=1/3 and for comparison without perturbation from resonant surface.